

DISSERTATION

**ROLE OF POLYGLUTAMYLATION IN NUCLEOSOME ASSEMBLY
PROTEIN 1 (NAP1) FUNCTION**

Submitted by

Vidya Subramanian

Department of Biochemistry and Molecular Biology

In partial fulfillment of the requirements for the

Degree of Doctor of Philosophy

Colorado State University

Fort Collins, CO

Summer 2008

UMI Number: 3332710

INFORMATION TO USERS

The quality of this reproduction is dependent upon the quality of the copy submitted. Broken or indistinct print, colored or poor quality illustrations and photographs, print bleed-through, substandard margins, and improper alignment can adversely affect reproduction.

In the unlikely event that the author did not send a complete manuscript and there are missing pages, these will be noted. Also, if unauthorized copyright material had to be removed, a note will indicate the deletion.

UMI[®]

UMI Microform 3332710

Copyright 2008 by ProQuest LLC.

All rights reserved. This microform edition is protected against unauthorized copying under Title 17, United States Code.

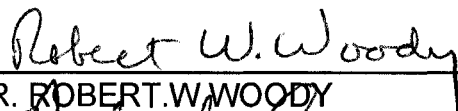
ProQuest LLC
789 E. Eisenhower Parkway
PO Box 1346
Ann Arbor, MI 48106-1346

COLORADO STATE UNIVERSITY

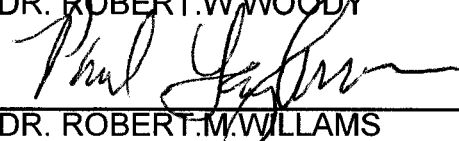
May 20th, 2008

WE HEARBY RECOMMEND THAT THE DISSERTATION PREPARED UNDER THE SUPERVISION OF VIDYA SUBRAMANIAN ENTITLED " ROLE OF POLYGLUTAMYLATION IN NUCLEOSOME ASSEMBLY PROTEIN 1 (NAP1) FUNCTION" BE ACCEPTED AS FULFILLING IN PART THE REQUIREMENT FOR THE DEGREE OF DOCTOR OF PHILOSOPHY.

Committee on Graduate Work



DR. ROBERT.W.WOODY



DR. ROBERT.M.WILLAMS



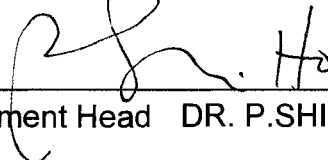
DR. PAUL.J.LAYBOURN



DR. OLVE.B.PEERSEN



Advisor DR. KAROLIN LUGER



Department Head DR. P.SHING HO

ABSTRACT OF DISSERTATION

ROLE OF POLYGLUTAMYLATION IN DROSOPHILA NUCLEOSOME ASSEMBLY PROTEIN-1 (dNAP1) FUNCTION.

PROJECT I

STUDY OF DNA ALKYLATING AGENTS ON NUCLEOSOMES- BIOCHEMICAL AND FUNCTIONAL ANALYSES

In the first part of this dissertation we attempted to understand the molecular mechanism of a sequence-specific, photoreactive DNA alkylating agent-NVOC. Most studies involving this class of compounds were restricted to analyses with unassembled (linear) DNA. We wanted to look at the activity of NVOC on conformationally distinct nucleosomal DNA since ~80% of cellular DNA exists as chromatin. We also wanted to determine any differences in the cross-linking/monoalkylation activity of NVOC between unassembled and assembled DNA substrates. DNA cross-linking agents are known to restrict any process involving DNA double-strand melting, such as replication. We wanted to investigate other basic cellular processes that might be affected by this drug-induced DNA modification.

We found that NVOC does indeed show a difference in the activity between nucleosomal versus assembled DNA. NVOC was found to preferentially mediate mono-alkylation rather than interstrand cross-linking of nucleosomal DNA. Linear DNA was, however, a better substrate for interstrand DNA cross-

links. We were able to quantitatively establish that NVOC-mediated DNA cross-links resulted in linear DNA templates that did not favor transcription and chromatin assembly *in vitro*. This study helped establish the effect of NVOC, a DNA cross-linking agent, on chromatin assembly using a quantitative method designed to determine the number of nucleosomes present on a DNA template.

PROJECT II

ROLE OF POLYGLUTAMYLATION IN DROSOPHILA NUCLEOSOME ASSEMBLY PROTEIN-1 (dNAP1) FUNCTION.

The organization of DNA into chromatin requires the systematic deposition of the histones onto the DNA template. Chromatin function requires the dynamic exchange of the histone components during replication and transcription. Deposition and exchange is mediated in part by a family of proteins generally referred to as histone chaperones.

It has been shown recently that recombinant yeast NAP1 (yNAP1) is capable of promoting ATP-independent histone exchange and nucleosome sliding *in vitro*, and this ability is specifically attributed to the highly acidic C terminal tail of the protein. *Drosophila* NAP1 (dNAP1) has a shorter acidic C terminus than yNAP1. Preliminary data in the lab suggests that recombinant wild-type dNAP1 is incapable of this nucleosome dissociation. Native dNAP1 purified from *Drosophila* embryos, on the other hand, is capable of nucleosome dissociation.

In this study we reveal the presence of a unique post-translational modification, polyglutamylation in native dNAP1, which restores the nucleosome dissociation function to recombinant dNAP1. We have also been able to identify two target sequences, as well as the number of glutamyl units associated with these modifications using mass spectrometric analysis (MALDI & MS/MS). The modification at the CTAD (C-terminal acidic tail domain) could compensate for the lesser amount of acidic amino acid in dNAP1 and may account for the gain in nucleosome dissociation function. The second polyglutamylation site is located at the NLS (Nuclear Localization Sequence) (based on the conserved core domain of yNAP1 and dNAP1).

Vidya Subramanian
Department of Biochemistry and Molecular biology
Colorado State University
Fort Collins, CO 80523
Summer 2008

ACKNOWLEDGMENTS

I would like to first thank my mentor- Karolin. She has been a great source of encouragement and inspiration. With her help I have learnt to think and work independently. Her ability to look at every piece of data and find the missing link has taught me a lot about how to design experiments and how to get maximum mileage out of them. She has never hesitated to venture into new areas of research and is quick to find resources that will help in this regard. Her enthusiasm for science is infectious and has been essential especially in my desperate moments of scientific despair. Most of all Karolin has taught me how important it is to hope for the best and prepare for the worst- a life lesson. Thank you Karolin.

I would like to extend a special thanks to all my committee members- Dr. Robert Williams (and collaborator), Dr. Robert Woody, Dr. Paul Laybourn and Dr. Olve Peersen. They have all been helpful in their own unique way. There hasn't been a single committee meeting where I haven't been able to find different solutions to the experimental problems I have faced. Thank you for your support, encouragement and critiques.

I thank Dr. Pascal Ducept in the Willams lab for teaching me more Organic Chemistry than I wanted to learn. I am extremely indebted to Dr. Rajeswari Edayathumangalam for her intensive training and focus on understanding basic principles, Dr. Yunhe Bao for his stash of Chinese rock CDs, Dr. Srinivas Chakravarthy for his philosophical take on science, Dr. YoungJun Park, my second mentor in the lab for being a huge source of inspiration and encouragement. I have always appreciated his work ethic and have learnt a lot working beside him- Thank you "The Parkster"!. The

irreplaceable Dr. Jay Chodaparambil for his unique perspective on life and science- thank you.

The Luger lab has been extremely protective and encouraging. Specifically I would like to thank Pam Dyer for being a great “mom” both in and out of lab. A special thanks to Dr. Mary Robinson for “Sunday with the Robinsons” and for teaching me how to knit and sew, Dr. Andy Andrews for destroying my thinking and forcing me to look at things differently, Dr. Wayne Lilyestrom for his initial lessons on snowboarding, Dr. Mark Van der Woerd for his “words of wisdom” and Dr. Uma Muthurajan for being my safety net and my one connect to home. To a great friend and a wonderful fellow NAPster-Kitty Brown, thank you for being my shrink and to my very hardworking and supportive juniors-Chenghua, Keely and Nick, thank you. A huge thanks to – Allison, Alysun, Greg, Tatsuya, Jeremy, Mike Cramer, Karen and Alex for making me the butt of all jokes. You have made it easier for me to deal with stress-thank you guys! To Beth, for taking care of all the nitty-gritty details thank you for all your help. I would like to thank all my classmates for being cohesive through the rough patches. I would like to extend a special thanks to the administrative staff for taking care of all the complicated paper work and making life easier for me. I thank the rest of the BMB department for their kind words and their friendship.

I would like to thank all my friends and relatives for being supportive and always checking to see if I have some sense of sanity left. Last but certainly not the least I would like to thank my parents-my father for teaching me math and science and my mother for her enthusiasm and spirit. Both of you taught me the importance of perseverance and to look at every obstacle as an opportunity and not a road-block; a lesson that has served me well during my 5 year graduate stint. Thank you for your trust, guidance, love and unrelenting support.

TABLE OF CONTENTS

Title Page	i
Signature Page	ii
Abstract and Layout of the Dissertation	iii
Acknowledgements	vi
Table of Contents	viii

Project I

Title: **Study of DNA alkylating agents on nucleosomes – Biochemical and Functional Analyses.**

Chapter 1: Review of Literature

1.1 Bioreductive Alkylating Agents: Function, Specificity and Derivatives

1.1.1 Function	1
1.1.2 Specificity	2
1.1.3 Derivatives	3

1.2 *In vivo* data demonstrating the effectiveness of the FR and FK series of drugs. 4

1.3 Phototriggered derivative of natural antitumor drug FR900482. 5

1.4 Cellular DNA exists as a heterochromatin 6

1.5 Specific aims pertaining to Project I 8

Chapter 2: Effects of Photo-chemically Activated Alkylating Agents of the FR900482 Family on Chromatin.

2.1	Abstract	9
2.2	Introduction	10
2.3	Experimental Procedures	13
2.4	Results	
2.4.1	Nucleosomal DNA cross-links inefficiently with compound 5 compared to free DNA.	18
2.4.2	Compound 5-mediated preferential monoalkylation of nucleosomal DNA compared to unassembled DNA.	19
2.4.3	Compound 5-mediated cross-linking of unassembled DNA represses <i>in vitro</i> transcription.	23
2.4.4	Compound 5-mediated cross-linking of plasmid DNA reduces efficiency of chromatin assembly.	25
2.5	Discussion	32
2.6	Acknowledgements	36
2.7	Supplementary Data	37

Chapter 3: Xray crystallography studies of the nucleosome core particle in complex with FK317 and Acr1.

3.1	Abstract	49
3.2	Introduction	
3.2.1	Structural studies involving NCP-mitosene complex.	50

3.2.2	Structural studies involving polyamide-NCP complex.	51
3.3	Experimental Procedures	53
3.4	Results	
3.4.1	Structural analysis of the FK317-nucleosome co-complex.	55
3.4.2	Structural analysis of the Acr1-NCP co-complex.	61
3.5	Discussion	
3.5.1	Structural analysis of the FK317-nucleosome co-complex.	64
3.5.2	Structural analysis of the Acr1-NCP co-complex.	65
3.6	Acknowledgements	66

Project II

Title: **Role of polyglutamylation in the function of *Drosophila* Nucleosome Assembly Protein 1**

Chapter 4:	Review of literature	67
4.1	Chromatin structure and function	67
4.2	Regulation of chromatin dynamics	69
4.2.1	Histone variants	69
4.2.2	Posttranslational Histone modifications	70
4.2.3	Chromatin remodelers	71
4.2.4	Histone chaperones	72
4.3	Nucleosome assembly protein 1 – Structure and function	73
4.4	Posttranslational NAP1 modifications and their functional impact	77
4.5	Specific aims of Project II.	80

Chapter 5: Role of polyglutamylation in the function of <i>Drosophila</i> Nucleosome Assembly Protein 1 (dNAP1).	
5.1 Abstract	81
5.2 Introduction	82
5.3 Experimental Procedures	84
5.4 Results	
5.4.1 Recombinant dNAP1 is compromised in its ability to dissociate nucleosomes <i>in vitro</i> .	89
5.4.2 Native dNAP1 capable of nucleosome dissociation <i>in vitro</i> .	91
5.4.3 The C terminus of native dNAP-1 is polyglutamylated.	95
5.5 Discussion	104
5.6 Acknowledgements	111
5.7 Supplementary Data	112
Chapter 6: Contributions to other research projects	117
Chapter 7: Future directions and Perspectives	118
References	122

CHAPTER 1 PROJECT I

STUDY OF DNA ALKYLATING AGENTS ON NUCLEOSOMES- BIOCHEMICAL AND FUNCTIONAL ANALYSES

REVIEW OF LITERATURE

1.1 BIOREDUCTIVE ALKYLATING AGENTS: FUNCTION, SPECIFICITY AND DERIVATIVES

Every DNA-modifying anti-cancer agent has a unique mode of action, which makes it selective and effective. DNA cross-linking drugs are particularly potent as they shut down all the basic cellular processes that involve DNA melting (1). Nitrogen Mustard (NM) and melphalan have been shown to be effective anticancer drugs in this regard. However, their harmful side effects have prevented their use in clinical trials. Ongoing research efforts are therefore directed at looking for drugs that specifically target cancerous cells. One such effort resulted in the discovery of a natural bioreductive alkylating agent- Mitomycin C (MMC), a representative compound of the mitosene class of compounds.

1.1.1 Function

Bioreductive alkylating agents are endowed with the ability to be activated under highly reductive conditions, resulting in the formation of a reactive bis-electrophilic mitosene species. The mechanism of activation of these compounds is best illustrated in Figure 1C. Proliferative cancer cells are known to harbor a reductive environment therefore making rapidly proliferative cancer cells a prime target for such drugs. The mitosene species has two reactive centers- the C10

carbamate and the C1 aziridine (Figure 1B). This affords the reactive species many options – inter and intrastrand cross-linking, monoalkylation via C10 or C1, protein-DNA cross-linking. Indeed various investigators have shown that mitosene-based compounds mediate all of the above (2-6).

1.1.2 Specificity

The reductive activation pathway both *in vivo* and *in vitro* results in the formation of the mitosene residue: a bis-electrophilic species that cross-links DNA through formation of a bis-alkylated adduct (7). Thus MMC has been found to be selective for oxygen-deficient tumor cells whose ability to undergo rapid proliferation provides an ambient reducing environment for its activation. However, this reactive species specifically targets the 5'CpG3' step in duplex DNA (2,8) Figure 1B. This selectivity is attributed to the distance between the exocyclic N2 atoms of the guanine residues in the 5'CpG3' step which is identical to the distance between the two reactive sites on the mitosene. Thus the geometric fit between the two reactive sites on the mitosene residue and the two exocyclic N7 atoms on guanine renders MMC specific to 5'CpG3'. The DNA-sequence specificity and the ability of these drugs to be bioreductively activated make them highly potent anti-tumor agents.

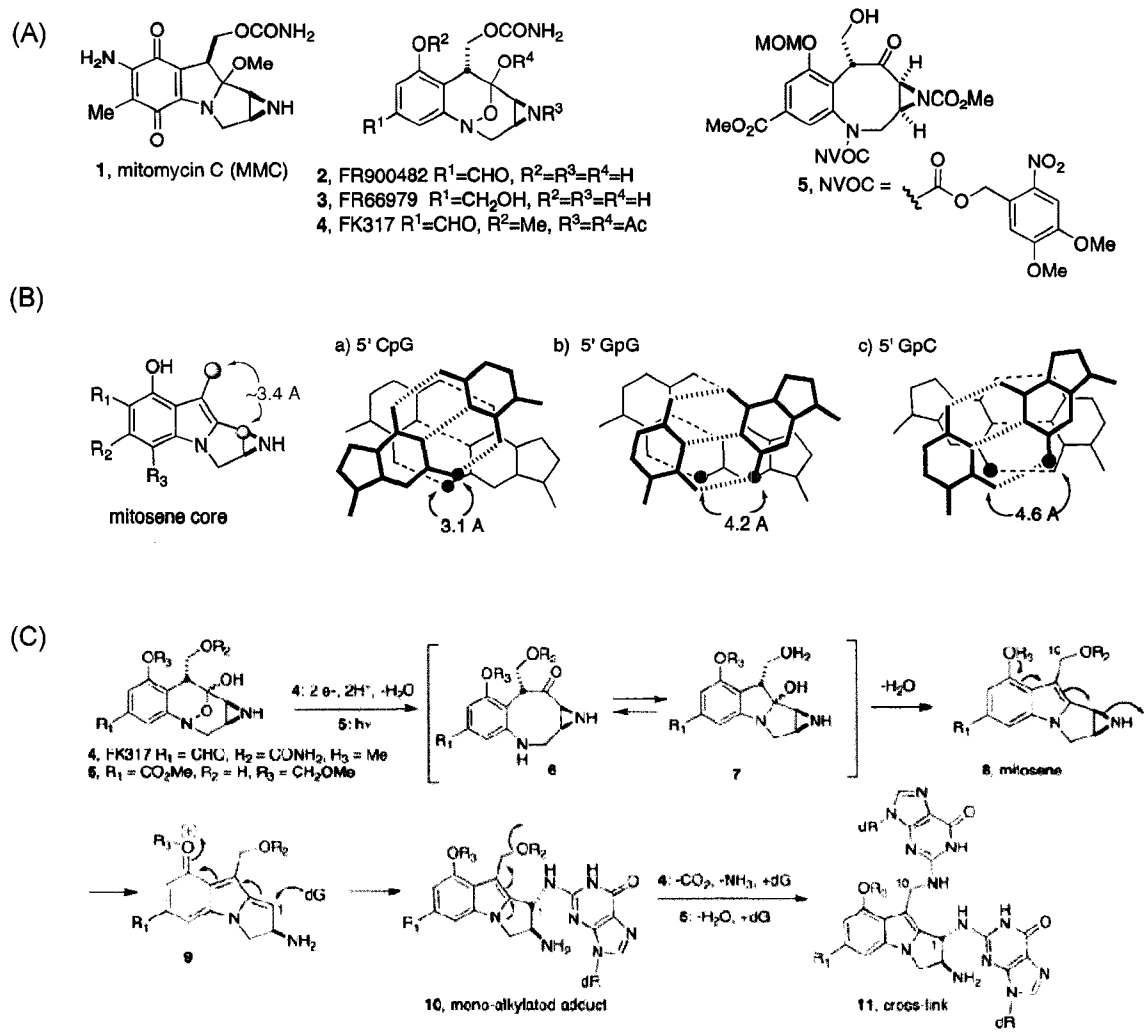


Figure 1: **Bioreductive Alkylating Agents- Structure, Specificity and Mechanism.**

(A) Chemical structures representing mitomycin C (MMC) **1**, natural derivatives FR900482 **2** & FR66979 **3**, semisynthetic derivative FK317 **4** and the phototriggered NVOC-derivative **5**. (B) 5'CpG3' specificity for interstrand cross-linking mediated by bioreductive alkylating agents. a),b) and c) represent the distances between the target exocyclic nitrogens in CpG, GpG as well as GpC steps. (C) Mechanism of activation and formation of the reactive bis-electrophilic mitosene moiety. The stepwise chemical representation of the reductive activation of FK317 **4** and the photochemical activation of NVOC **5** resulting finally in the formation of a reactive mitosene species.

1.1.3 Derivatives

Mitomycin C has been in the spotlight for several years, but the overwhelming side effects of this drug necessitated discontinuing its use in clinical trials. This stimulated the need for drugs with similar mechanism of action but with less severe side effects. The search for alternative drugs within the same class of compounds was pursued by a Japanese company- Fujisawa Pharmaceutical Company. They were successful in the isolation of two important natural compounds- FR900482 and FR66979 (9). These were obtained from fermentation harvests of *Streptomyces sandensis*. The structure of the two derivatives along with their mechanism of action is provided in Figure 1 A & C (6). The company has also been successful in the synthesis of two clinical candidates- FK317 and FK973 that are both semisynthetic derivatives of the natural antitumor drug FR900482. The semisynthetic drugs have the same basic chemical structure as FR900482 compound and a similar mechanism. FK317 and FK973 show better biological profiles during clinical trials (10).

1.2 IN VIVO DATA DEMONSTRATING THE EFFECTIVENESS OF THE FR AND FK SERIES OF DRUGS.

The FR class of drugs is well represented by FR900482, which has been shown to form covalent cross-links between HMG I/Y and the minor groove of DNA, thus providing the first evidence for drug-mediated cross-links between an oncoprotein and DNA in living cells. This initiated efforts towards the use of these drugs as possible replacements for mitomycin C due to their reduced host toxicity

and enhanced interstrand DNA as well as protein-DNA cross-linking. While both the FK317 derivative and FR900482 have similar chemical structures, they have markedly different biological profiles. In clinical trials, FR900482 and FK973 were shown to trigger vascular leak syndrome (VLS) induced by necrosis, while FK317 did not. *In vivo* experiments conducted by treating Jurkat cells with these drugs demonstrated that the difference in biological activity is possibly due to the fact that FK317 exhibits a necrosis-apoptosis switch while FK973 induces VLS *via* a necrosis pathway (10). Thus FK317 has advanced into phase II trials in Japan.

1.3 PHOTOTRIGGERED DERIVATIVE OF NATURAL ANTI-TUMOR DRUG FR900482.

Since all the FR series of compounds are limited by the requirement of hypoxic reducing conditions, the Williams lab (Colorado State University), were looking at ways to design and synthesize masked pro-mitotense drugs. These caged photocleavable derivatives would provide the advantage of efficient cross-linking and controlled release of the reactive mitotense species. As a result of these efforts, the phototriggered NVOC (6-nitroveratryloxycarbonyl chloride) derivative of the natural antitumor drug FR900482 was prepared, which we will be referring to as NVOC for convenience throughout this report (11). The chemical structure and method of activation of NVOC is provided in Figure 1A, compound 5.

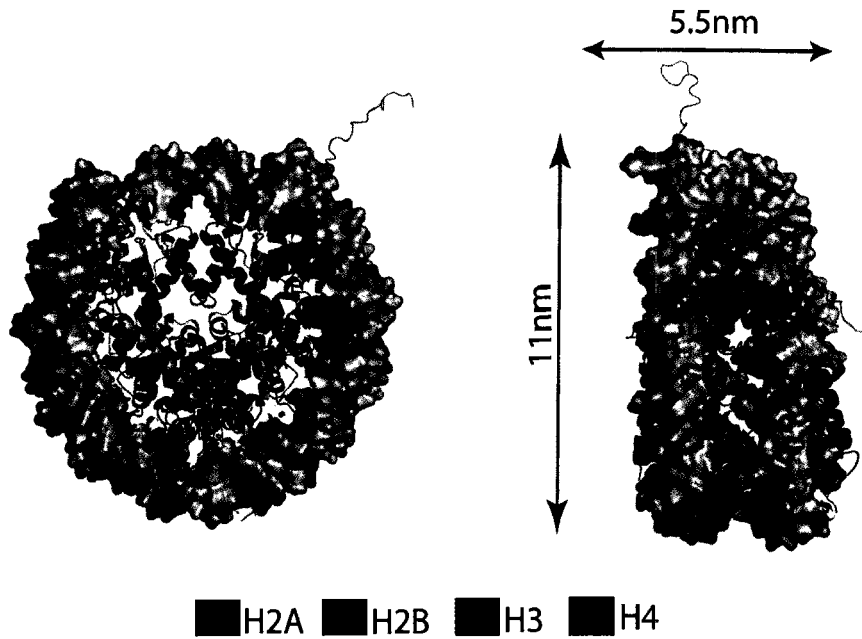
1.4 CELLULAR DNA EXISTS AS HETEROCHROMATIN

Most eukaryotic DNA is close to 2 meters long and is packed into the cell by association with basic histones protein to chromatin (12). Chromatin constitutes the highest level of compaction of cellular DNA (reviewed in (13)). The basic

repeating unit of chromatin is the nucleosome core particle (NCP, Figure 2) (14). This unit consists of an octamer containing two copies of four histone proteins in the form of one tetramer (H3-H4)₂ and two dimers (H2A-H2B) around which 147bp of DNA are wrapped in 1.7 turns of a tight superhelix. The nucleosomal DNA, however, is not an ideal superhelix, i.e. while normal DNA has a periodicity of 10bp/turn, the nucleosomal DNA has a periodicity of 10.7bp/turn. The major and minor grooves in the nucleosomal DNA are highly compressed and deep in the region that faces the histones, but more extended on the outside (15,16). Moreover the regions outside are more flexible and plastic relative to those associated with histones (14,16). The nucleosome complex is critical for transcriptional regulation. Thus, histones not only play a role in DNA compaction but also mediate transcriptional regulation based on their ability to regulate the accessibility of DNA, as well as their ability to interact with a variety of components of the transcription machinery.

Earlier studies on the activity of MMC on nucleosomal DNA revealed that crosslinking of 154bp 5S nucleosomal DNA is compromised when compared to unassembled DNA (17). However the study did not characterize the nature of the modified DNA products, i.e. if the cross-links were protein-DNA, interstrand DNA or monoalkylated DNA adducts.

Our study aims at dissecting the differences in the mitosene-based drugs on assembled and unassembled DNA. We also wish to investigate the molecular mechanism of these photoreactive DNA alkylating compounds by looking at the quantitative effect of these agents on transcription and chromatin assembly.



Luger, et.al , Nature, 1997

Figure 2: **Structure of the Nucleosome.** (A) Top view and (B) Side view of the nucleosome. The dimensions of a single nucleosomal unit are indicated along side the mononucleosome structure. The color scheme used for the protein octamer core is explained below.

1.5 SPECIFIC AIMS FOR PROJECT I

1) Effect of photoactivable mitosene-based drug NVOC on nucleosomal DNA.

1A. Determination of the efficiency of cross-linking of the photoactivatable drug in comparison with chemically activated mitosene-based drug on both nucleosomal and linear DNA templates.

1B. Determination of the nature of drug-mediated modification (extent of cross-linking versus monoalkylation) on nucleosomal and linear DNA.

1C. To determine if the sequence specificity of the mitosene-based drug is conserved in the case of nucleosomal DNA.

2) Functional analysis to dissect the molecular mechanism of action of the drug.

2A. Determine the quantitative effect of NVOC on chromatin assembly.

2B. Determine the effect of NVOC on *in vitro* transcription.

CHAPTER 2

EFFECTS OF PHOTOCHEMICALLY ACTIVATED ALKYLATING AGENTS OF THE FR900482 FAMILY ON CHROMATIN.

2.1 ABSTRACT

Bioreductive alkylating agents are an important class of clinical antitumor antibiotics that crosslink and monoalkylate DNA. Here we use a synthetic photochemically activated derivative of FR400482 to investigate the molecular mechanism of this class of drugs in a biologically relevant context. We find that the organization of DNA into nucleosomes effectively protects it against drug-mediated crosslinking, while permitting mono-alkylation. This modification has the potential to form covalent crosslinks between chromatin-associated proteins and nucleosomes. Using *in vitro* approaches, we found that interstrand crosslinking of free DNA results in a significant decrease in basal and activated transcription. Finally, crosslinked plasmid DNA is inefficiently assembled into chromatin. Our studies suggest new pathways for the clinical effectiveness of this class of reagents.

2.2 INTRODUCTION

Many anticancer agents act by impeding rapid proliferation that is characteristic of cancer cells. While some impact cytoskeletal dynamics and cell-signaling pathways, others affect basic cellular processes such as replication and transcription. Compounds that fall into the latter class include interstrand DNA crosslinking / DNA alkylating agents. DNA crosslinking affects DNA-related processes specifically via the formation of covalent bonds between both DNA strands. This is a potent drug-mediated modification associated with severe cytotoxicity. The detailed effects of drug-mediated DNA alkylation on cell proliferation are yet to be determined, since such lesions are likely to be removed and repaired via DNA base-excision repair mechanisms (18,19).

Bioreductive alkylating agents include families of bifunctional compounds that are capable of forming monoalkylated DNA and interstrand DNA crosslinks under highly reducing conditions. The specific targeting of these drugs to cancer cells has been rationalized by their ability to be activated under the hypoxic conditions that prevails in cancer cells as a result of their high replication rate (20). A representative clinically significant drug is Mitomycin C (MMC, **1**; Figure 1A) (7). MMC is the most thoroughly studied member of this class of compounds and has been in clinical use for over thirty years as an antitumor agent (5,21,22). FR900482 (**2**, Figure 1A), a natural metabolite obtained along with FR66979 (**3**, Figure 1A) from *Streptomyces sandaensis* No. 6897, is structurally and functionally related to MMC (23,24) but was dropped from clinical development in Phase I studies due to the development of vascular leak syndrome in patients.

More recently, a semi-synthetic derivative FK317 has exhibited promising antitumor activity (24-29) and has advanced from Phase I to Phase II human clinical trials. FK317 (**4**, Figure 1A) shares structural similarities and properties with FR900482 (**2**, Figure 1A), but exhibited fewer side effects, in particular with respect to vascular leak syndrome, when compared to FR900482 (10,25-29).

MMC can be activated *via* a one-electron or two-electron reduction pathway to form a highly reactive bis-electrophilic mitosene species that is capable of both mono-alkylating and crosslinking DNA. In contrast, FR900482 and FK317 are activated specifically by a two-electron reduction pathway to form a structurally and functionally related bis-electrophilic mitosene species that is likewise capable of mono-alkylating and crosslinking DNA. In all three instances, it has been demonstrated that mitosenes preferentially crosslink B-form DNA at 5'CpG3' steps in the minor groove (5,6,10). Mitosene formation appears to be the rate-limiting step in the formation of the final drug-mediated lesion (2). The solution structure of mono-alkylated DNA indicates that the mono-adduct represents an intermediate species in a reaction that finally results in the formation of an interstrand crosslinked product (3,30,31). Recently a new generation of synthetic mitosene progenitors based on FR900482 that can be activated with alternative chemical signals not requiring reductive activation (11) was reported. These agents can potentially obviate the slow generation of the mitosene, and also allow for controlled release of these highly reactive species. In particular, the totally synthetic NVOC-derivative related to FR900482 (**5**, Figure 1A) is activated photochemically and exhibits biochemical reactivity similar to FK317 (11)

including the characteristic 5'CpG3' sequence specificity for interstrand crosslinking.

The striking preference of all mitosene-based drugs for crosslinking 5'CpG3' steps is thought to be due to the geometrical arrangement of the two electrophilic sites on the mitosene which closely aligns with the distance between the opposing dG residues at a 5'CpG3' step in B-form DNA (Figure 1B). This requirement has been shown to be less stringent for mono-alkylation (3,32). While the sequence specificity for both mono-alkylation and interstrand crosslinking was originally determined on free B-form DNA (16), the interactions of this class of drugs with DNA in the context of nucleosomes has not been studied in detail. This is a significant concern since ~ 80 % of all eukaryotic DNA is organized in nucleosomes. Nucleosomal DNA conformation deviates significantly from that of unassembled B-form DNA and as such, the identification of the covalent interactions of these drugs in an environment more closely resembling that of chromosomal DNA as packaged in the nucleus of living cells is particularly relevant. A previous study revealed a decrease in the levels of MMC-mediated interstrand crosslinking on nucleosomal DNA when compared to free DNA (33). However, MMC-mediated mono-alkylation on linear versus nucleosomal DNA could not be demonstrated conclusively. Furthermore, the effects of DNA crosslinking on transcription and chromatin assembly have not been investigated in detail.

Here we describe the effect of a photochemically activated NVOC-derivative (**5**; Figure 1A) on two distinct free and nucleosomal DNA templates that are both

146 base pairs in length. Apart from base composition, the templates differ in the number and location of 5'CpG3' steps (Figure 1B). We investigated the ability of **5** to crosslink or alkylate free and nucleosomal DNA. We observed a dramatic decrease in crosslinking of nucleosomal DNA and a commensurate increase in mono-alkylation. Compound **5** significantly inhibits *in vitro* transcription and nucleosome assembly. Our studies conclude that crosslinking of free DNA mediated by **5** may affect cellular proliferation by targeting two vital processes – chromatin assembly and transcription.

2.3 EXPERIMENTAL PROCEDURES

Drug stock solution

Compound **5** was prepared according to published procedures (11). A stock solution of 10 mg/ml (15.8 mM) of **5** was prepared in 100% DMSO and placed in a light-safe tube to prevent photo-decay. Appropriate dilutions were made in 100% DMSO.

Nucleosome preparation

The 146bp 5S and α -satellite DNA templates were prepared as mentioned in (34) and the corresponding nucleosomes were reconstituted using recombinant full length *Xenopus* histone octamer via salt dialysis as described earlier (35).

DNA crosslinking and alkaline agarose electrophoresis

The final volume of the crosslinking reaction was 20 μ l. The final concentration of free DNA (both 5S and α -satellite) in these reactions was 6.25 μ M, and 12.5 μ M for nucleosomal DNA. The samples were irradiated in clear Eppendorf tubes

at 25 °C for an hour with an ultraviolet lamp (Rayonet) containing 350 nm bulbs (11) (34), and incubated in the dark at 4 °C. Excess drug was removed from free DNA samples by ethanol precipitation. In order to remove excess drug and histones from compound **5**-treated nucleosomal samples, the 20 µl reaction mixture was treated with 5.2 µl of 4M NaCl, 4 µl of 20 mg/ml glycogen and 60 µl of 100% ethanol. The nucleosomes were then pelleted by spinning the samples at 13.2 K rpm for 30 minutes. Histones were removed by Proteinase K treatment in a volume of 100 µl containing a final concentration of 0.1 mg/ml of Proteinase K (Sigma-Aldrich). The samples were incubated at 37°C for at least an hour followed by phenol-chloroform extraction and ethanol precipitation. All samples (both nucleosomal and free DNA) were analyzed by 1.4% alkaline agarose electrophoresis (36). The gels were run at 75 volts for 50 to 55 minutes and stained with SyBr Gold (Invitrogen, Molecular Probes™). The appropriate bands were quantified using the Image Quant Analysis (version 5.1) software.

Analysis of mono-alkylation

Free and nucleosomal DNA samples were subjected to NVOC treatment, and DNA was isolated from nucleosomes as described above. 10µg of extracted DNA were radiolabeled at the 5' end with ATP using standard protocols in a final volume of 50 µl and in the presence of T4 polynucleotide kinase (NEB). The radiolabeled DNA was then subjected to phenol-chloroform extraction and ethanol precipitation to remove enzyme and excess radiolabel in the reaction mix. The resulting samples were analyzed by 8% PAGE in the presence of urea (34). The gel was first pre-run at 30 W for about 30 minutes (until the

temperature of the gel was monitored to be around 50 °C) and then run at 30 W for 40 minutes in 1XTBE buffer. The gel was dried and exposed to a Phosphorimager screen for 10 to 15 hours. The screen was then scanned and visualized using the Image Quant Analysis (version 5.1) software.

In vitro chromatin assembly

The p4TxRE/G-less plasmid template, native *Drosophila* core histones, recombinant ACF and dNAP1 were purified as described (37). The *in vitro* assemblies were performed as described in (37). The standard chromatin assembly reaction was 98 μ l and contained 2.1 μ g of plasmid DNA (0.994 pmoles of 3.2 kp plasmid DNA), 1.505 μ g of purified native *Drosophila* core histones (0.11 nmoles of each histone), 12.012 μ g of purified recombinant dNAP1 (0.2145 nmoles of dNAP1 monomer) and 0.36 μ g of purified recombinant *Drosophila* ACF (1.285 pmoles of ACF peptide), in 10 mM HEPES pH 7.6, 50 mM KCl, 5 mM MgCl₂, 5% glycerol, 1% PEG, 3 mM ATP, 0.01% NP40, an ATP-regenerating system (30 mM phosphocreatinine and 1 μ g/ml creatinine phosphokinase) and 140 ng BSA. The reaction was performed at 27 °C for 4-12 hours. Micrococcal nuclease digestion was performed as described (38).

Quantitative Agarose Gel Electrophoresis (QAGE)-Multigel Analysis

To determine the number of assembled nucleosomes, the average surface charge density of unassembled and assembled DNA template had to be quantitated (39,40). The mobility of the species (μ) was calculated as a function of the agarose concentration by electrophoresis performed on nine gels each of

different concentrations of agarose varying from 0.2-1.0%, embedded in a 1.5% agarose frame and run at 1 V/cm. The values of μ_o' (gel free mobility) and μ_o (μ_o' corrected for the electro osmotic effects of the buffer) were estimated as described (39,40). In this study the 18-lane template was used to run unassembled DNA with its corresponding assembled species in the same gel frame. Both the frame and running gel were cast in TAE buffer (40 mM Tris acetate, 1 mM EDTA pH 7.8) or E Buffer (40 mM Tris HCl, 0.25 mM EDTA pH 7.8) as indicated and the corresponding EEO (electroendosmosis) values were used to calculate μ_o . The assembly reaction containing 2.1 μg of assembled DNA along with 1 μg of intact T3 phage (migration standard) was loaded such that 0.23 μg of assembled DNA was present in each well. The same amount of supercoiled unassembled DNA was loaded along with the T3 control. The gels were run at room temperature (48 volts for 6 hours) with running buffer circulating for the duration of the experiment. With the μ_o values thus obtained for unassembled and assembled DNA templates, the number of assembled nucleosomes were calculated as reported (39,40).

The p4TxRE/G-less plasmid was treated with NVOC in a manner similar to that of unassembled DNA as mentioned previously in the same section and subjected to similar QAGE-Multigel analyses.

In vitro Transcription Assay

The *in vitro* transcription assay was carried out in a final reaction volume of 30 μl containing 1 mM acetyl CoA, 150 ng of DNA (treated or untreated as mentioned)

and 70 μg of CEM (HTLV-negative human T-cells). For activated transcription reactions the same conditions were used along with 100 ng of Tax and 100 ng of CREB. The reactions were incubated at 30°C for an hour. The samples were then incubated with 250 μM ATP, 250 μM CTP, 12 μM UTP and 0.8 μM [$\alpha^{32}\text{P}$] UTP (3,000 Ci/mmol) for 30 min at 30 °C. This allows for transcription through the 380-bp G-less cassette in the p4TxRE/G-less plasmid (41). The read-through transcripts were cleaved after treating these reactions with RNase T1 (100 units/reaction) at 37 °C for 30 minutes. RNase T1 is an endoribonuclease that specifically degrades single-stranded RNA at the G residues. This enzyme is therefore extremely useful for detection of RNA transcript levels from DNA templates containing the G-less cassette. The reaction was terminated by addition of 123 mM NaCl, 0.5% SDS and 2.5 mM EDTA, and the samples were subjected to Proteinase K treatment at 50 °C for 30 minutes. The transcripts were then extracted *via* precipitation with a final concentration of 0.48 M ammonium acetate and 0.3 mg/ml of carrier tRNA. In this step an appropriate amount of radiolabeled DNA fragment was added as a recovery standard. The precipitated samples were analyzed on a urea-6.5% polyacrylamide gel. The gel was subsequently dried and visualized by Image Quant Analysis (version 5.1). The software was used to quantitate the transcript yields under the various conditions indicated. The transcript levels in each lane were normalized against the recovery standard (internal control). The highest signal (due to activation with Tax and CREB) was assigned the number 1 and all the other normalized transcript levels were then represented as fractions of the highest value.

2.4 RESULTS

2.4.1 Nucleosomal DNA is crosslinked inefficiently by compound **5** compared to free DNA.

The preference of mitosene-based drugs for 5'CpG3' dinucleotide steps results from the favorable geometric arrangement of the electrophilic sites of the drug and the target sites on linear B-form DNA (Figure 1B). Nucleosomal DNA, although still classified as B-form, is distorted compared to unassembled DNA due to the high degree of bending upon superhelix formation (16). To test the effect of this distortion on the efficiency of crosslinking, we compared two different 146 base pair DNA sequences in the context of highly positioned nucleosomes; a palindromic DNA fragment derived from human α -satellite DNA and an asymmetric fragment derived from the *Xenopus laevis* 5S rRNA gene. While the former has been used routinely to generate homogenous nucleosome species mainly for crystallization purposes (35) the latter has been used extensively for biochemical analyses. The two sequences differ significantly in the number and location of 5'CpG3' steps (Figure 3).

Free DNA and assembled nucleosomes (5S and α -sat nucleosomes) that had been separated from any remaining free DNA by preparative gel electrophoresis were treated with **5** and analyzed by native PAGE (Figure 4A & B). Even at a 60-fold molar excess of **5**, nucleosomes remained intact and exhibited no release of free DNA. DNA was isolated from nucleosomes, and the degree of crosslinking in free and nucleosomal DNA was analyzed by alkaline

agarose electrophoresis (Figure 4C-F). The percentage of crosslinks as a function of molar excess of drug is plotted in Figure 4G. As expected from the differences in the number of 5'CpG3' sites on α -sat DNA compared to 5S DNA (1 versus 9 in each 146 bp DNA fragment, Figure 3), free 5S DNA is crosslinked much more efficiently than free α -sat DNA (Figure 4C versus 4D respectively). In both cases, the level of crosslinking is reduced significantly in nucleosomes (Figure 4E & 4F for 5S nucleosome and α -sat nucleosome respectively), indicating that the inherent distortions in nucleosomal DNA and the partial protection by histones inhibit the formation of interstrand crosslinks.

2.4.2 Compound 5-mediated preferential monoalkylation of nucleosomal DNA compared to unassembled DNA.

Alkaline agarose gel electrophoresis allows us to distinguish between crosslinked and uncrosslinked species, but does not possess the resolution to visualize mono-alkylation. In contrast, denaturing PAGE allows for good resolution of the unmodified single-stranded DNA, monoalkylated single-stranded DNA, and crosslinked DNA strands. Figure 5A shows the analysis for free and nucleosomal α -satellite DNA. A crosslinked DNA control, purified from a denaturing gel, was loaded as a control (Figure 5A, lane 2). Even though the α -sat DNA template has only one 5'CpG3' site (Figure 3), two positional crosslinked isomers were identified as indicated in Figure 5A. These isomers are formed due to the difference in orientation of the reactive mitosene residue in the 5'CpG3' step, which is largely dependent on which of the reactive centers on the mitosene moiety reacts with the exocyclic N2 amine on guanosine (6). The nucleosomal

(A)

5S DNA

ATCCAGGGATTATAAGCCGATGACGTCATAACATCCCTGACCCCTTAAATAGC
TTAACTTTTCATCAAGCAAGAGCCTACGACCATACCATGCTGAATATACCGGTTT
TCGTCCGATCACCGAACTGAACGAGCATAGGGCTCGT

Alpha-satellite DNA

ATCAATATCCACCTGCAGATTCTACCAAAAGTGTATTTGGAAACTGCTCCATCAA
AAGGCATGTTTCAGCTGAATTCCGCTGAACATGCCTTTTGATGGAGCAGTTTCCA
AATACACTTTTGGTAGAATCTGCAGGTGGATATTGAT

(B)

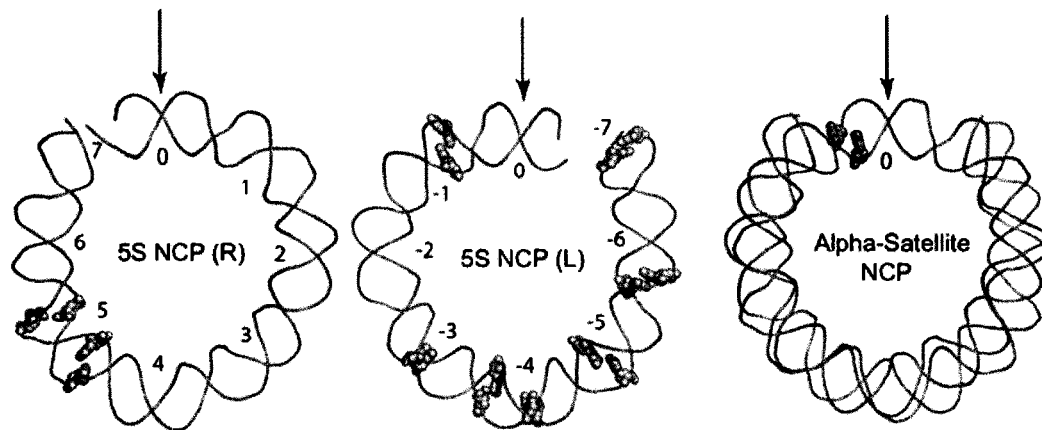


Figure 3: The two DNA fragments differ in the number and location of 5'CpG3' dinucleotide steps. (A) Sequence of the two DNA fragments under investigation. The asymmetric 5S DNA template contains nine 5'CpG3' steps highlighted (pink), the palindromic alpha-satellite DNA contains a single 5'CpG3' step (green).

(B) Representation of target site in a structural context. The left and middle panels represent the two halves of the 5S DNA (5S nucleosome (R) and (L) respectively), with the dyad indicated as 0. The numbers $\pm 1-7$ represents the superhelical axis location (SHL) of nucleosomal DNA. Since the structure of the 5S nucleosome is not known, we show a projection of the target sites onto the structure of the α -sat nucleosome as a model. The right-most panel is a graphical representation of the NVOC target site on α -satellite nucleosomal DNA. The arrows indicate the location of the symmetry dyad.

Figure 4

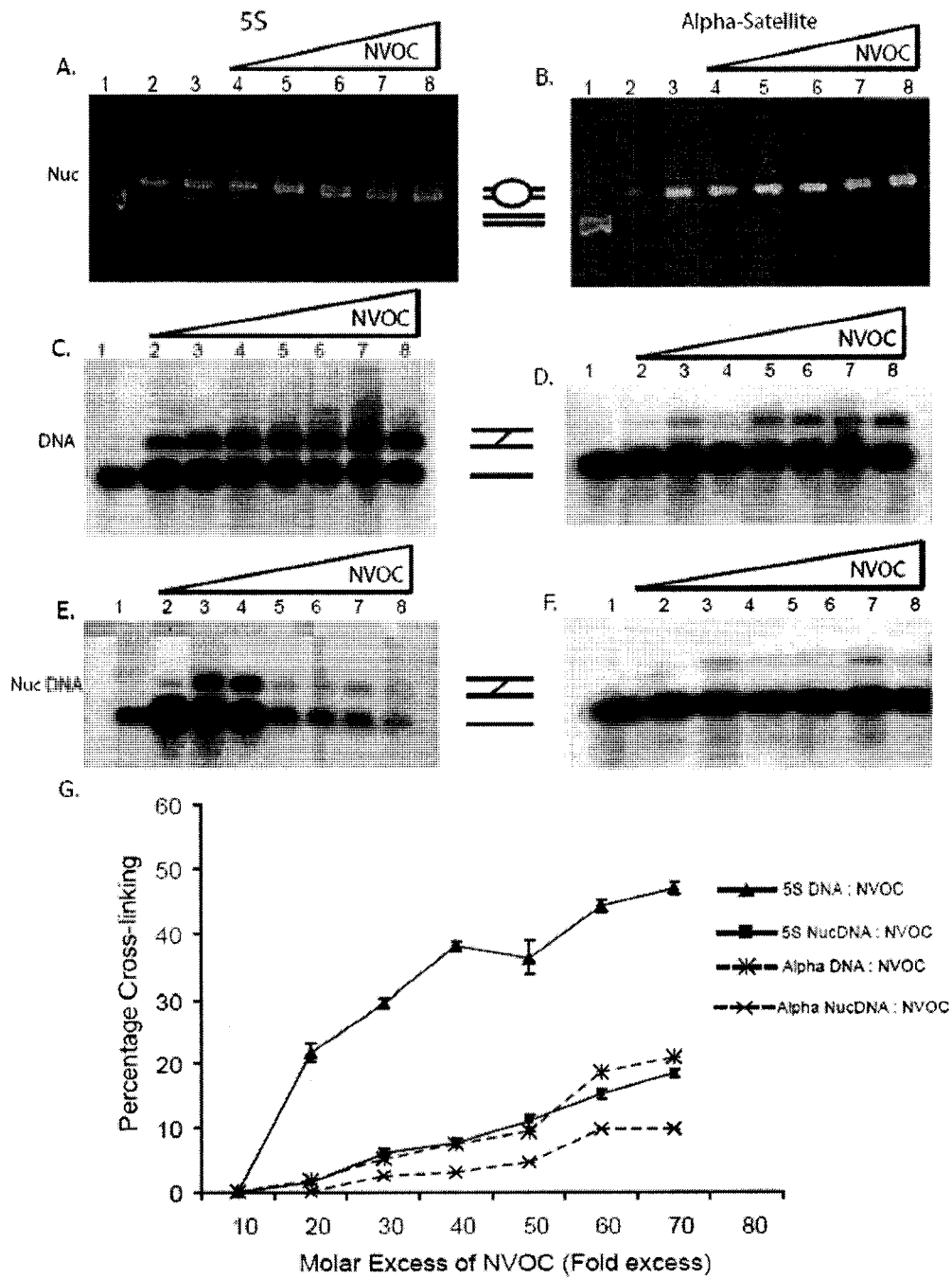


Figure 4: Reduced crosslinking mediated by the NVOC-derivative 5 on nucleosomal DNA. Panels (A) and (B) represent nucleosomes reconstituted with 5S DNA respectively, treated with increasing molar ratios of NVOC. The samples were analyzed on a 5% native PAGE gel stained with ethidium bromide to determine any appearance of free DNA due to NVOC-induced nucleosome dissociation. Lane 1 in panel A and B indicate free DNA while lane 2 in both panels shows nucleosome controls without the drug. Lane 3 shows nucleosome treated with UV radiation without the drug, while lanes 4-8 show a 1:1, 1:10, 1:20, 1:40 and 1:60 ratios of nucleosome to NVOC, in both panels. Panels (C) and (D) show denaturing alkaline agarose gels of 5S and α -sat DNA treated with increasing ratios of NVOC. Lane 1 in both panels shows untreated DNA, while the DNA in lanes 2-8 was treated with 1:1, 1:5, 1:10, 1:20, 1:40, 1:60 and 1:80 molar ratios of NVOC. Panels (E) and (D) show denaturing alkaline agarose gels of 5S and α -sat nucleosomal DNA treated with increasing ratios of NVOC. Lane 1 in both panels represents untreated DNA, while lanes 2-8 represents a 1:1, 1:5, 1:10, 1:20, 1:40, 1:60 and 1:80 ratios of nucleosome to NVOC. The alkaline agarose gels were stained and visualized using Sybr Gold and the intensity of the crosslinked and uncrosslinked bands were determined using the ImageQuant v 5.1 software. (G) Graphical representation of the efficiency of NVOC-mediated crosslinking on DNA/nucleosomal α -satellite and 5S DNA. The efficiency of crosslinking was determined from the ratio of the intensity of the crosslinked band to the sum of the intensities of the crosslinked and uncrosslinked bands and values thus obtained were plotted as NVOC-mediated percentage crosslinking as a function of the fold excess of NVOC (over DNA/nucleosomal DNA).

template therefore appears to have a much higher abundance of the monoadduct than observed for free DNA, demonstrating that α -satellite nucleosomal DNA is preferentially monoalkylated. Since only a single mono-alkylated species is apparent, we suggest that the sequence preference for 5'CpG3' may be maintained in the context of the nucleosome even for mono-alkylation by **5**.

The same experiment was repeated with 5S DNA which contains nine (as opposed to one) 5'CpG3' sites. No significant mono-alkylated species were observed on free 5S DNA at a 40-fold molar excess of drug (Figure 5B, lane 3). Instead, we observed a family of multi-alkylated products whose migration rates are slower than the mono-adduct species but faster than the more prominent crosslinked species. Nucleosomal 5S DNA treated with similar amounts of **5** is predominantly multi-alkylated, whereas crosslinks are barely visible (Figure 5C, lanes 2 and 3). We conclude that the NVOC-derivative **5** is bifunctional and can cause both interstrand DNA crosslinking as well as alkylation. The outcome depends entirely on the conformational state of the DNA.

2.4.3 Compound 5-mediated crosslinking of unassembled DNA represses *in vitro* transcription.

Histones are transiently removed from DNA during transcription, often with the help of ATP-dependent chromatin remodeling factors and perhaps also histone chaperones (42,43). This generates a window of opportunity for efficient crosslinking of nucleosome-free DNA by mitosene-based drugs. To investigate

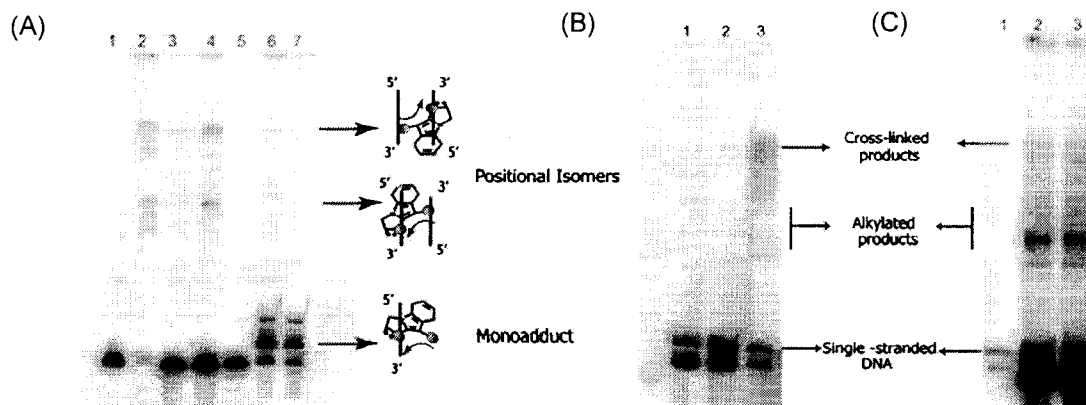


Figure 5: Preferential NVOC-mediated mono-alkylation of nucleosomal DNA compared to linear DNA. Urea-8% polyacrylamide gel (8%DPAGE) analysis was conducted on [γ^{32} -P] ATP labeled nucleosomal and free DNA. (A) DPAGE analysis on NVOC-treated α -sat DNA/nucleosomal DNA. Lane 1: α -sat DNA, lane 2: Crosslinked α -sat DNA control. The two different orientation isomers are illustrated at the side of the gel. Lane 3 and 4: α -sat-DNA treated with a 20- and 40-fold molar excess respectively of NVOC to DNA. Lane 5: Nucleosomal α -sat-DNA treated with proteinase K; lane 6 and 7: Nucleosomal DNA treated with 20- and 40-fold molar excess of NVOC respectively. (B) DPAGE analysis of free 5S DNA. Lane 1: 5S DNA. The two bands correspond to the difference in charge and hence migration of the two complimentary strands of 5S DNA. Lanes 2 and 3: 5S DNA treated with 20- and 40-fold molar excess of NVOC respectively. (C) DPAGE analysis of 5S nucleosomal DNA. Lane 1: Nucleosomal 5S DNA treated with proteinase K, lane 2 and 3: Nucleosomal 5S DNA treated with 20 and 40 molar excess of NVOC respectively. The concentration of DNA used in these reactions was 6.25 μ M, and that of the nucleosomes was 12.5 μ M.

the effect of crosslinking on basal and activated transcription, we employed a previously established *in vitro* system (37,41) that utilizes a well-characterized plasmid template (p4TxRE/G-less). The plasmid contains 178 5' CpG3' dinucleotide steps that are distributed quite uniformly along its entire length, with the exception of the 380-bp long G-less cassette. We made use of an *in vitro* assembly system consisting of purified assembly factors, which recapitulates many aspects of *in vivo* chromatin assembly (37).

Transcript levels were monitored under basal and activated conditions in the absence and presence of the co-activators Tax and CREB (44). Under both conditions the crosslinked template showed a significant reduction in transcription levels when compared to a control that had not been photo-activated by light. Figure 6B is a quantitative representation of the data shown in Figure 6A. Basal transcript levels from crosslinked DNA template decreased 5 - fold compared to untreated template. Activated transcript levels dropped 25 -fold when compared to the transcript levels of the inactive-NVOC reaction.

2.4.4 Compound 5-mediated crosslinking of plasmid DNA reduces efficiency of chromatin assembly.

Mitosene-based drugs are particularly effective in rapidly dividing cancer cells where DNA synthesis and concomitant chromatin assembly are frequent events. We therefore wanted to quantify the effect of DNA crosslinking and alkylation on the efficiency of *in vitro* chromatin assembly. The same p4TxRE/G-less templates (untreated and treated with compound **5**) that were used for the *in vitro*

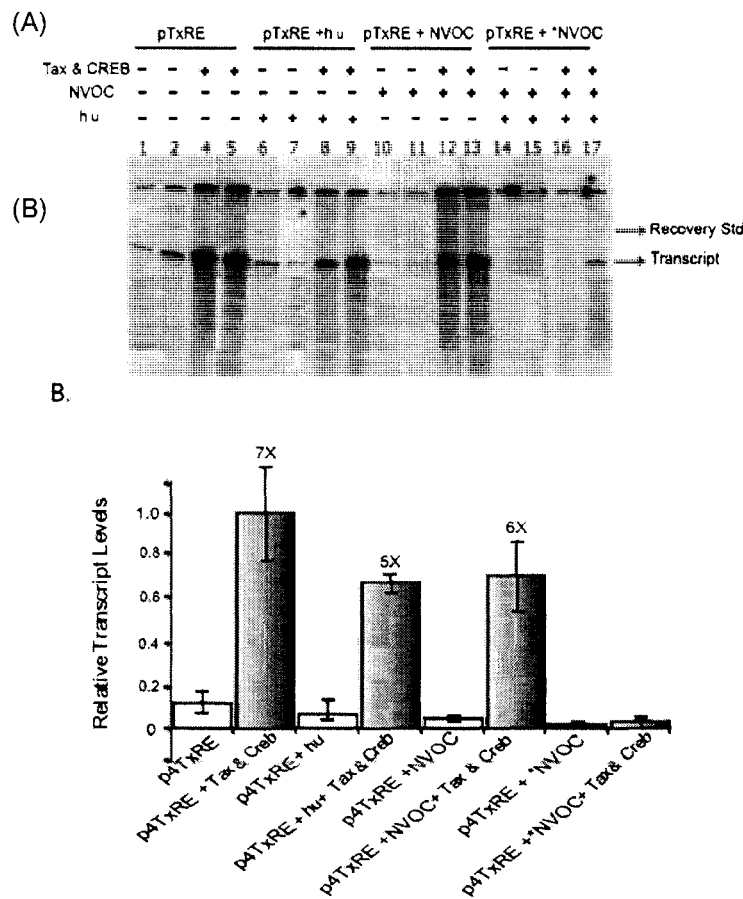


Figure 6: Decreased levels of *in vitro* transcription from crosslinked DNA templates. (A) *In vitro* transcription assay indicating a decrease in transcript levels only in the presence of NVOC-mediated crosslinked product. * indicates activated NVOC. Each transcription reaction contains 150ng of the p4TxRE template and 60 μ g of the nuclear extract- CEM from HTLV-negative human T cell line. 100ng of the purified recombinant Tax and 100ng of purified recombinant CREB were added to the reaction where indicated. (B) Quantitation of the transcript levels was done using ImageQuant.

transcription assay above were employed for this assay.

The plasmid was treated with a 40-fold molar excess of compound **5** prior to assembly to ensure complete saturation of all available sites. Crosslinking was verified by linearizing the plasmid, followed by analysis by alkaline gel electrophoresis (data not shown). Crosslinked plasmid was purified from unreacted DNA and free **5** by gel elution under native conditions, exploiting the fact that crosslinked plasmid exhibits a slower electrophoretic mobility than untreated plasmid (data not shown). Untreated and **5**-treated supercoiled plasmids were assembled into chromatin using the purified chromatin remodeling factor ACF1 and the histone chaperone dNAP1 (45). The assemblies were assayed by micrococcal nuclease digestion and quantitative agarose gel electrophoresis-multigel analysis. Micrococcal nuclease (MNase) digestion confirmed that the nucleosomes reconstituted onto untreated DNA template are spaced on average 165-170 bp apart (Figure 7A, lanes 2-5). Interestingly, chromatin assembled on **5**-treated plasmid DNA was resistant towards digestion with MNase, whereas no effect was found if the plasmid was treated with light in the absence of **5**. A DNA band corresponding to mononucleosomes was visible only at the highest MNase concentrations (Figure 7A lane 15). This could be due to the fact that crosslinked DNA is a poor substrate for most nucleases (45). This was addressed in a control experiment in which the effect of **5** treatment on the sensitivity of unassembled plasmid DNA towards digestion with MNase was assayed (Figure 7A, right panel). Whereas untreated DNA is digested rapidly

and completely, crosslinked plasmid DNA exhibited increased resistance towards digestion.

The results shown in Figure 7A raise the possibility that chromatin assembly is inefficient on a crosslinked DNA template. To further investigate this, we used Quantitative Agarose Gel Electrophoresis - Multigel Analysis (QAGE), a method which has been used successfully in the past for the analysis of chromatin to determine parameters such as average surface charge density and particle deformability (39,40). More precisely, this method allows us to quantitate the average surface charge density of unassembled DNA and assembled DNA, thus effectively 'counting' the number of nucleosomes on any given DNA fragment. The same analysis was also performed with the free DNA sample. A typical example is shown in Figure 7B. Ferguson plots (semi logarithmic plots of migration distance μ versus agarose percentage; Figure 7C) allow for the determination of μ_0 and μ_0' . The μ_0' values for all the species in Figure 7 are listed in Table 1. Crosslinked DNA species and the untreated DNA species do not vary significantly in their μ_0' values. This demonstrates that there is no difference in surface charge densities in the free DNA upon treatment with compound **5**. This not only validates the technique but also establishes the fact that any change in nucleosome assembly on the **5**-treated and untreated with compound **5**. This not only validates the technique but also establishes the fact that any change in nucleosome assembly on the **5**-treated and untreated plasmid is not associated with charge.

Figure 7

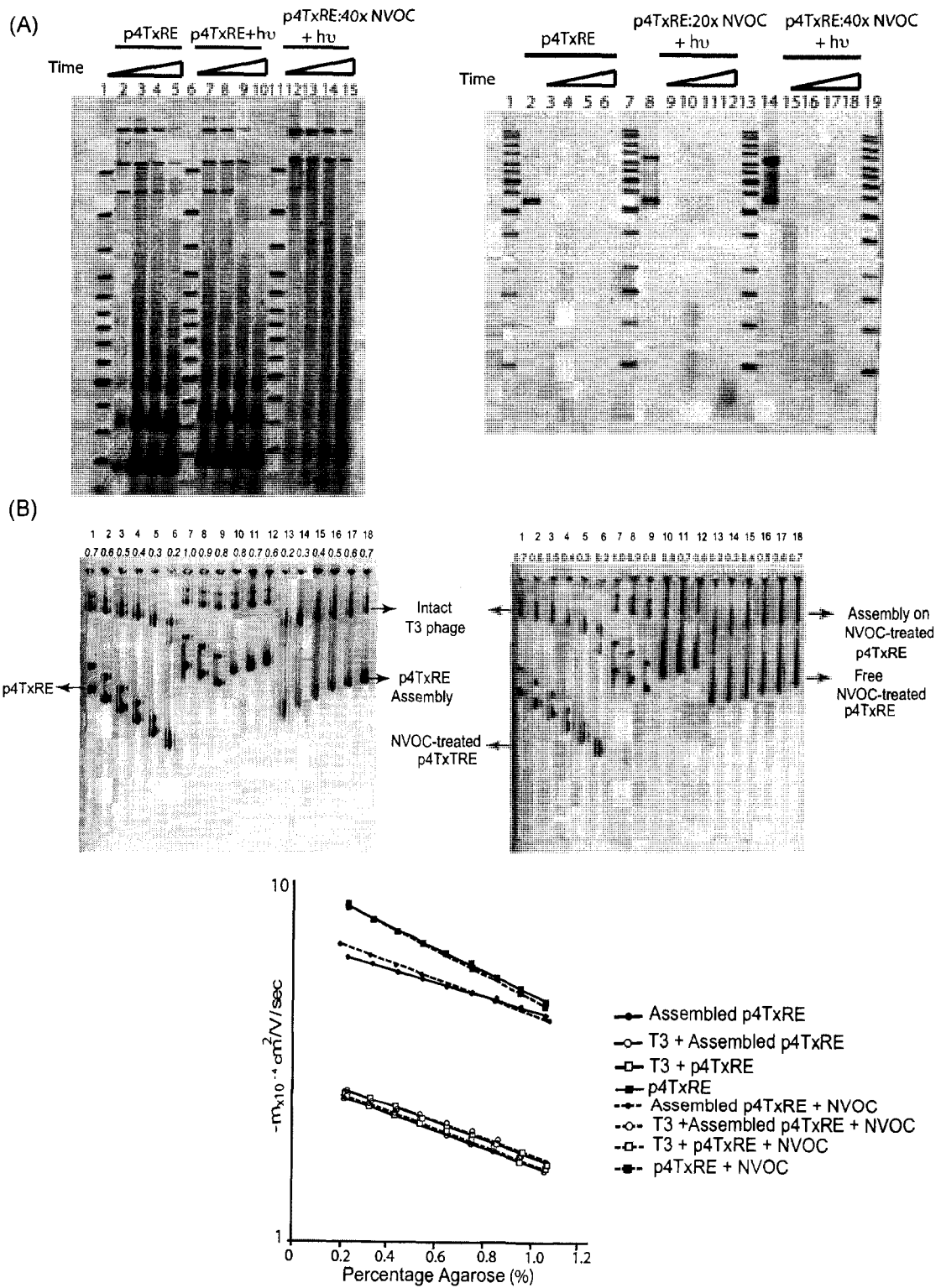


Figure 7: Crosslinking of DNA affects the efficiency of chromatin assembly. (A)

Qualitative analysis of the assembled template by micrococcal nuclease digestion. The various templates used in these analyses are indicated above the lanes. The left panel represents the micrococcal nuclease digestion on chromatin templates at different time points (1, 2, 4 and 8 minutes, respectively). The right panel represents the micrococcal nuclease digestion analyses on untreated and NVOC-treated p4TxRE. Lanes 2, 8 and 14 represent untreated p4TxRE, p4TxRE treated with 20 molar excess NVOC and p4TxRE treated with 40-fold molar excess NVOC respectively. Lanes 3-6, 9-12 and 15-18 represent the digestion times of 0.5, 1, 2, and 4 minutes. (B) The right and left panels represent the QAGE analyses performed on untreated p4TxRE/assembled p4TxRE and NVOC-treated p4TxRE/ assembly with crosslinked p4TxRE respectively. The numbers over each lane indicates the agarose concentrations. (C) The QAGE results are represented quantitatively in a Ferguson Plot. The y-axis has been set to logarithmic scale. Intact T3 phage was used as a migration control as well as in determination of the unknown μ_0 value for unassembled and assembled DNA. The plot is first used to determine the gel-free mobility (μ_0'). The values obtained in these plots are listed in Table 1.

Table 1

Quantitative analysis of the data presented in Figure 7C. Number of nucleosomes were calculated as described in materials and methods. Experiments were repeated three times.

Samples	$\mu\text{c cm}^2 / \text{V/se c (x10}^{-4}\text{)}$ Surface Charge density	Number of Nucleosomes
p4TxRE/G-less	-2.27635	
Assembled p4TxRE/G-less	-1.6764	18.5 + 2
NVOC-treated p4TxRE/G-less	-2.47647	
Assembled NVOC-treated p4TxRE/G-less	-1.9661	14.5 + 1

The μ_0' values listed in Table I were used to calculate the number of nucleosomes assembled on the two templates(39,40). This analysis shows that an average of 18.5 nucleosomes is assembled on the untreated p4TxRE/G-less plasmid. On 3245 base pairs, this converts to a repeat length of 175 bp, a number that corresponds well to the repeat length established by MNase (Figure 7A, left panel). On crosslinked DNA, an average of 14.5 nucleosomes was assembled. This 22% reduction in the number of nucleosomes assembled on the 5-treated DNA template when compared to an untreated DNA template is reproducible and indicates that crosslinking indeed has an inhibitory effect on chromatin assembly under physiological conditions.

2.5 DISCUSSION

Bioreductive alkylating agents are an important class of anticancer drugs that act through their ability to covalently crosslink two strands of DNA, thus impeding DNA replication of rapidly dividing cancer cells. The synthetic NVOC derivative (5) is a photo-activated compound that generates in high chemical yield a doubly electrophilic mitosene species that is structurally and mechanistically homologous to the mitosenes generated by bioreductive activation of FK317, MMC and congeners. Here we showed that interstrand crosslinking of nucleosomal DNA by compound 5 is suppressed while at the same time, the extent of mono-alkylation markedly increases. Our finding that crosslinked DNA

is inefficiently transcribed and assembled into chromatin suggests additional mechanisms by which mitosene-based drugs display their cytotoxic effect.

It has been shown previously that the efficiency of MMC-induced crosslinking on nucleosomes was reduced compared to free DNA (33). In the present study we have significantly extended this finding by demonstrating the preferential formation of mono-alkylated over crosslinked products at the nucleosomal dyad. Nucleosomal DNA is distinct from unassembled DNA in its helical parameters (16). The exact geometry of each given CpG step depends on its rotational and translational position with respect to the histone octamer. By using nucleosomes assembled on α -satellite DNA, we have the opportunity to directly measure the distance between the reactive centers of the only CpG step that is located near the nucleosomal dyad (14). The distance measured between the two opposing exocyclic amine residues in the minor groove at this particular location in the nucleosome is 3.95Å, whereas the distance between the same reactive centers on unassembled B-form DNA is 3.4Å. This 0.5Å difference is significant in light of the estimated distances between reactive centers in other dinucleotides that are NOT crosslinked on B-form DNA. For example, the distance between the target sites in a GpG step is ~ 4.2Å and in a GpC step it is around 4.6Å.

Apparently, nucleosomal DNA is too structurally constrained to allow for mitosene-mediated interstrand crosslinking. Instead, monoalkylation at presumably the same site is observed. What then is the biological significance of mitosene-mediated alkylation of nucleosomal DNA? Alkylation has been considered a less cytotoxic modification compared to interstrand DNA

crosslinking as it is easily corrected by the nucleotide base excision repair machinery (18,19). However, it remains to be investigated how efficiently this type of damage is repaired in the context of chromatin. Mono-alkylation has also been proposed as a suitable intermediate for the formation of crosslinks. Earlier studies have shown that congener FR66979 can cause protein-DNA crosslinks *via* drug-mediated mono-alkylation of DNA and the oncoprotein HMG A1 *in vitro* (46). Similar crosslinks were observed *in vivo* upon treatment with FR900482 and FK317 (47). This opens the interesting hypothesis that mono-alkylation of nucleosomal DNA, especially at the nucleosomal dyad, could result in the crosslinking of chromatin-associated protein to nucleosomal DNA, with far-reaching implications on chromatin dynamics and DNA accessibility.

About 80% of all eukaryotic DNA is organized in nucleosomes, leaving only parts of the linker DNA and the occasional highly active promoter histone-free. The processes of replication, transcription and DNA repair require transient exposure of DNA (48,49). This may represent a window of opportunity for mitosene-derived drugs to crosslink the two strands of DNA. This modification is likely to be refractory to all processes that require melting of the DNA double helix. Our studies show that basal as well as activated transcription from crosslinked DNA templates is severely impaired. This defect stems from the inability of the polymerase to initiate transcription, since the G-less cassette is free of crosslinks.

The potential effect of DNA crosslinking on chromatin assembly has largely been ignored in investigations of the mechanisms of mitosene-based cytotoxicity.

Using a defined *in vitro* assembly system, we found a 22% decrease in nucleosome occupancy on a crosslinked template. The majority of chromatin is assembled during S-phase, where the histones are deposited on the newly replicated DNA by Chromatin Assembly Factor-1 (CAF-1) (50). Suppression of the p60 subunit of CAF-1 by RNAi results in a slightly reduced efficiency of chromatin assembly (51). These cells exhibited cell cycle arrest and programmed cell death. Thus, it appears that a relatively small decrease in assembly could be a sufficient signal to induce cell-cycle arrest in the S-phase, especially in rapidly dividing cells. Since post-transcriptional chromatin assembly is also a key process for quiescent cells, it is possible that mitosenes may be toxic for non-dividing cells through these mechanisms.

These studies reveal new and hitherto unresolved possible mechanisms for how mitosene-based anti-tumor agents may exert their cytotoxic effect in rapidly proliferating cells. We are continuing to study the molecular interactions of such agents in the context of dynamic processes of chromatin assembly and there remains the possibility for the formation of additional covalencies between the DNA-bound drug and histones as well as other proteins closely associated with the complex processes of replication and transcription.

2.6 ACKNOWLEDGEMENTS

This work was done in collaboration with Dr. Robert. M. Williams' Lab in the Chemistry Department at Colorado State University. I would like to thank Drs. Konesky, Lu, Nyborg and Stargell for guidance and reagents, and P. N. Dyer for help with histone and DNA preparation. I would also like to thank Fujisawa Pharmaceutical Co. (now Astellas) for the generous gift of FK317. I would like to thank Dr. Williams and his post doctorate student Dr. Pascal Ducept for their help, support and input.

2.7 SUPPLEMENTARY DATA

2.7.1 Drug-induced protein DNA crosslinks

Since the mitosene-based agents demonstrated a higher propensity to mono-alkylate nucleosomal DNA than B-form DNA, we decided to investigate the possibility of histone-DNA crosslinks mediated by the mono-alkylated nucleosomal DNA adducts. We believed that this might be a possibility largely due to the presence of the nucleophilic arginine residues of the histone octamer to the minor groove of the nucleosomal DNA. If intranucleosomal drug-mediated crosslink does indeed take place, this could cause the nucleosome to be in lock-down and resist any cellular mechanism that involved nucleosome dynamics (replication, transcription, DNA repair etc.). In an attempt to answer this question, we looked at two methods that would give us an indication of intra-nucleosomal crosslink's: tyrosine quenching assay and high salt nucleosome dissociation with labeled octamer components.

a) Tyrosine quenching assay

This assay is a simple spectroscopic technique that allows for the investigation of the physical and chemical properties of DNA-histone interactions without any histone labeling (52,53). The technique is based on the efficiency of fluorescence quenching by energy transfer between the tyrosine residues present in the histones and the DNA bases in a nucleosome. Since nucleosome stability decreases with increasing salt concentration due to the subsequent decrease in the electrostatic interactions between histones and DNA, this technique allows for the analysis of nucleosome stability under similar conditions (52,53).

According to Oohara and colleagues, nucleosomes subjected to high salt undergo dissociation in three transitions: at 0.55M NaCl they undergo unidentifiable structural changes (stage I), at 0.95M salt the H2A/H2B dimer dissociates from the nucleosome (stage II), and in the final stage at 1.45M salt where the H3/H4 tetramer dissociates (stage III). This method can therefore help in determining the transitional stage during nucleosome dissociation in crosslinked nucleosome that is stabilized as a function of salt concentration.

RESULTS

The characteristic tyrosine emission spectrum versus salt concentration in the context of nucleosomes is represented by a sigmoidal curve. At low salt, the nucleosomes are stable and hence the DNA bases quench the tyrosine emission. As the salt concentration increases, the DNA unwraps from around the histone core, and hence the intensity of tyrosine emission is increased (or less quenched by DNA bases). Stabilization of the nucleosome (in this case due to intranucleosomal crosslinks) results in the increase in tyrosine emission at higher salt concentration when compared to wild-type nucleosomes. Thus while the curve will remain sigmoidal for a “super stable” nucleosomes, it should show a shift to the right with respect to the wild-type nucleosome dissociation pattern. Figure 8 shows that the difference in emission pattern between untreated and treated nucleosomes may not be significant. The emission pattern of the 5S NVOC-treated nucleosomes overlaps with that of the untreated control (Figure 8A). This may be indicative of the absence of any *global* drug-mediated stabilization of the nucleosome. In the case of α -nucleosome however, a small

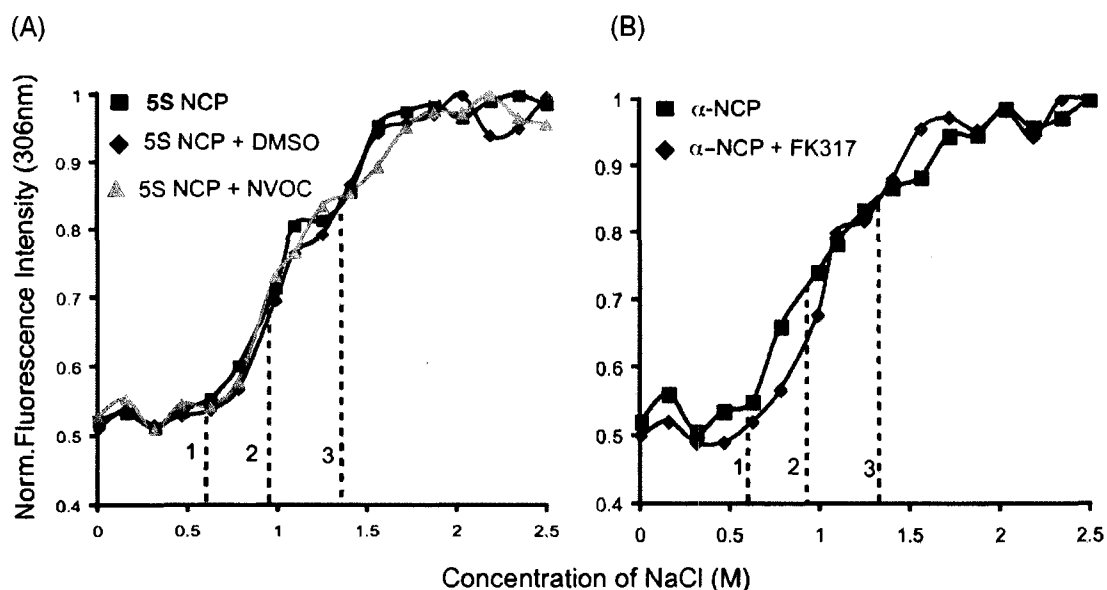


Figure 8: Tyrosine quenching experiments to determine difference in the stability of FK/NVOC treated nucleosomes due to possible protein DNA-crosslinks. The tyrosine emission intensity values were normalized and plotted as a function of salt concentration. The plots indicate dotted lines, which denote various stages of nucleosome dissociation at different salt concentrations. Stage 1 is associated with unidentifiable structural changes in the nucleosome at 0.55M NaCl. Stage 2 is characterized by H2A/H2B dissociation from the nucleosome at 0.95M NaCl and the final stage 3 is seen at 1.45M NaCl where the H3/H4 tetramer dissociated for the nucleosome. The comparison of these stages between treated and untreated nucleosomes provides an efficient method to determine the target of drug-mediated crosslinking. (A) Represents the tyrosine fluorescence plots for untreated and NVOC-treated 5S nucleosomes. (B) Represents the tyrosine fluorescence plots of untreated and FK317-treated α -satellite nucleosomes. These experiments were not repeated more than once.

difference was observed in the stage II of nucleosome dissociation, indicating that there might be increased resistance to H2A/H2B dimer dissociation in FK317-treated nucleosomes (Figure 8B).

b) Monitoring any local drug-mediated protein-DNA complexes using double-labeled octamer.

In order to establish the presence of *local* crosslinks, double-labeled octamers (Alexa Fluor® 488 –AF 488 [Molecular Probes] labeled H2BT112C and Alexa Fluor® 546-AF 546 [Molecular Probes] on H4T71C) were used to reconstitute nucleosomes. The double-labeled nucleosome was treated with 40-fold molar excess of the NVOC-derivative and subjected to UV activation for 30 min. The untreated and treated nucleosomes were then subjected to dialysis in 2M KCl overnight. Under high salt conditions, the nucleosomes dissociate completely and the presence of any crosslinked complexes can then be visualized and identified by virtue of the nature and presence of fluorescent tag (Figure 9A & B). In other words, one can discern if the covalently crosslinked complex contains dimer or tetramer components.

RESULTS

Figure 9A & B depicts the various possible conjugated DNA-protein adducts that can be monitored based on the fluorescent tag that is seen after high salt dialysis of the drug-treated nucleosomes. Figure 9C seems to suggest that

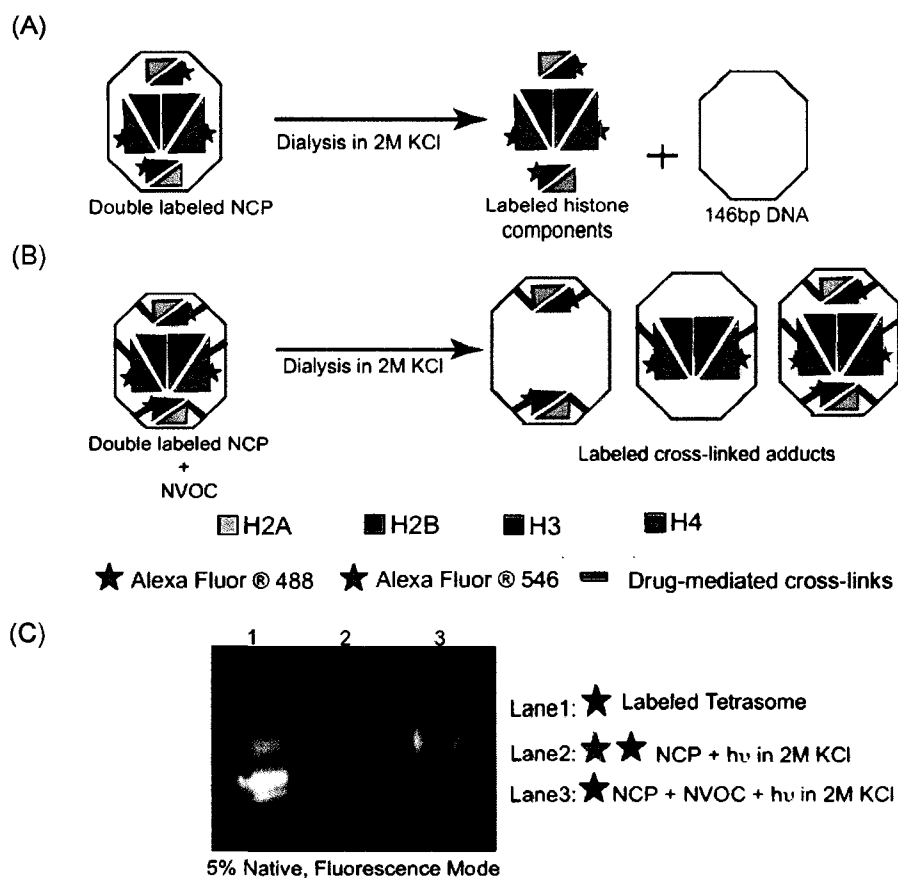


Figure 9: Identification of NVOC-mediated histone-DNA complex using dual-label octamer. (A) Schematic of the dissociation of doubly labeled nucleosomes in high salt resulting in the release of the histone components as well as the 146bp DNA. (B) Schematic of the NVOC- treated nucleosomes subjected to high-salt dissociation resulting in the release of protein-DNA complexes that can be identified by the nature of the fluorescent signal seen subsequent to high salt dialysis. (C) 5% Native gel viewed under fluorescent mode. Lane 1: Labeled tetrasomes. The red star indicates that the band was appeared red due to the AF546. Lane 2: nucleosomes subjected to UV without NVOC, no concrete fluorescence indicating complete dissociation. Lane 3: NVOC-treated nucleosome dissociation results in a species similar to a tetrasome with an AF546 signal.

dissociation of the NVOC-treated nucleosomes leaves behind a complex whose migration on a 5% Native PAGE is similar to that of a tetrasome. Further the fluorescent signal from this complex is characteristic of AF 546, a tag that was used to label H4 (a tetramer component). This could demonstrate the presence of a relatively stable NVOC-mediated tetramer-containing DNA-protein complex.

Thus while tyrosine quenching experiments did not reveal any significant *global* stability to 5S nucleosomes on treatment with NVOC, the dual-labeled octamer dissociation assay reveals otherwise. This contradiction, along with the fact that the distances between the histone arginines and exocyclic N2 of the guanine base measured in the nucleosome structure were all greater than the reactive distance of 3.4Å making histone-DNA crosslinks inconceivable, is further indication that the presence of protein-DNA crosslinks in nucleosomes, remains elusive. Further analysis is, however, required to confirm the formation of this crosslinked complex.

2.7.2 Alternative method for quantifying *in vitro* chromatin assembly

In an attempt to corroborate the multigel analysis, we decided to look at other methods that would allow confirmation of the quantity of nucleosomes assembled on a p4TxRE template (as mentioned earlier in Chapter 2). An AtomForce Microscope (AFM) was used for visualization (data shown) and quantitation (data not shown) of the *in vitro* chromatin assembly. AFM is a high-resolution scanning probe microscope that is capable of resolution in the nanometer range. The height of the various components during visualization is dependent to large extent on the diameter of the tip that probes the surface. Previous attempts at

visualizing nucleosomes using the AFM have been successful (54). However, in most cases the DNA template used for chromatin assembly is a 208-12mer DNA containing a highly positioning nucleosome sequence (54,55). In this study we use a random plasmid DNA sequence for assembly. It is important to note that the *in vitro* chromatin assembly used for AFM analysis is also used routinely for transcription assay. The quantitation of nucleosomes (using QAGE/Multigels) confirmed by AFM can therefore provide valuable information to subsequent transcription assays that may be performed with the same assembly template.

RESULTS

The images obtained in air for untreated and NVOC-treated p4TxRE plasmid DNA (Figure 10 A & B respectively) show that there might be some morphological difference between uncrosslinked and crosslinked DNA. The chromatin assembly was imaged on a GD-APTES surface, which not only tethers the nucleosomes to the mica surface, but also immobilizes the free dNAP1 and ACF1 proteins present in the *in vitro* assembly assay. These are seen as white spots in Figure 10C. The chromatin assembly is sparsely dispersed on the surface largely due to the low concentrations of these arrays in the reaction. The enlarged image in Figure 10D represents the best image we have obtained so far of the *in vitro* assembled chromatin. The height profile (not shown) did indicate the presence of 15-19 nucleosomes, however the close proximity of the nucleosomes on the template did not allow for accurate interpretation of data. In order to obtain discernable data we have to image subsaturated chromatin

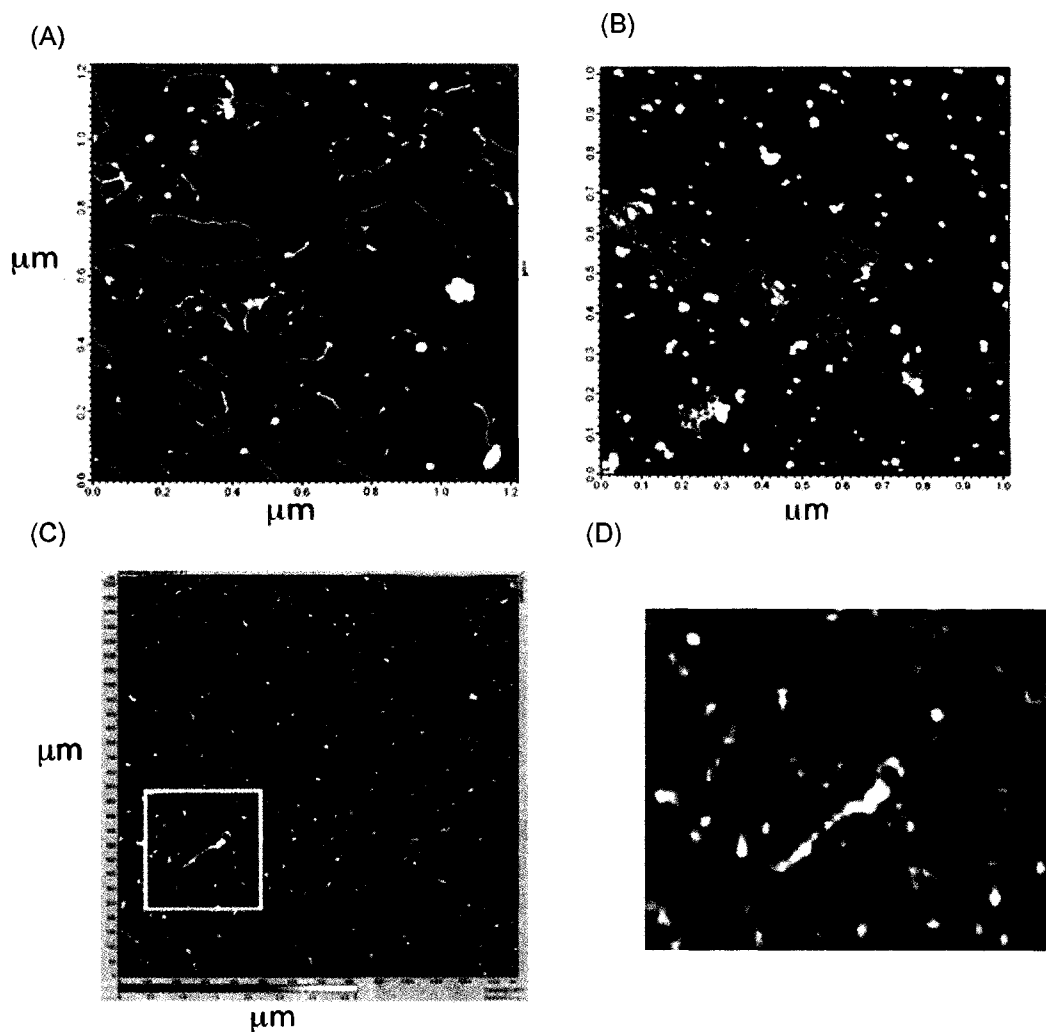


Figure 10: **Atomic Force Microscopy images of untreated, treated p4TxRE and assembled p4TxRE.** The surface used for DNA imaging in air was mica treated with nickel chloride. The surface used for chromatin assembly was mica treated with glutaraldehyde APTES. The concentration of DNA used in these scans was $1\mu\text{g/ml}$ and for the chromatin assembly the concentration of DNA was $2.1\mu\text{g/ml}$. (A) $1.2\mu\text{m} \times 1.2\mu\text{m}$ image scan of untreated p4TxRE. (B) $1.2\mu\text{m} \times 1.2\mu\text{m}$ image scan of NVOC-treated p4TxRE. (C) $1.35\mu\text{m} \times 1.35\mu\text{m}$ image scan of the in vitro chromatin assembly. (D) An enlarged image of the yellow highlighted box in panel C. Height profiles for the chromatin assembly indicated 15-19 nucleosomes occupying the plasmid template.

assemblies. AFM imaging along with multigel analysis will help us confirm quantitation of nucleosomes via two independent methods.

Unpublished 2D topology gel data in Dr. Paul Laybourn's Lab (Colorado State University, Fort Collins), shows that the same chromatin assembly (used for Multigel analysis and AFM) does indeed contain 18 nucleosomes. 2D topology gels are routinely used to determine efficiency of chromatin assembly (37,56) and are based on the principle that incorporation of a single nucleosome creates a negative supercoil on relaxed DNA. Thus by counting the number of negative supercoils one can determine the number of nucleosomes incorporated. We believe therefore that three independent methods confirm that p4TxRE can occupy 18 uniformly spaced nucleosomes (saturated assembly) when subjected to our *in vitro* chromatin assembly reaction.

2.7.3 Experimental Procedures

Preparation of 5S and alpha satellite nucleosome core particles

Purification of 146bp DNA (both palindromic α -satellite and 5S DNA): The 5S DNA derived from the 5S rRNA gene (57) as well as the α -satellite palindromic DNA and the individual recombinant *Xenopus* histones were purified as described in (34). The recombinant histones were then refolded to form octamers and subsequently used to reconstitute nucleosomes as described in (34). The nucleosomes were then heat shifted for 1 hr at 37°C and analyzed for their homogeneity and integrity by running these samples on 5% Native PAGE gels using 0.2X TBE as the running buffer (34). The use of recombinant histones,

purified DNA and heat shifting ensures a single stable nucleosome species in terms of positioning on the DNA.

Tyrosine Quenching Experiments

These fluorescence readings were made with the AVIV AT 105 spectrofluorometer (AVIV Instruments, Lakewood, NJ, USA) with temperature control. The temperature was maintained at 20°C. In these experiments 0.3µM nucleosomes were used in a final buffer volume of 125µl containing 20mM Tris-Cl pH 7.5, 1mM EDTA pH 8.0 and 1mM DTT, brought to a final concentration of 2.5M NaCl and maintained at 25°C. In case of drug-treated nucleosomes, the same concentration of NVOC-treated and FK317-treated nucleosomes was used. The nucleosomes were treated with 40-fold molar excess of the NVOC/FK317. This was based on the alkaline agarose gel results (Figure 4), which indicated substantial crosslinking at a 40 molar excess of the agents. Tyrosine fluorescence was measured at an emission wavelength of 306nm and an excitation wavelength of 275nm. The absolute values of emission signals were normalized using the formula $A_n = A/A_n$. A_n is the normalized value, A is the absolute value and A_n is the highest emission value. The normalized emission values were plotted against salt concentration for both the treated and untreated nucleosome substrates.

Preparation of fluorescently labeled octamer

Site-directed mutagenesis was conducted on the plasmid containing the full-length histone H2B and H4 to generate H2BT112C and H4T71C mutants. The recombinant *Xenopus laevis* full-length H2A and H3 as well as the mutant

histones generated above were purified as described in (34). The purified mutant histones were unfolded in 6M guanidinium hydrochloride and incubated at room temperature for 1 hr. The unfolded protein was quantified spectrophotometrically as mentioned in (34). The Alexa Fluors® are water-soluble dyes and are usually added at a 3-fold molar excess to histone concentration for a labeling efficiency of 90-95% (on histones) (unpublished data). An appropriate stock solution of these dyes is made in 50mM phosphate buffer at pH 7.0 and a suitable volume is added to the unfolded histones. This histone:dye solution is then incubated in the dark at room temperature overnight. All procedures from this step on are carried out in the dark. The overnight mixture is then cleared of excess fluorescent dye by applying the sample on a Superdex G25 resin column and using 6M guanidinium chloride as an elution buffer. The resulting labeled histones are then quantified and added in equimolar amounts with the other unlabeled histones for octamer refolding. The resulting labeled octamer was purified over a size-exclusion column and the corresponding 5S-DNA containing nucleosomes were reconstituted as described in (34). The nucleosomes were treated with 40-fold molar excess NVOC-derivative. The control included nucleosomes irradiated with UV in the absence of the drug.

Atomic Force Microscopy

The instrument used for liquid imaging of the chromatin assembly was Nanoscope III AFM (Digital Instruments) using a Si₃N₄ cantilever (Molecular Imaging). The plasmid DNA was imaged in air (dry imaging) using a Nanoscope III AFM (Digital Instruments). The surface chemistry for air imaging of plasmid

DNA involves incubation of the mica surface with 10mM NiCl₂ along with 20μl of treated/untreated DNA at a concentration of 1μg/ml for 15 min. The surface is then air dried with a steady stream of nitrogen gas. The assembly was prepared as described in (37) and Chapter 3 with untreated plasmid DNA template. The surface preparation for viewing chromatin assemblies *in situ* involved treating the mica surface with 0.1% glutaraldehyde in 99% APTES (aminopropyltriethoxysilane, Sigma Aldrich). The glutaraldehyde treatment tethers the chromatin to the mica surface and hence allows for convenient visualization of the assembly in liquid (58).

CHAPTER 3

X-RAY CRYSTALLOGRAPHY STUDIES OF THE NUCLEOSOME CORE PARTICLE IN COMPLEX WITH FK317 AND Acr1

3.1 ABSTRACT

The ambiguity surrounding the possibility of protein-DNA complex mediated by mitosene-based compounds led us to consider co-crystallization of the mitosene-derivatives with nucleosomes. The co-crystallization trials resulted in the determination of the structure of FK317 in complex with α -satellite nucleosome at 3.3Å. Based on the crystal statistics it remains questionable if the structure obtained is complete, but some aspects of the structure help explain the subtle changes observed in the tyrosine quenching experiments (Chapter 2) with α -satellite nucleosome and FK317.

We also attempted the co-crystallization of another sequence-specific pyrrole-imidazole polyamide intercalator (acridine) agent-Acr1 with nucleosomes. The crystallization attempts yielded a 3.0Å structure, which presented a single Acr1 molecule bound to nucleosomal DNA in the minor groove.

3.2 INTRODUCTION

3.2.1 Structural studies involving nucleosome-mitosene complexes

Previous structural studies with mitosene-based compounds and their substrate includes the structure of mono-alkylated mitomycin C (MMC) -DNA complex (5) and computational characterization of MMC-crosslinked DNA (59). In both these solution studies, Nuclear Magnetic Resonance (NMR) was used to resolve the structure of these complexes. The substrates used in these studies were deoxyoligonucleotides (8-9bp and 6bp respectively). In both cases, the MMC mitosene-residue was found to reside in the slightly widened minor groove in the 5'CpG3' step of the oligonucleotide. The structural analysis revealed that the specificity for crosslinking is largely due to the ability of the mitosene residue to sterically accommodate and orient the reactive residues with respect to the target sites. The less stringent requirement of 5'CpG3' during mono-alkylation is largely due to the hydrogen bond formed between the C'10 carbamate in the mitosene residue with the exocyclic amino group from deoxyguanine in the subsequent step. The solution structure of mono-alkylated MMC-DNA complex also revealed that the mitosene moiety is placed asymmetrically across the minor groove and the plane of the mitosene-residue was found stacked over the unmodified strand, with its face exposed to the solvent (3). DNA perturbations in the form of a 3.0Å base pair displacement towards the major groove as a result of MMC-minor groove binding were also observed in the same study.

Previous studies indicate no attempts were made to look at the structure of mitosene-based drugs in complex with nucleosomes. Based on the preliminary

results we obtained from the previous chapter, we attempted to co-crystallize α -satellite nucleosomes with FK317. FK317 was chosen for this purpose, since its treatment was less invasive when compared to the NVOC-derivative (UV irradiation in the dark at room temperature for 1 hr followed by incubation for at least 3 hr at room temperature before setting up crystal trays) and would allow for systematic, homogenous modification of nucleosomes. Results from such a co-crystal structure would help us determine the CpG-specific nature and the preferred mode of activity (crosslinking versus monoalkylation) of these drugs on conformationally distinct nucleosomal DNA.

3.2.2 Structural studies involving polyamide-nucleosome complexes

Pyrrole-imidazole polyamides are sequence-specific minor-groove binding agents. The design of these compounds was based on the same principle as that of sequence-specific DNA-binding proteins. In the case of proteins, the specificity is rendered largely by critical contacts between the amino acid side chains and the edges of the DNA bases. In the case of polyamides, the side-by-side pairing of pyrrole and imidazole groups allow for sequence selectivity and the curvature in these compounds aids suitable accommodation in the narrow minor groove (60,61).

Polyamides have been used previously to study the accessibility of nucleosomal DNA (62). The bivalent polyamide clamp was found to bind to the nucleosome “supergroove” and increase resistance to nucleosome dissociation on dilution (63). The same clamp was also used as a tool to trap intermediates of nucleosomal DNA dynamics (64). In most cases these agents result in moderate

structural distortions in nucleosomes, which includes increased minor groove width by 1.5-2.0Å and propagation of these distortions towards the free ends of DNA in the nucleosome (region free of histones) (62). As a result of their sequence selectivity, these agents can be used as ligands that compete for nucleosomal DNA interactions with proteins like sequence-specific transcription factors. There are two options by which this competition can be executed: first, by direct steric interference and, second by causing allosteric change in the structure of the DNA-binding site. Polyamides conjugated to intercalators like acridine are known to propagate allosteric inhibition of protein-DNA complex (65). This was mediated in a bimodal fashion; the polyamide portion of the ligand provides specificity in the binding of the conjugate, while the acridine moiety was found to cause proximal unwinding due to its ability to intercalate between DNA bases. Since the polyamides target minor grooves of DNA, the intercalating agent is poised to cause changes in the DNA structure that would potentially inhibit major-groove binding factors. The unwinding of the DNA proximal to the polyamide was monitored via quantitative DNase I footprinting analyses as well as topological gels (65).

In order to visualize the acridine-mediated structural changes in the major groove of nucleosomal DNA due to sequence-specific polyamide binding in the adjacent minor groove, we pursued attempts to co-crystallize the Acr1 conjugate with α -satellite nucleosomes. Results from this co-crystal structure will not only corroborate published biochemical data (65), but will help understand the effect of intercalating agents on nucleosomes. Typically, the nucleosomes are resistant

to intercalators (like psoralen) due to conformational incompatibility of the DNA, but the use of these conjugates provides a good platform to look at the effects of these agents on nucleosomal DNA.

3.3 EXPERIMENTAL PROCEDURES

Nucleosomes with 146bp alpha-satellite palindromic DNA (derived from the human α -satellite DNA) were prepared on a large scale and purified according to the methods described in (34). The concentrated nucleosomes were then mixed with 40-fold molar excess of activated drug (FR900482 and FK317) (in 90% DMSO as mentioned in Chapter 2) such that the final concentration of α -sat nucleosomes in the hanging drops were \sim 5.9mg/ml and in sitting drops was \sim 8.0mg/ml. In case of Acr1, a 20-fold molar excess of the drug was added. This drug does not require activation. The co-crystal trays were set up and incubated at 19°C. Crystals containing FK317 grew in 37.5mM KCl and 30mM MnCl₂, while those containing FR900482 grew in 27.5mM KCl and 40mM/45mM MnCl₂ (Figure 11 A-D). Co-crystals with Acr1 were found in conditions containing 35mM KCl and 42.5mM MnCl₂.

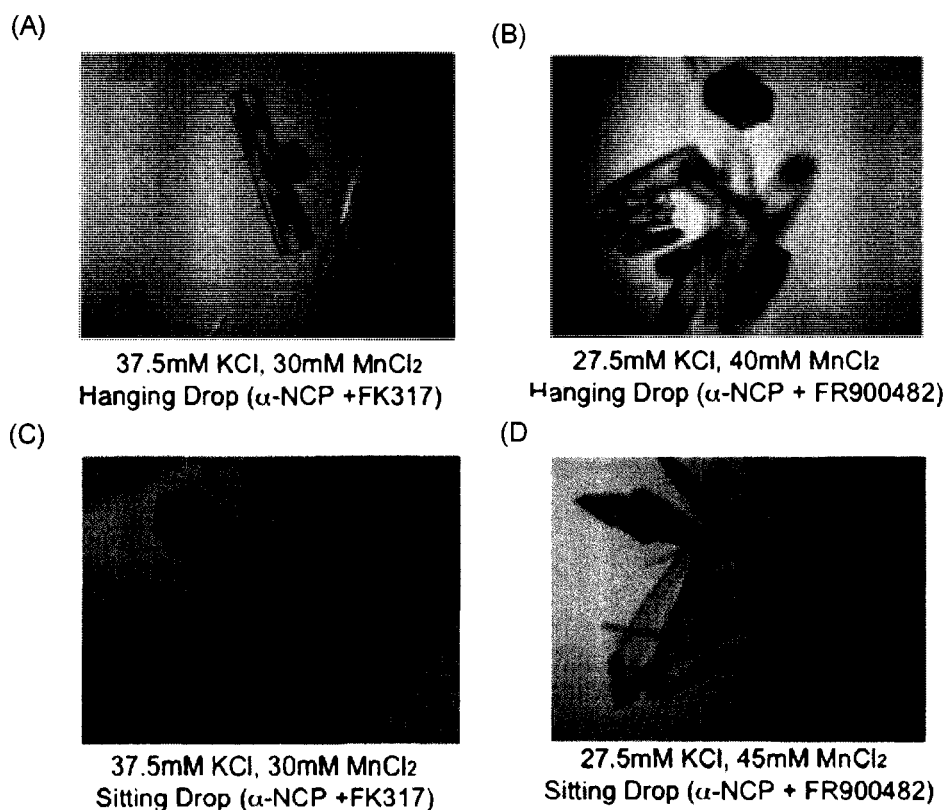


Figure 11: Crystallographic conditions for α -satellite nucleosome co-crystals with FK317 and FR900482. Initial screening conditions were identified for co-crystals α -satellite nucleosomes with FK317 and FR900482 via hanging drops and the same conditions were used to set up sitting drops. The concentration of nucleosomes used for hanging drop was \sim 5.9mg/ml and for sitting drops the concentration of nucleosomes used was \sim 8.0mg/ml. (A) & (C) represents a hanging and sitting drop containing co-crystals of α -satellite nucleosome treated with FK317, respectively. (B) & (D) represents a hanging and sitting drop containing co-crystals of α -satellite nucleosome treated with FR900482 respectively.

3.4 RESULTS

3.4.1 Structural analysis of FK317-nucleosome complex

The calculated difference density maps revealed the presence of an FK317 mitosene-moiety nestled in the minor groove of nucleosomal DNA (Figure 12 A,B & C). The orientation of the residue is similar to published studies, in that the mitosene residue appears stacked against one of the DNA strands (5,59). The mitosene-residue is asymmetrically placed in the minor groove of nucleosomal DNA, but it does not appear to be solvent-exposed. The location of the FK317 mitosene residue is adjacent to a 5'GpG3' also a known target site for intrastrand crosslinking mediated by the mitosene class of compounds (4). MMC-mediated intrastrand crosslinking is known to induce a 14.6° bend per lesion (4). Mitosene-based crosslinking reactions are known to result in covalent crosslinks mainly via the C1 and the C10 electrophilic groups. Figure 12 demonstrates that these reactive centers are not at the optimal distance and orientation for covalent binding. Moreover the distances between the other possible groups within the mitosene-moiety capable of crosslinks and DNA targets range from 2.3-3.8Å. These distances are larger than the optimal distance for covalent interactions (less than 2Å). Earlier studies revealed that FR900482 is capable of crosslinking a minor groove-binding protein HMG I/Y at the exocyclic nitrogen on guanine residue (within 2-3Å distance) (47). It was hypothesized that this interaction was via the C10 residue on the mitosene species and an adjacent arginine moiety. The nearest arginine in the structure was found to be at a distance of 6.05Å from H2B and hence incapable of covalent crosslinks with the mitosene moiety.

TABLE II

 α -sat nucleosome -FK317 co-crystal

<u>Data Collection</u>	
Space Group	P2 ₁ 2 ₁ 2 ₁
Unit Cell dimensions	a = 104.9, b = 109.0, c = 175.6
Resolution range	50-2.99Å
Unique Reflections	45991
Completeness % (Overall/Highest resolution bin)	92/80.1
R _{merge} (overall/ last shell)	0.051 / 0.488
<u>Refinement</u>	
Total number of atoms in the final model	12012
R-factor / R _{free}	0.2571/0.3243
Mosaicity	0.74
Resolution range Å	50- 3.3Å
B Factor (DNA/Protein)	112.751 / 36.172

TABLE III

 α -sat nucleosome -Acr1 co-crystal

<u>Data Collection</u>	
Space Group	P2 ₁ 2 ₁ 2 ₁
Unit Cell dimensions	a = 105.8, b = 109.35, c = 182.4
Resolution range	50-2.97Å
Unique Reflections	49270
Completeness % (Overall/Highest resolution bin)	96.1 / 93.4
R _{merge} (overall/ last shell)	0.07 / 0.47
<u>Refinement</u>	
Total number of atoms in the final model	12458
R-factor / R _{free}	0.2740/0.283
Mosaicity	0.810
Resolution range Å	20- 3.0Å
B Factor (DNA/Protein)	95.97 / 44.627

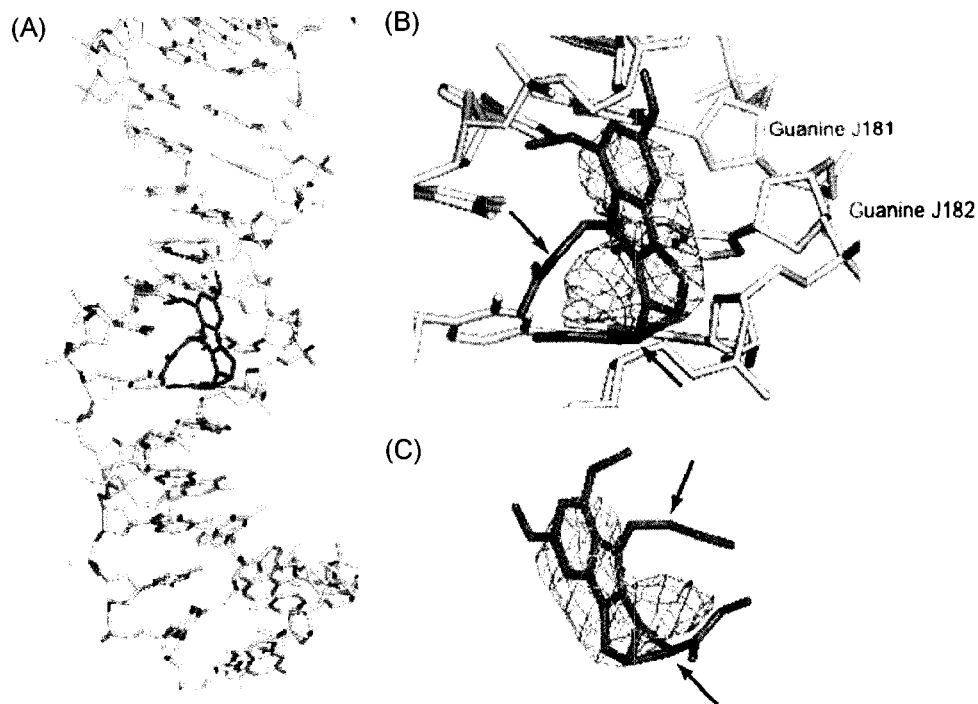


Figure 12: Co-crystal structure of FK317 with α -sat nucleosome after preliminary refinement. (A) Section of the co-crystal structure depicting nucleosomal DNA (in white) with the FK317 mitosene-moeity (green). (B) A closer view of the FK317-mitosene residue with the corresponding Fo-Fc difference density map (colored wheat). All the density maps for this structure were calculated at 3.3Å and the contour levels were set at 2.0. The DNA bases adjacent to the mitosene-residue are labeled along the sides of the J DNA chain. (C) The structure of the FK317-mitosene residue in the co-crystal structure with the difference density map. The arrows denote the position of the reactive centers within the mitosene-moeity.

The position of the mitosene-residue does not allow for favorable covalent interactions with any of the known target residues on DNA/protein (Figure 13). It is possible that the location of the residue is sustained by a series of hydrogen bond interactions with the DNA phosphodiester bond, since the target exocyclic N2 on guanines remain outside hydrogen bonding distance (3.05Å). It still remains unclear as to what the effect of the FK317 mitosene residue at this location has on the adjacent nucleosomal DNA structure (Figure 13). No critical change in DNA structure was observed in the vicinity of the drug. We are however still at the preliminary stages of refinement. Closer examination revealed that the aromatic mitosene species was placed at a distance of around 13-15Å from tyrosine residues in H2A and H2B. This observation may help explain the subtle change seen in the tyrosine-quenching profile of untreated and FK317-treated α -satellite nucleosome (Figure 8A). The latter indicated a shift in the tyrosine emission pattern particularly in the range of 0.55-0.75M NaCl (Figure 8A). The nucleosomes in this salt range are known to be devoid of the H2A/H2B dimer. Thus a shift in the tyrosine quench pattern towards the right (with respect to the wild-type) could be explained by the presence of the highly aromatic mitosene in the vicinity of the tyrosine residues, which could continue to quench tyrosine fluorescence subsequent to histone dimer removal (tyrosine-quenching can take place between 14-18Å of separation) (52,53). If this is the case, then the position of the reactive compound is indeed between the nucleosomal DNA and H2A/H2B dimer. We are however still unable to explain the nature of the interactions that the mitosene species makes with nucleosomal DNA as well as

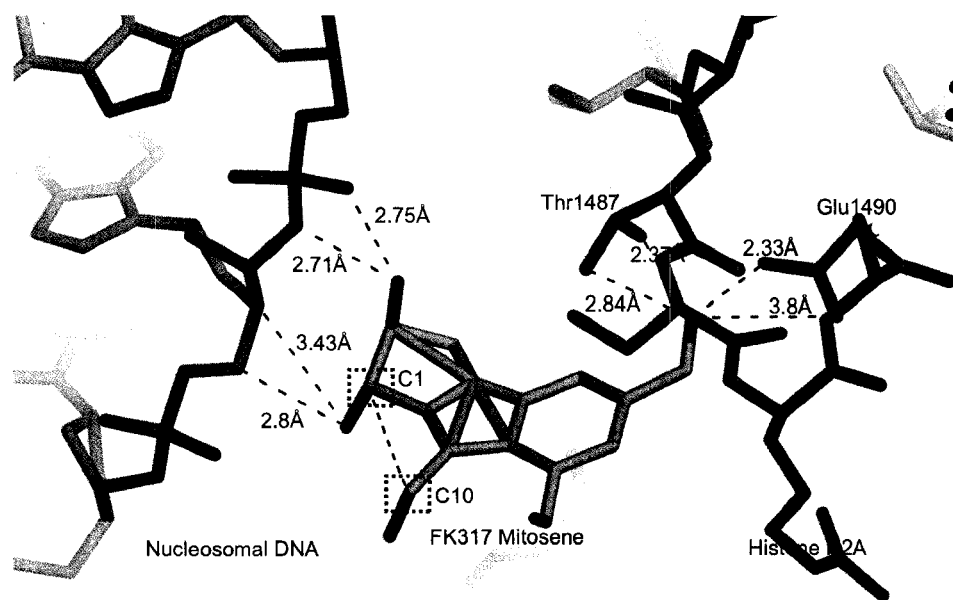


Figure 13: Representation of the possible H2B residues and DNA binding partners for the FK317 mitosene moiety. Nucleosomal DNA is represented in grey, the H2B residues are depicted in red and the FK317 mitosene moiety is represented in wheat. The reactive centers within the mitosene moiety C1 and C10 are indicated via dashed boxes. The color assignments for the individual atoms are as follows: pale red corresponds to oxygen, green corresponds to a carbon and magenta indicates nitrogen atoms. The blue dashes represent the distances between the various selected atoms.

its ability to stack adjacent to 5'GpG3' step. The electron density maps revealed a strong difference density peak adjacent to the first peak for the drug density. We suspected that there might be a chance of covalent dimerization of the drug in the crystal conditions. To alleviate these doubts we refined the model by introducing various possible covalent dimers of the FK317 mitosene (based on the position of the reactive carbon that might facilitate this process). Figure 14 is a list of the various ligands used for refinement as well as their corresponding R_{free} and B factors. The model with the FK317 mitosene was found to have the lowest R_{free} value and hence the most plausible model.

3.4.2 Structural analysis of Acr1-nucleosome complex

The difference density maps obtained from the Acr- α sat nucleosome co-crystals revealed a strong signal as shown in Figure 15 A at a contour level of 2.5. The polyamide portion of the conjugate was first built into the density as shown in Figure 15 A,B. The introduction of the polyamide portion of the ligand resulted in a subsequent drop in the overall R_{free} value. The location of linker and the acridine moiety in the structure remains uncertain due to lack of well-defined electron density in this region. The Fo-Fc map for the polyamide reveals the presence of residual density that might correspond to the acridine moiety (Figure 15 B). The acridine component of the conjugate complex is yet to be built in, but a projected structure of the conjugate complex in the nucleosomal context is represented in Figure 15 B & C. Independent examination of the difference densities of the DNA surrounding the polyamide reveals local structural changes

in the form of propeller twists about 2-4 base pairs upstream of the intercalating acridine as depicted by the arrows in Figure 15 A. These changes propagate to the major groove adjoining the polyamide-bound minor groove and have not yet been built into the model. The current structure is therefore only a partially refined model and will require further refinement for complete structural analysis.

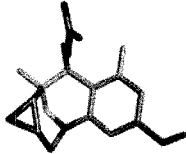
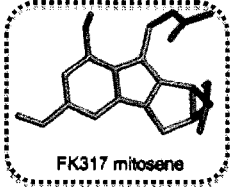
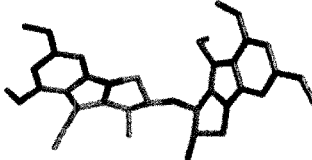
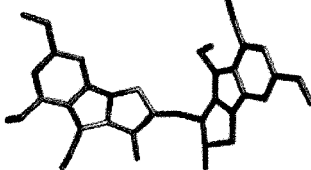
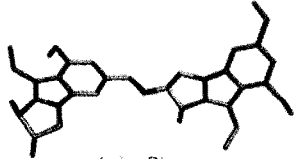
Ligands	Final Rwork/Rfree	B Factor		
		DNA	Protein	ligand
 FR900482 mitosene	0.2545/0.3255	112.741	/36.162/	43.064
 FK317 mitosene	0.2538/0.3243(1)	112.991	/ 36.193 /	32.88
 Azindine Dimer	0.2534/0.3269	112.931	/36.352/	32.61
 Carbamate Dimer	0.2546/0.3276	113.221	/36.642/	20.31
 Imine Dimer	0.2563/0.3266	112.40	/35.822/	38.38

Figure 14: List of the various structures that were built into the difference density maps with the corresponding R_{free} and B factors. The highlighted box represents the best solution for the co-crystal structure.

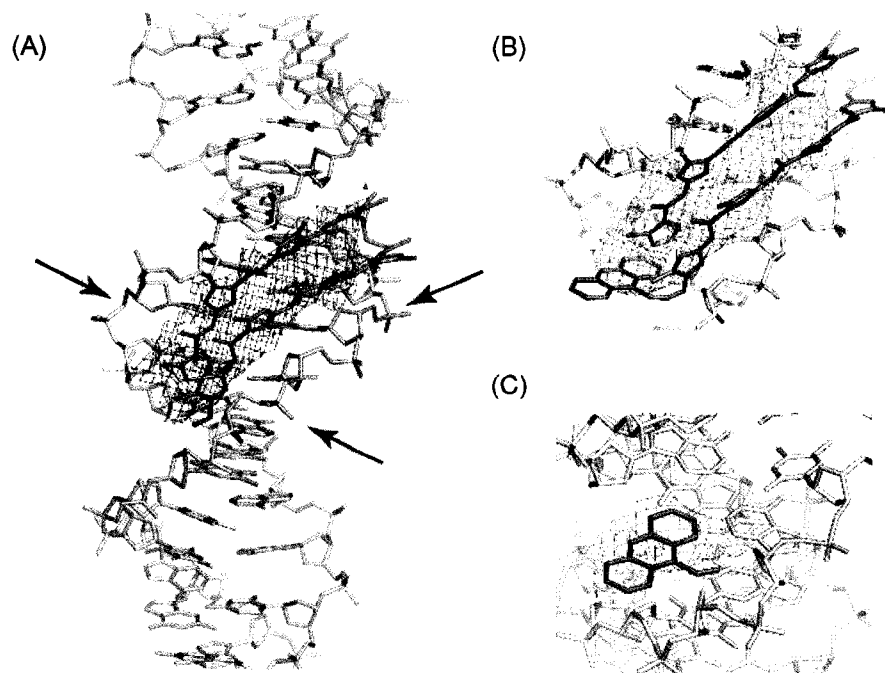


Figure 15: Preliminary co-crystal structure of Acr1 with α -nucleosome. (A) Section of the co-crystal structure depicting nucleosomal DNA (white) with the polyamide component (green). The black arrows represent the DNA bases that show difference densities corresponding to propeller twist changes. (B) The projected structure of the acridine-polyamide conjugate in the minor groove of nucleosomal DNA with the corresponding Fo-Fc difference density map (in red). All the density maps for this structure were calculated at 3.0Å and the contour levels were set at 2.3. (C) The intercalating acridine ligand is represented along with the corresponding Fo-Fc map.

3.5 DISCUSSION

3.5.1 Structural analysis of FK317-nucleosome complex

The analysis of the co-crystal structure of FK317 and α -nucleosome remains inconclusive in terms of the nature of the interaction between the mitosene moiety and nucleosomal DNA. This may be largely due to compromised resolution of the co-crystals and low occupancy of the drug. Attempts were made to augment resolution (different crystal conditions and higher nucleosome concentrations) and increase drug interaction with nucleosome (soaks with FK317, NVOC-treated nucleosomes). None of these attempts yielded any improvement in terms of resolution or occupancy. Nonetheless the partial co-crystal structure helped us determine that the distance for effective mitosene-mediated protein-DNA crosslinks is $\sim 6.05\text{\AA}$. This separation can be correlated to the distance between reactive centers contained within two covalently linked mitosene residues. Thus the dimers listed in Figure 14 could prove to be effective as drug-mediated intranucleosomal DNA-protein crosslinkers. These studies also revealed the need for mitosene-drugs that have a higher activity on nucleosomal versus B-form DNA. This would allow for higher occupancy of the drug molecule on nucleosomes and hence provide a more defined model for drug binding.

The high-resolution co-crystal structure of mitosene agents with nucleosomes will allow us to understand the nature of interaction of this class of compounds with cellular DNA and hence its function as an anticancerous agent.

3.5.2 Structural analysis of Acr1-nucleosome complex

The partially refined co-crystal structure of Acr1 with α -nucleosomes reveals the presence of a large signal corresponding to a polyamide molecule. The density corresponding to a second polyamide molecule at the symmetry-related site is poor. This could be due to the low occupancy of the second polyamide site. The overall structure of the nucleosome is maintained on Acr1-polyamide binding as indicated by the preliminary least square analyses. The overall rmsd between the co-crystal structure and the original nucleosome structure (1AOI) was found to be $\sim 0.73\text{\AA}$. The present structure is only partially refined, but the difference density generated indicates local structural changes in the major groove DNA adjoining the site of polyamide binding in the minor groove. This is in accordance with published data that suggests that the polyamide-acridine conjugates are capable of inducing DNA sequence specific structural changes which propagate to the neighboring major groove, resulting in the eviction of major-groove binding transcription factors like GCN5 (65). Further refinement of the current model is required for accurate analysis of the proposed DNA structural changes.

The structure of the Acr1- α nucleosome co-complex is critical in understanding the effect of these conjugate intercalators on nucleosomal DNA. This will provide some insights into the extent of structural changes in major groove DNA and its consequences for protein binding at the molecular level.

3.6 Acknowledgements

A special thanks to Dr. Raji Edayathumangalam and Dr. Uma Muthurajan for their training and input, Dr. Robert Williams and Dr. Peter Dervan for the chemical ligands used in this co-crystallization study and, Pam Dyer for the reagents necessary to perform these experiments.

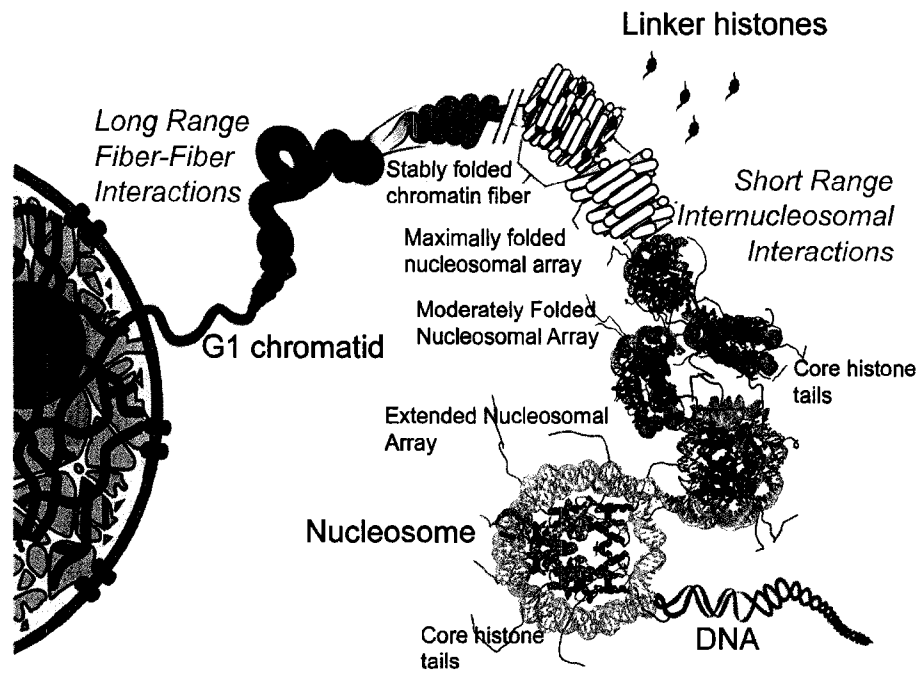
PROJECT II
ROLE OF POLYGLUTAMYLATION DROSOPHILA NUCLEOSOME
ASSEMBLY PROTEIN 1 (dNAP1) FUNCTION.

CHAPTER 4

REVIEW OF LITERATURE

4.1 CHROMATIN FUNCTION, STRUCTURE AND DYNAMICS

The ability of the cell to pack an enormous amount of DNA into the nucleus is largely due to the presence of highly basic proteins called histones (Figure 16). The basic monomeric unit in this hierarchy is called the nucleosome (Figure 2). A conventional nucleosome contains two copies each of major type histones H2A, H2B, H3, H4 and 146bp of DNA wrapped around this protein core in 1.7 tight left-handed superhelical turns (Figure 2). Nucleosomal DNA is highly compact due to the presence of extensive hydrogen bonding contacts between the DNA phosphate backbone and the histone octamer core. The octamer is made up of the (H3-H4)₂ that protects almost 80bp of nucleosomal DNA and renders a two-fold symmetry to the nucleosome core particle (NCP). The H2A/H2B dimers bind either side of the tetramer and protect ~ 30bp each of nucleosomal DNA.



Adapted from Hansen 2002

Figure 16: Hierarchy of DNA compaction. The basic unit of chromatin- the nucleosome is represented at the bottom of the DNA compaction ladder (69).

DNA in “compact” chromatin has to be accessible for basic cellular processes like transcription, replication and DNA-damage repair. A number of mechanisms are involved in the maintenance of a compact yet dynamic chromatin structure. Evidence for the dynamic nature of chromatin was first shown *in vitro* by demonstrating transient site-exposure due to dissociation and re-association of the nucleosomal DNA ends in mononucleosomes (70-72). Studies *in vivo* suggest complete nucleosome dissociation during replication and transcription (73-76). In particular, it was found that RNA polymerase II elongation required release of H2A/H2B dimer (77). Higher order chromatin dynamics is largely mediated by changes in intra and inter-nucleosomal interactions (Figure 16). Thus changes in the mononucleosome structure can translate to changes in higher order chromatin structure (78).

4.2 REGULATION OF CHROMATIN DYNAMICS

The factors that allow for changes in nucleosome structure include incorporation of histone variants, posttranslational histone modifications, chromatin remodelers and histone chaperones.

4.2.1 Histone Variants

Incorporation of non-allelic histone variants alter nucleosome dynamics via subtle changes in the intra as well as inter nucleosomal stability (35,79). Histone variant expression, unlike that of major type histones, is not restricted to the S phase. Histone variants have distinct differences in amino acid sequence compared to their major-type counterparts. For example, H2A variants - H2A.X, H2A.Z, Macro H2A, and H2A.Bbd - exhibit 86%, 60%, 65% and 40% sequence similarity with

the major H2A protein. H3 variants - H3.3 and CenpA - share 96% and 62% sequence similarity with major type histone-H3. Interestingly, the H2A.Z variants are more conserved across the species when compared to the major type histones (80), indicative of an indispensable function of the variants that cannot be carried out by their major-type histone counterparts (79).

Histone variant-containing nucleosomes have been shown to exhibit differences in nucleosome stability (81,82). Moreover, differences in the sequence of histone tails (between variants and major type histones) result in differences in histone modification patterns, which in turn change the landscape for binding of a gamut of proteins including chromo- and bromo-domain containing proteins. The surface charge distribution on the nucleosomal surface is largely due to the octamer and is known to play a very important role in higher order nucleosome structure both in solution studies and in crystal packing (14). Histone-variant containing nucleosomes show differences in this charge distribution (62), which in turn could result in differences in the stability and packing of the resulting higher order chromatin structure (83,84).

4.2.2 Posttranslational Histone Modifications

Covalent posttranslational histone modifications play a critical role in the regulation of nucleosome fluidity. These modifications can occur at the exposed octamer surface and also within the histone core (85). Nucleosomes with these chemical adducts present suitable targets for proteins that are capable of altering chromatin structure (86,87). The most extensively studied modifications are those that are present on histone tails. They have been shown to affect

chromatin folding and chromatin fiber stability either directly by charge neutralization of the basic histone tails or indirectly by altering the target site for chromatin-binding proteins (88,89).

Histones are substrates for acetylation, methylation (mono-, di-, trimethylation), phosphorylation, ubiquitylation, and sumoylation (90). Linker histone H1 is also a known substrate for phosphorylation, lysine methylation, and ADP-ribosylation. The functional implications of these modifications vary depending on the combinatorial pattern of other modifications in their vicinity - histone code hypothesis (91).

4.2.3 Chromatin Remodelers

Chromatin remodelers are multi-subunit complexes that are capable of mediating chromatin dynamics by altering histone-DNA interactions in an ATP-dependent manner within the nucleosome (92). Remodelers are divided into various classes on the basis of different protein composition and functions, and include SWI/SNF (BAF), imitation switch (ISWI), INO80, rsc/rat (SWR1), and Mi-2/CHD groups (93). They are highly conserved in eukaryotes and play an important role in development (94,95). The association of these complexes with the nucleosome remains unclear, but it has been shown that the ISWI group of proteins contain a conserved SANT domain that interacts with histone tails (specifically H4) and a SLIDE domain that interacts with DNA (96-98). In terms of chromatin-related functions, SWR1 complex is a H2A-Htz1 exchanger in yeast thus allowing for the deposition of histone variant Htz1 (similar to H2A.Z in higher eukaryotes). Remodeler complexes are also known to be associated with histone-modifying

enzymes. NuA4 is a HAT (histone acetyl transferase) and shares subunits with the SWR1 complexes (99).

The RSC (remodels structure of chromatin) complex ejects and/or translocates the octamer *in vitro* (100). The consequence of nucleosome remodeling can therefore result in complete disassembly by transfer of the histone components to the associated histone chaperones or relocation of the intact octamer on nucleosomal DNA (92,93). Remodelers are known to be in close physical and genetic association with histone chaperones. For example, SWI/SNF and Asf1 interactions have been demonstrated in *Drosophila* (101). Similar interactions of remodelers with different histone chaperones are listed in (102).

4.2.4 Histone Chaperones

Histone chaperones prevent unintended interactions between the highly basic histones and DNA and allow for proper nucleosome formation. The fundamental properties of these proteins include histone binding and their ability to regulate nucleosome dynamics via transport, transfer and storage of histones. Not all histone chaperones are capable of the above functions *in vivo*. In order to simplify the understanding of histone chaperone function these proteins are broadly classified as: (a) Independent chaperones - eg. Asf1; (b) proteins that are part of multi-chaperone complexes (e.g. CAF-1 Chromatin assembly Factor-1); and (c) chaperones that function within large chromatin-remodeling complexes (102). Some histone chaperones like RbAp48 are found to be a member of all three categories as it is capable of autonomous function, is a component in the

CAF-1 complex, and is associated with the ISWI and CHD families of chromatin remodelers.

Histone chaperones have been thought to be specific with respect to their binding partners and, depending on their binding with replicative variants or replacement variants, they are involved in replication-dependent and replication-independent chromatin function (103,104). Histone chaperones are therefore also classified based on their histone-binding partners, e.g Anti silencing Factor - 1 (Asf1) is an H3-H4 chaperone, while Nucleosome Assembly Protein-1 (NAP1) is an H2A-H2B chaperones. Linker H1 is also known to have its chaperone, namely NASP (104,105). While the long stretch of acidic amino acid sequences in the histone chaperones accounts for basic histone-binding ability, the specificity of this binding capability has not been addressed to date (106-110).

In the work presented here we are specifically interested in the NAP family of histone chaperones and its chromatin-related function.

4.3 NUCLEOSOME ASSEMBLY PROTEIN 1 (NAP1)- STRUCTURE AND FUNCTION

NAP1 is a representative member of the NAP subfamily of histone chaperones. This class of proteins includes NAP1-Like Protein (NAP1L 1-5), SE translocation (SET), Testis-specific protein-Y (TSPY) and many others (108) (Figure 18). It is a highly acidic protein with ~25% of the amino acids being negatively charged at physiological pH. In yeast, *NAP1* is a non-essential gene, while in *Drosophila* and mouse, *NAP1* knockout result in embryonic lethality (111-113).

The high-resolution crystal structure of yNAP1 reveals a novel non-coiled coil motif that constitutes the dimerization domain and a conserved four-strand anti-parallel β -sheet (108) (Figure 17). Asf1, nucleoplasmin, nucleolin, dNLP-core and SET/ TAF- β /INHAT are histone chaperones that contain the conserved antiparallel β -sheet, indicative of a potentially important role in histone binding (106,110,114-116).

Co-immunoprecipitation studies in *Drosophila* embryo extracts revealed dNAP1 to be associated with H2A-H2B dimer suggesting presence of the histone-dimer-NAP complex *in vivo* (117). On the other hand, *in vitro* analyses revealed that yNAP1 shows preferential binding to (H3-H4)₂ tetramer largely mediated by the N-terminal histone tails (118). *Xenopus* NAP1 is also known to bind linker histone H1 and result in its deposition onto linker DNA (105). NAP1 has a number of histone-binding partners, but the exact region of interaction for these complexes remains unknown. NAP1 is also in the midst of a complex network of cellular processes that largely depend on the nature of its protein-binding partner (119). For example, HIV-Tat protein interacts specifically with the core and the C-terminal domain of hNAP1. This interaction was found to be critical for regulation of viral gene expression (120). NAP1 is known to interact

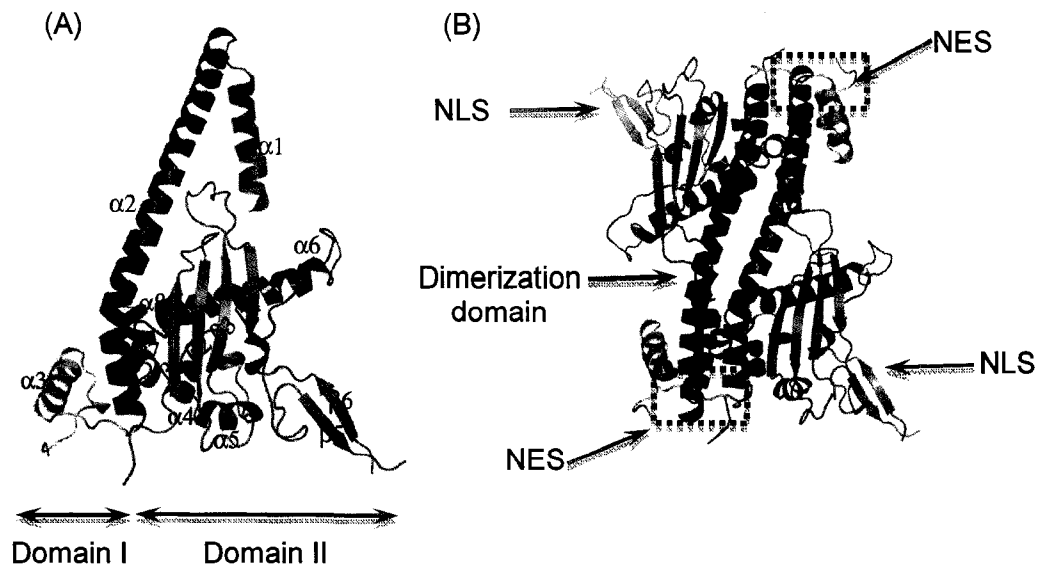


Figure 17: Structure of yNAP1. (A) The yNAP1 monomer structure represents the various components of Domain I and Domain II. The $\beta 1$ - $\beta 5$ anti-parallel β -sheet is characteristic of the NAP1 family of proteins. The subdomains A,B,C and D are represented as blue, yellow, green and red respectively. (B) The yNAP1 dimer structure. The location of the various domains and their functions are indicated by grey arrows. NLS refers to the nuclear localization sequence and NES refers to the nuclear export sequence (121).

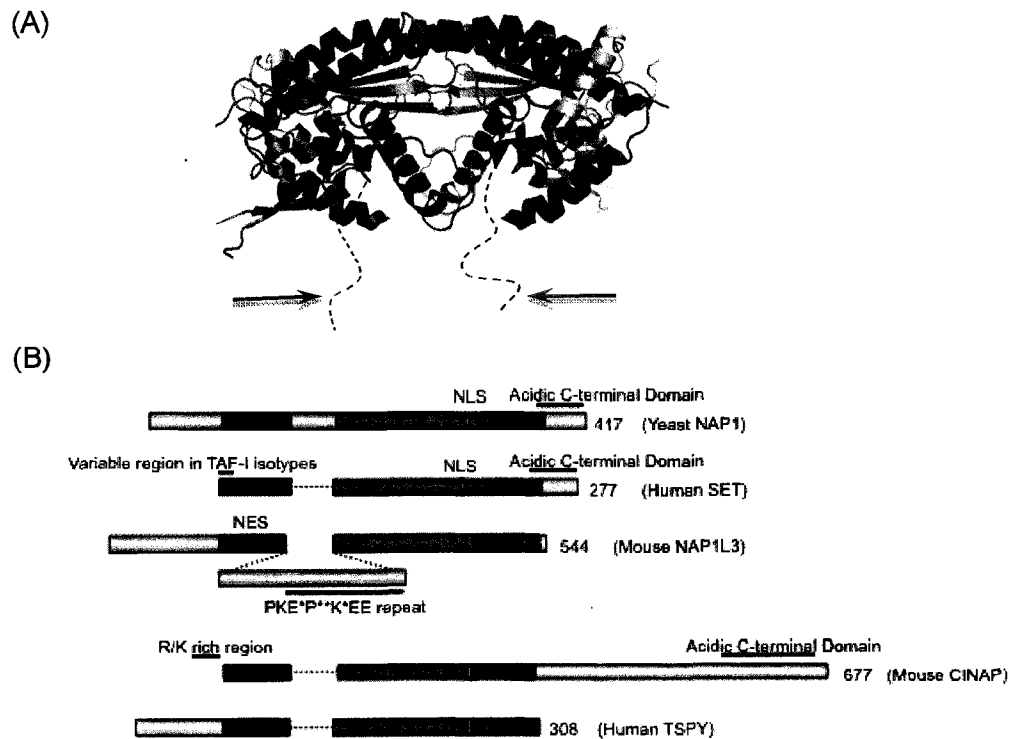


Figure 18: NAP family of proteins. (A) Structure of the representative member- yNAP1. The dotted lines and the grey arrows represent the unstructured acidic C terminal tail. The tail is not a part of the model. (B) Alignments of members of the NAP protein family, i.e., yeast NAP1, human SET, mouse NAP1L3, mouse CINAP, and human TSPY, are shown. The position and length of the acidic C-terminal domain are with mitotic regulators like Gin4 kinase and Sda1 (122,123), indicating potential cell regulatory roles.

4.4 POSTTRANSLATIONAL NAP1 MODIFICATIONS

NAP1 is substrate to a variety of posttranslational modifications, but the functional implications of most of these modifications (with the possible exception of phosphorylation) have not been studied. dNAP1 interacts with casein kinase-2 (CK2) and is found to be phosphorylated at three locations. Two of the phosphorylation sites are at the PEST (Proline, Glutamic acid, Serine and Threonine rich) domains, while the third is close to the nuclear localization sequence (NLS) (124). It was therefore proposed that phosphorylation of dNAP1 regulates protein degradation as well cellular localization. yNAP1 is also a substrate of CK2 and was found to have at least 11 phosphorylation sites. This modification was found to promote nuclear localization of yNAP1 (125). Human NAP1 interacts with transcription coactivator p300 in HeLa cells and is a substrate for p300-mediated acetylation (126). NAP1 in *Arabidopsis thaliana* is known to be farnesylated. This membrane-anchor modification enables NAP1 to be localized to the nucleus during cell division, proliferation and subsequent leaf development (127).

Recently hNAP1 and hNAP-2 as well as other NAP family proteins, including SET/PHAPII, nucleolin and nucleoplasmin B23, have been shown to be subject to a unique acidic, branched modification-polyglutamylolation (128,129). The enzyme that mediates this modification was identified as TTLL4 (Tubulin-Tyrosine Ligase-Like 4 protein family) in HeLa cells (129). In hNAP1 this modification was found at two putative target sites at the C-terminus (Glu-356, Glu357). The impact of this modification on NAP1 function remained unknown. It

was hypothesized that the presence of the acidic modification increased the affinity of histone binding to NAP1.

Interestingly, NAP1 is subjected to another branched modification-polyglycylation (130). The same study also identified TTL10 as the NAP1 polyglycylase. Mutational analyses revealed that the C-terminus residues - Glu 359 and Glu 360 - are target sites for glycylation. It is speculated that the polyglycylation undoes the effect of polyglutamylation, largely due to the proximity of the target sites and due to the differences in the charge rendered by both these modifications. The various posttranslational modifications and their proposed function is summarized in Figure 19.

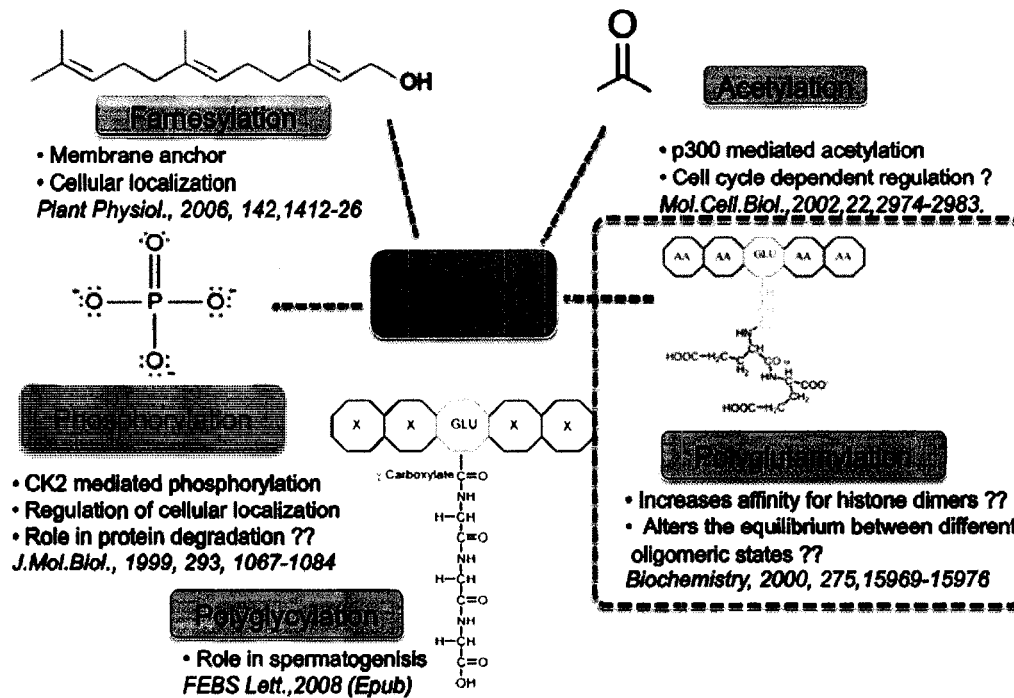


Figure 19: Schematic of the variety of posttranslational modifications and their potential functions.

4.5 SPECIFIC AIMS FOR PROJECT II

1. Characterization of the histone chaperone activity of dNAP and yNAP as a function the acidic C terminus.
 - 1A. Determine the ability of recombinant purified dNAP to mediate nucleosome dissociation *in vitro*.
 - 1B. Determine the ability *Drosophila* NAP1 with the yeast NAP1 CTAD to mediate nucleosome dissociation *in vitro*.
2. Characterization of the role of the polyglutamylate modification in dNAP1 histone chaperone activity.
 - 2A. Determine the ability of the purified native dNAP1 to mediate nucleosome dissociation *in vitro*.
 - 2B. Determine the presence and location of the polyglutamylate modification on native dNAP1 via Mass Spectrometry and anti-polyglutamylate-specific antibodies (GT335).
 - 2C. To determine the distribution of the polyglutamylated versus unmodified dNAP1 between the nuclear and cytoplasmic fraction of the *Drosophila* embryos as well as during various developmental stages.

CHAPTER 5

THE ROLE OF POLYGLUTAMYLATION IN DROSOPHILA NUCLEOSOME ASSEMBLY PROTEIN-1 (dNAP1) FUNCTION.

5.1 ABSTRACT

NAP1 isolated from mammalian cells is known to aid chromatin assembly *in vitro*. The localization of NAP1 in *Drosophila* embryos revealed that it is predominantly nuclear during the S phase and cytoplasmic during the G2 phase, in keeping with its role in chromatin assembly. Yeast nucleosome assembly protein 1 (yNAP1) also promotes nucleosome assembly along with nucleosome sliding and nucleosome disassembly *in vitro*. Nucleosome sliding and disassembly functions have been attributed mainly to the length and acidic amino acid content of the unstructured C-terminal tail (131). Sequence alignment of dNAP1 and yNAP1 reveals that dNAP1 has a shorter C-terminal acidic domain (CTAD). In this study we have shown that recombinant dNAP1 is unable to disassemble nucleosomes *in vitro* and this function is restored when the CTAD of dNAP1 was replaced with that of yNAP1. We also demonstrate that the functionally deficient dNAP1 CTAD is compensated for *in vivo* by posttranslational polyglutamylation. We have identified two potential target sites for this modification - one at the C terminus, which we hypothesize enables NAP-related nucleosome function, and the second at the NLS.

5.2 INTRODUCTION

Non-specific histone-DNA interactions are alleviated by the presence of escort proteins called histone chaperones (132). This function is based on the ability of these proteins to bind histones, thereby aiding in their incorporation, storage and transfer (102). Histone chaperones therefore play a fundamental role in the regulation of transcription, replication, cell-cycle regulation, histone metabolism, apoptosis, development and differentiation.

The Nucleosome Assembly Protein (NAP) family of histone chaperones includes: NAP1, NAP1-Like Proteins (NAP1L 1-5), SE translocation (SET), Testis-specific protein-Y (TSPY) and many others (108,121) (Figure 18). It is a highly acidic protein with ~25% of the amino acids being negatively charged at physiological pH. In yeast, *NAP1* is a non-essential gene, while in *Drosophila* and mouse, *NAP1* knockout result in embryonic lethality (111-113). Higher eukaryotes have a large number of NAP homologues that regulate tissue-specific functions. For example, NAP1L2 protein expression is seen specifically during neuronal development (113,133), and TSPY functions to regulate spermatogenesis (134). The amino acid sequence alignment showed no significant sequence homology among the various NAP family members, but the recent structure of yNAP1 revealed the conserved central NAP domain as the unifying motif among the NAP family members (108,121) (Figure 17). It has been proposed that the conserved domain may therefore be involved in the binding of the histone partners.

The NAP1 subfamily is characterized by a highly acidic stretch at the C-terminal domain (CTAD) (121,131). The CTAD in yNAP1 is required for ATP-independent, NAP1-mediated nucleosome disassembly, exchange and sliding *in vitro* (131). In the absence of the acidic tail, yNAP1 is unable to execute these functions but remains capable of promoting nucleosome assembly (131) *in vitro*, indicating the essential role of the CTAD in modulating nucleosome structure. This results in either complete nucleosome disassembly, or in variant histone dimer exchange, or in nucleosome sliding (131). While the presence of acidic CTAD is conserved among the various NAP1 species, the length and the number of acidic amino acids is not. In particular, dNAP1 contains 21 acidic amino acids at the CTAD compared to 30 in yNAP1. Is the dNAP1 CTAD sufficient in executing *in vitro* nucleosome dissociation like yNAP1?

This is particularly interesting in light of studies indicating that NAP1 & NAP2 isolated from HeLa cells are polyglutamylated (128). Polyglutamylation is a branched acidic polypeptide modification generated by sequential addition of glutamyl units. It was first identified in tubulin and later in human NAP1 and NAP2 (128,135). Polyglutamylation is a post-translational modification that generates lateral acidic side chains on proteins by sequential addition of glutamate amino acids (135). This modification has been extensively studied in the context of α - β tubulin (128,135). In case of human NAP1 the number of glutamyl residues range from 6-12 units (128). Further the study also provided evidence for the presence of this branched polypeptide modification in the C-terminus of human NAP1.

Recent studies revealed other substrates for polyglutamylation in HeLa cells, including histone chaperones-SET/PHAPII, nucleolin, nucleoplasmin B23 and several transcription factors (129). The same study also revealed that the main polyglutamylase in HeLa cells is TTLL4 (Tubulin-Tyrosine Ligase-Like protein family) and this enzyme was found to copurify with its substrates (e.g. NAP1). While no obvious target consensus sequence for TTLL4 has been defined as of now, the substrates for polyglutamylation contained glutamate-rich stretches in their primary sequence.

In this study, native dNAP1 purified from *Drosophila* embryos is found to be capable of NAP-mediated nucleosome disassembly *in vitro* while the recombinant dNAP1 remains incapable of the same. Western blot analyses reveal at least two polyglutamylated native dNAP1 species and subsequent mass spectrometric analyses showed the presence of 10 glutamyl units associated with the C terminal domain of both these species. We believe that polyglutamylation of the CTAD restores the nucleosome-dissociation function of dNAP1 CTAD *in vitro*.

5.3 EXPERIMENTAL PROCEDURES

Purification of the various recombinant NAP1 constructs

The various NAP1 constructs used in this study are depicted as schematics in Supplementary Figure A1. The GST-tagged full-length γ NAP1 (1-417) and truncated GST- γ NAP1 (74-365) constructs were expressed and purified as described in (118). Recombinant His-tagged rdNAP1, dsNAP1 and Δ C dNAP1 constructs were expressed (in *E.coli*) and purified as in (117). Domain-swap

NAP1 was constructed using Splice Overlap Extension by PCR (SOE-PCR) (136). This method does not require restriction sites to fuse two different DNA fragments.

Purification of native dNAP1 from Drosophila embryos

The frozen *Drosophila* embryos were a generous gift from Dr. Jim T.Kadogana and Dr. Paul J.Laybourn. The 8-hr, preblastodermal, dechorionated embryos (at least 50grams) were washed and homogenized to prepare S190 extracts. These extracts were then subjected to chromatographic purification as described in (137). In order to further improve the purity of the native dNAP1 obtained from the final Q sepharose purification step, the fractions containing dNAP1 were pooled and subjected to an ammonium sulfate cut. 4.0M ammonium sulfate pH7.5 was added to the pooled dNAP1 fractions to a final concentration of 1.8M. The mixture was incubated for 30 min and subjected to centrifugation in a Beckman rotor at a speed of 18,000rpm for 1.5 hr at 4°C. This ammonium sulfate cut helps to remove hydrophobic contaminants in the native dNAP1 fractions. The resulting supernatant was dialyzed overnight with at least three buffer changes, at 4°C in buffer A containing 10mM Tris pH 7.5, 1mM EDTA pH 8.0, 10% glycerol, 100mM NaCl and 2mM DTT. After dialysis, the supernatant is subjected to anion exchange purification using a MonoQ column (HR 5/5, Amersham,G.E Health sciences). Native dNAP1 was eluted with a linear gradient (15 column volumes) from 0.1-1M NaCl in 10mM Tris pH 7.5, 1mM EDTA pH 8.0, 10% glycerol, and 2mM DTT. The appropriate fractions were pooled and dialyzed in Buffer A for subsequent use.

Nuclear and cytoplasmic extracts were purified from *Drosophila* embryos as described in (117,137).

Western Blot Analysis

Native dNAP1 was probed with polyclonal anti-rabbit dNAP1 antibodies (a generous gift from Dr. Takashi Ito) at a 1:5000 dilution. The polyglutamylation modification was detected by probing with monoclonal anti-mouse polyglutamylation antibodies (mAb GT335) (128) at 1 1:5000 dilution. The blots were visualized using the chemiluminescent ECL PLUS Western Blot detection System (Amersham, G.E Health sciences). The yeast extracts were probed with polyclonal anti-rabbit yNAP1 antibodies generated against the yNAP1 peptide – EERLALDYSIGEQLKDKLIPC (QCB Biologicals) at a 1:5000 dilution. All samples (unless specified) were analyzed on 15% SDS-PAGE.

Preparation of DNA, Histones and Nucleosomes

The 146bp 5S DNA derived from 5S rRNA gene (57) was prepared as described previously in (34). The recombinant wild type histones H2B, H3 and H4 as well as mutant H2AK119C were expressed and purified as described in (34). Histone H2AK119C was labeled with 7-diethylamino-3-(4'-maleimidylphenyl)-4-methylcoumarin (CPM) as previously described in (138). The labeled histone was then refolded with wild type H2B to form labeled dimer and with H2B,H3 and H4 to form CPM-labeled octamer (34). Nucleosomes were reconstituted with CPM-labeled octamer by dialysis against decreasing salt (34). The samples were analyzed by 5% native PAGE gel in 0.2X TBE running buffer.

Nucleosome Dissociation Assays

The assay was performed with 3.5 μ M of labeled nucleosomes incubated with increasing amounts of the different constructs (Supplementary Figure A1) in Buffer A. The above reactions were incubated at 4°C for 10-12 hr. The samples were then analyzed on a 5% Native PAGE gel. The gel was viewed without any stain in fluorescent mode at 365nm, followed by ethidium bromide staining for visualization of DNA and coomassie staining for detection of protein content. Controls including labeled histone dimer complex with the various NAP1 constructs were prepared by incubation of 8 μ M labeled histone H2A/H2B dimer with 8 μ M of the NAP1 constructs in Buffer A for 10 hr at 4°C.

Mass Spectrometric Analysis

In-gel digestion was performed by first excising the band from an 18% SDS PAGE gel containing the protein of interest. The excised pieces were then washed with 100 μ l of 100mM NH₄HCO₃/50% acetonitrile (ACN) for 15 min with gentle vortexing. This was done until all the dye was removed from the gel slice. Once the final supernatant was removed, 100 μ l of 100% ACN were added and incubated for 5 min. Subsequently the ACN was removed and the sample allowed to air dry for 5 min. This process enables the dehydration of the sample and enables it to efficiently imbibe the proteolytic enzymes. 100 μ l of DTT (100 μ l of 10mM in 100mM NH₄HCO₃) was added and incubated at 60°C for 30 min. The supernatant is removed and supplemented with 100 μ l of iodoacetamide (IAA-55mM in 100mM NH₄HCO₃) and incubated in the dark at room temperature for 30 min. The treatment with DTT helps reduce the sulfhydryl groups and the

subsequent IAA treatment modifies the reduced SH groups thus preventing the formation of a disulfide bond. The supernatant was aspirated and the gel pieces were washed with 100mM NH_4HCO_3 /50% ACN followed by 100 μl of 100% ACN as mentioned above. The dehydrated samples were then infused with 15ng/ μl of porcine trypsin (Roche, Proteomics Grade) [and 12.5ng/ μl for Asp-N (Roche, Proteomics Grade)] in a final reaction volume of 40 μl containing 100mM NH_4HCO_3 . This reaction mixture was incubated overnight at 37°C. The supernatant was saved and the residual digested fragments were extracted with 50% ACN/0.1% trifluoroacetic acid (TFA). The sample was dried using a Speed Vac and resuspended in minimum volume of 0.1% TFA. The sample digest was mixed with α -cyano-4-hydroxycinnamic acid (10 mg/ml in 50% ACN, 0.1% TFA), spotted on the MALDI target and allowed to dry. The sample was then analyzed using an Ultraflex-TOF/TOF mass spectrometer (Bruker Daltonics, Billerica, MA) in positive ion and negative ion, reflector mode. The negative mode allows for better charge uptake by acidic polypeptides. Appropriate calibrations were performed for both these modes.

5.4 RESULTS

5.4.1 Recombinant dNAP1 is compromised in its ability to dissociate nucleosomes *in vitro*.

The ability of NAP1 to dissociate nucleosomes and hence modulate nucleosome structure in a CTAD-dependent manner was first demonstrated in (131) using recombinant yNAP1 and ΔCTAD yNAP1. Here we used the same assay to test the activity of the various NAP1 constructs listed in Supplementary Figure A1.

Recombinant full-length GST-yNAP1 was used as a positive control, while the N- and C- terminal truncated version GST-(74-365)-yNAP1 was used as a negative control. The N terminus of yNAP1 appears to be non-essential for nucleosome dissociation *in vitro* since the Δ CTAD yNAP1 (1-365 yNAP1) construct is also incapable of mediating nucleosome dissociation. The assay consists of CPM-labeled H2AK119C-containing nucleosomes incubated in the presence of the various recombinant NAP1 constructs. GST-tagged versions of yNAP1 constructs are preferred in order to distinguish the bands corresponding to NAP1-histone-dimer complex from nucleosomes, since their migration on a 5% native PAGE gel is very similar (131).

In Figure 20, Panel A is a schematic showing the principle behind NAP1-mediated nucleosome dissociation/disassembly. Panel B reveals the expected change in nucleosome structure when incubated with increasing molar ratios of full-length yNAP1. The NAP1-dependent disassembly is associated with nucleosome repositioning, tetrasome formation, release of DNA, and at higher molar ratios, decrease in fluorescent signal from nucleosomes and a subsequent increase in fluorescent signal from NAP1-histone-dimer complex (Figure 20B) (131). Figure 20C on the other hand reveals no change in nucleosome configuration when incubated with the truncated GST(74-365) yNAP1 construct. Recombinant dNAP1 incubated with labeled nucleosomes revealed no change in nucleosome structure, similar to the truncated GST(74-365) yNAP1 construct (Figure 20D). This indicates the chromatin-related functional deficiency of dNAP1 CTAD. Exchanging the CTAD of dNAP1 with that of yNAP1 resulted in a protein

(dsNAP1) that was capable of nucleosome disassembly (Figure 20E), indicating that dNAP1-mediated modulation of nucleosome structure requires the CTAD of yNAP1. The loss of function observed with recombinant dNAP1 could be attributed to the lack of sufficient acidic amino acids at its C terminal domain since there is a subsequent gain of function with dsNAP1 which contains the yNAP1 CTAD (Figure 20E), known to have significantly more acidic amino acids. Independent experiments performed with labeled nucleosomes incubated with recombinant dNAP1 and free polyglutamic acid tails *in trans* did not result in disassembly (data not shown), further suggesting that the optimal acidic tail has to be in structural context with the rest of the NAP1 domain (*in cis*) for effective nucleosome dissociation function *in vivo*.

The inability of dNAP1 and GST-(74-365) yNAP1 constructs to disassociate nucleosomes could be explained by the inability of these constructs to bind histone-dimers. To eliminate this possibility we performed qualitative mobility shift assays with all the NAP1 constructs in the presence of CPM-labeled histone dimers. No significant deficiencies in histone binding were observed (Supplementary Figure A2).

5.4.2. Native dNAP1 is capable of nucleosome dissociation *in vitro*.

The presence of a sufficiently acidic CTAD is essential for dNAP1-mediated change in nucleosome structure *in vitro*. This is indicated by the inability of recombinant dNAP1 to disassemble nucleosomes and the ability of dsNAP1 construct to do the same *in vitro*. Previous studies indicate that native dNAP1 and recombinant dNAP1 are both capable of chromatin assembly (MCB,

16,1996,3112-3124). But is native dNAP1 any different from recombinant dNAP1 in its ability to alter nucleosome structure?

To test this possibility we isolated dNAP1 from 8hr, preblastodermal, dechorionated *Drosophila* embryos. Purification of native dNAP1 (ndNAP1) from 50grams of embryos using the protocol described in the Experimental Procedure section yielded ~1mg of native dNAP1 at ~95% purity (Figure 21A). Purified native dNAP1 was tested for its ability to dissociate nucleosomes *in vitro* via the previously mentioned fluorescence assay. Figure 21B reveals the ability of the native dNAP1 to alter nucleosomes. The fluorescent scan, staining with ethidium bromide and coomassie reveals that the increasing molar ratios of native dNAP1 result in nucleosome repositioning and subsequent appearance of free DNA characteristic of nucleosome disassembly. The nucleosome-altering function is seen at higher concentrations of native dNAP1 as well, while recombinant dNAP1 at these concentrations remains inert towards nucleosomes (Figure 21C).

Figure 20

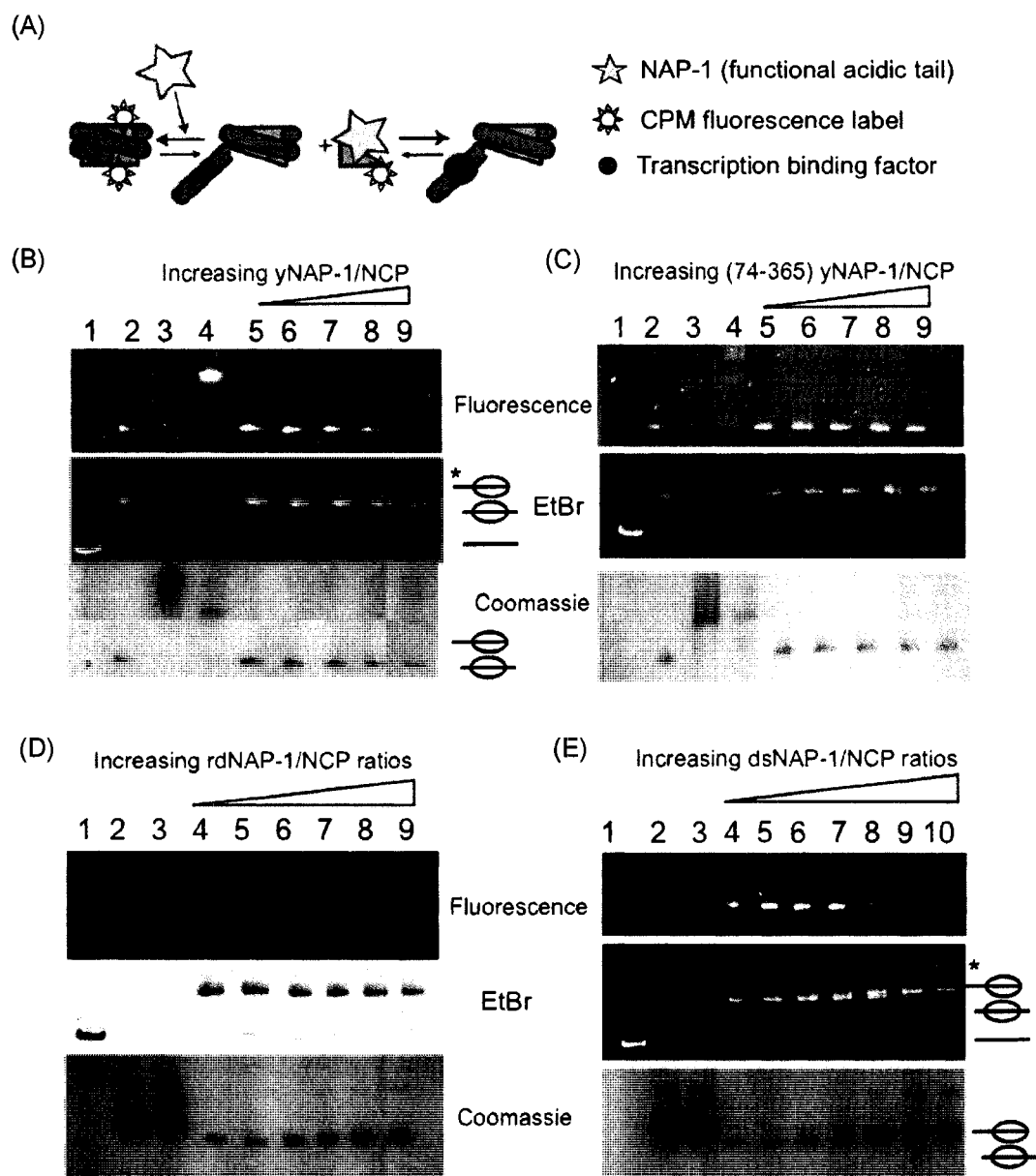


Figure 20: Recombinant dNAP1 (rdNAP1) is incapable of nucleosome disassembly due to a shorter and less acidic CTAD. (A) Schematic of the mechanism of NAP1-mediated nucleosome dissociation. Chaperone-mediated nucleosome disassembly is associated with release of free DNA, formation of tetrasome and formation of fluorescent NAP1-dimer complex. * Represents the migration of the tetrasome complex on 5% Native PAGE gels. In all the panels, Lane 1: Free 5S DNA, Lane 2: CPM-labeled H2A-containing nucleosomes, Lane 3: Recombinant NAP1 constructs, Lane 4: Fluorescent NAP1-histone dimer complex, Lane 5-10 contains increasing molar ratios of NAP1 (dimer)/nucleosome ratios (1:1, 2:1, 4:1, 8:1, 16:1, 20:1 respectively). (B) & (C) are controls representing the effect of GST-yNAP1 and GST-(74-365)yNAP1 respectively on nucleosome integrity. (D) & (E) indicate the effects of increasing His-dNAP1 and His-dsNAP1 on nucleosome disassembly function via histone-dimer removal. All the reactions, run on 5% Native PAGE gels were first analyzed in the fluorescent mode before visualization with ethidium bromide for DNA detection and coomassie for protein detection.

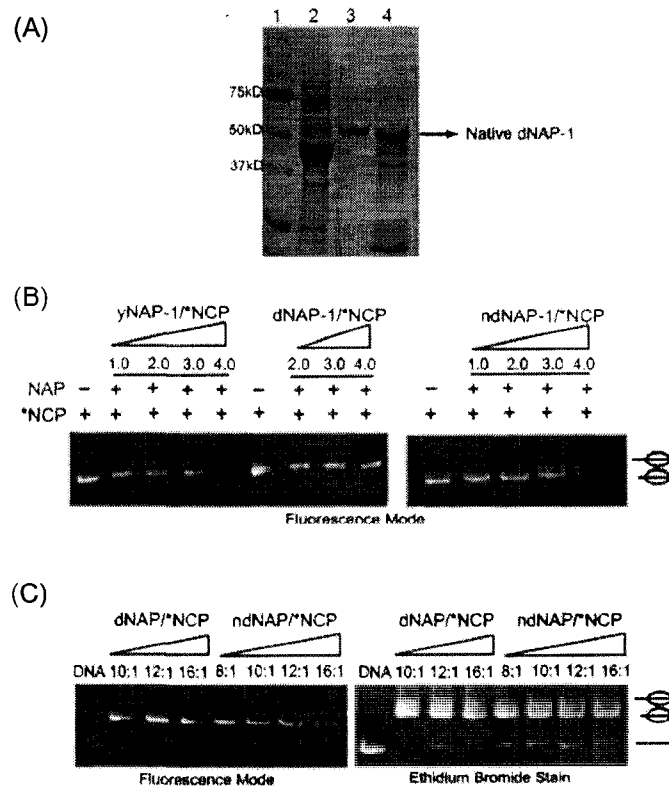


Figure 21: Native dNAP1 is capable of nucleosome disassembly *in vitro*. (A) Native dNAP1 was purified to homogeneity and was analyzed on a 15% SDS-PAGE gel stained with coomassie. Lane 1: Protein molecular weight marker, Lane 2: Partially purified extract (The fraction purified subsequent to the Q sepharose purification), Lane 3: Recombinant dNAP1 (rdNAP1) and Lane 4: Purified native dNAP1 (ndNAP1) (final purified product subsequent to ammonium sulfate cut and purification over a MonoQ column). (B) Effect of increasing ratios of dNAP1 and native dNAP1 on fluorescently labeled nucleosome. (C) Represents higher ratios of dNAP1 and native dNAP1 to labeled nucleosome to show dose-dependent effect of NAP1-mediated nucleosome disassembly. The dissociation reactions were analyzed on a 5% Native gel and visualized first in the fluorescent mode followed by ethidium bromide staining to visualize the DNA. The dissociation assays were performed as described in the experimental procedures.

This confirms that native dNAP1 is indeed capable of nucleosome dissociation though not as efficiently as yNAP1 and dsNAP1 (as indicated in Figure 21C). Thus dNAP1 isolated from *Drosophila* embryos is capable of modulating chromatin structure while recombinant dNAP1 is not. Native dNAP1 differs from recombinant dNAP1 in that it is a substrate for a plethora of posttranslational modifications. We were particularly interested in determining first the presence of a unique branched, acidic polypeptide modification: polyglutamylation, previously identified in human NAP1 and NAP2 (128) and then the effect of this modification on NAP1 function.

5.4.3 The C terminus of native dNAP1 is polyglutamylated.

The presence of an acidic posttranslational modification like polyglutamylation could compensate for the reduced acidic amino acid content at the C-terminal domain of dNAP1, thus making native dNAP1 CTAD competent for *in vitro* nucleosome dissociation. To test this hypothesis, we first probed the purified native dNAP1 fraction for polyglutamylation with anti-rabbit dNAP1 antibodies and anti-mouse mAb GT335 antibodies (for polyglutamylation) (Figure 22A & B). The result clearly indicates the presence of the polyglutamylation modification on native dNAP1. It is important to note that the mAb GT335 is highly specific to the branched polypeptide modification and does not recognize random linear stretches of glutamates as exemplified by the inability of these antibodies to recognize the recombinant yNAP1 and dNAP1 polypeptides, both of which contain long stretches of glutamates at the C-terminus (Figure 22A & B). The native dNAP1 fraction was also detected with secondary probes containing

distinct fluorescent tags on anti-mouse and anti-rabbit secondary antibodies (mentioned in experimental procedures) to ensure co-localization of the two signals to the same band (Supplementary Figure A3.iii.), indicating that the modification does indeed exist on dNAP1. Future mass spectrometric analyses also confirm the presence of polyglutamylation on the native dNAP1 protein. Closer examination of the native dNAP1 fractions on a higher percentage PAGE gel (Figure 22C-E) indicated three bands corresponding to dNAP1 (Figure 22C & D). Two of the three bands interacted with mAb GT335 (Figure 22D & E), indicating the presence of a mixed population of polyglutamylated and non-polyglutamylated dNAP1 species. A mixture of competent and non-competent native dNAP1 CTAD species could explain why at the same molar excess, nucleosome disassembly with native dNAP1 was not as complete as with yNAP1 (Figure 21B).

In order to determine if the modification supplements the dNAP1 CTAD making it competent to modulate chromatin structure, we identified the location and extent of the polypeptide modification on native dNAP1 using mass spectrometric techniques. In-gel digests were performed on both polyglutamylated native dNAP1 bands identified in Figure 22E. The same procedure was also conducted on recombinant dNAP1 that was unreactive to the GT355 antibody. The in-gel digests and mass spectrometric analyses aid direct examination of the modification status of dNAP1 as it exists *in vivo*. Two different proteolytic enzymes were used in this study- Asp-N and Trypsin. Asp-N has target sites on dNAP1 that enable digestion of the C-terminal region into small

fragments. Trypsin has digestion sites that generate peptide fragments from the core domain of dNAP1, which are suitable for subsequent MALDI and MS/MS analyses. The digestion profiles of recombinant dNAP1 and the polyglutamylated native dNAP1 bands- K_H and K_L (K_H and K_L represent the Higher and the Lower polyglutamylated bands in Figure 22E.) in the negative reflector mode are represented in Figure 23A for Asp-N and Figure 23B for trypsin digestion.

From the comparative mass spectrometric peptide patterns generated from native dNAP1 and recombinant dNAP1, difference peaks between recombinant dNAP1 and native dNAP1 (K_H and K_L) that yielded positive and reproducible results are highlighted in Figure 23 (with Asp-N and Trypsin). Table IV is a summary of the mono MH- (molecular ion) values with the peptide sequences of interest, the number of glutamyl units as well as the mono MH- value seen solely in the native dNAP1 spectra. This information allows us to perform the MS/MS analysis on these individual peaks to confirm the appropriate target sequence as well as to determine the approximate residue within the sequence that is polyglutamylated. Figure 24 shows the raw MS/MS data for the difference peak with an MH- value of 2328.895. Table IV indicates the values and the appropriate sequence of the corresponding ions generated, when the residue Glu 342 was assigned the target for 10 glutamyl units. The calculated masses of the a and b ions indicate successful identification of Glu-342 as the target residue containing 10 glutamyl units. Similar analysis of the difference peak in the trypsin digest spectra between recombinant dNAP1 and native dNAP1 (K_H) (Figure 24B) indicated the possibility of a second polyglutamylation site within the core domain

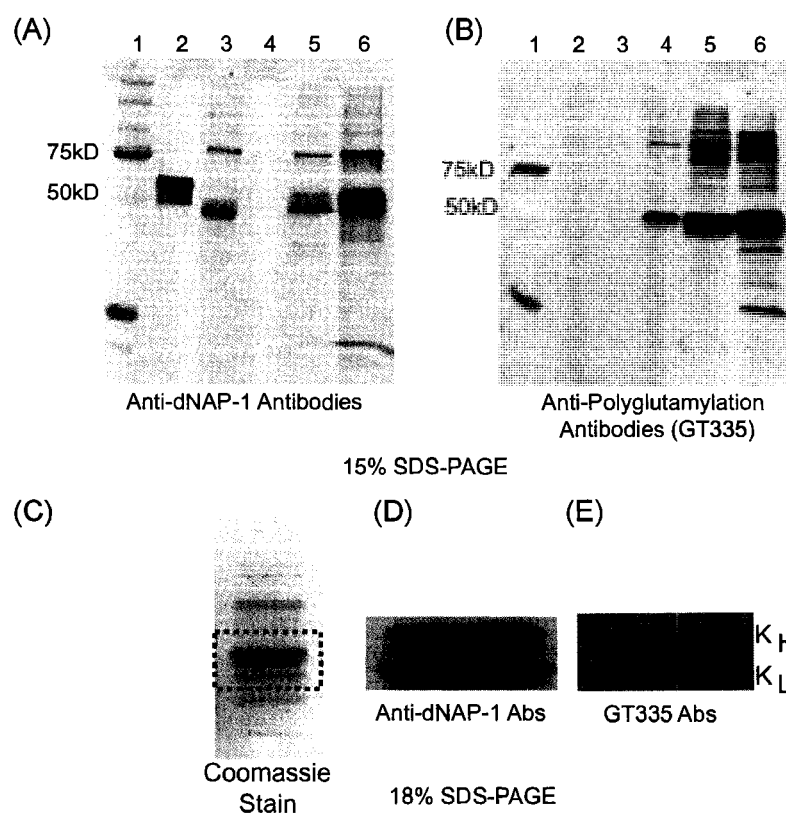


Figure 22: Native dNAP1 is polyglutamylated. (A) & (B) represent western blot analysis indicating the presence of dNAP1 and polyglutamylation, respectively, in native dNAP1 fractions I and II. The same samples were analyzed on two different gels and were probed with the corresponding antibodies indicated below the blot. Lane 1: Protein molecular weight marker, Lane 2: recombinant yNAP1, Lane 3: rdNAP1, Lane 4: Waste, Lane 5: native dNAP1 fraction I and Lane 6: native dNAP1 fraction II. The above samples were analyzed on 15% SDS-PAGE gels. (C) Representation of the purified ndNAP1 fraction II on an 18% SDS PAGE gel stained with coomassie. The sample was analyzed on separate gels and probed with dNAP1 (D) and GT335 (E) antibodies. The two bands represented in the Panel D were assigned K_H (higher band) and K_L (lower band) for convenience during subsequent mass spectrometric analysis.

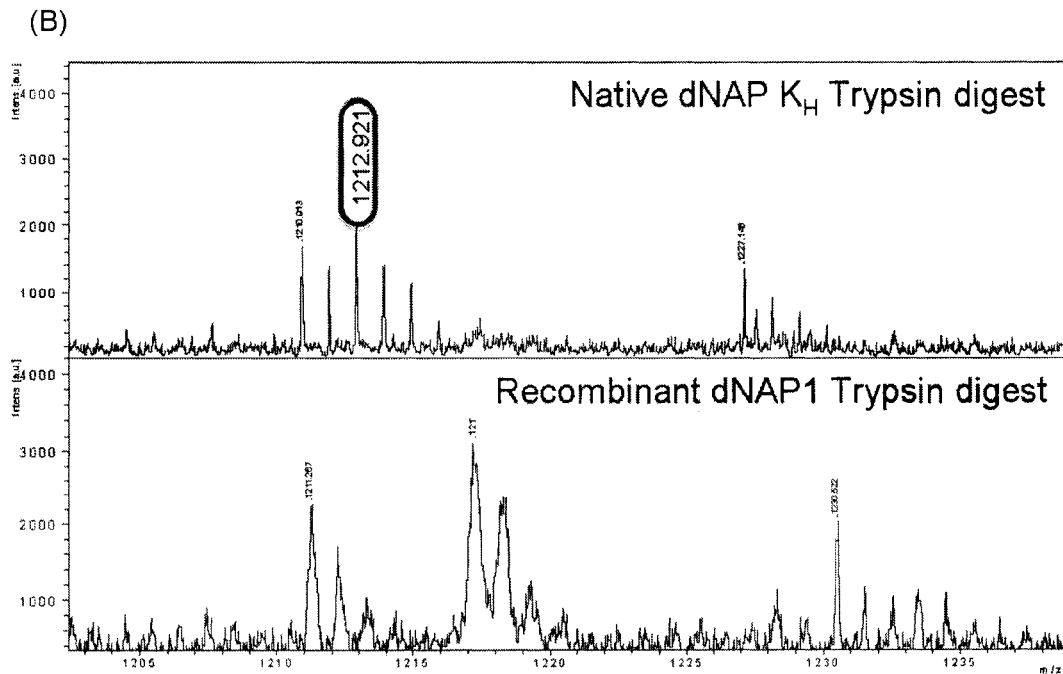
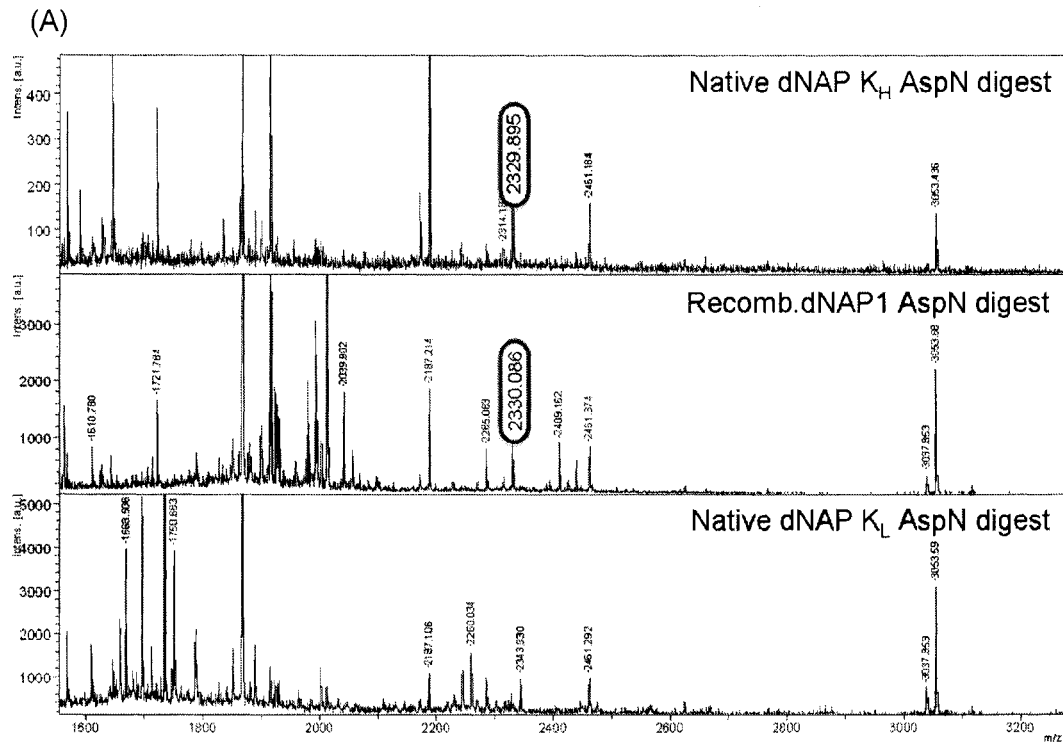


Figure 23: Peptide mass spectra comparing native dNAP1 K_H and K_L species with rdNAP1. (A) MALDI spectra of the peptides generated by digestion of native dNAP1 (K_H & K_L) and rdNAP1 species with Asp-N in negative reflector mode. The m/z values range between 1550-3200. (B) MALDI spectra of the peptides generated by digestion of native dNAP1 (K_H) and rdNAP1 species with trypsin in negative reflector mode. The m/z values range between 1200-1250. The highlighted residues correspond to m/z values that were significant in ndNAP1 (K_H and K_L) spectra and absent in rdNAP1 spectra. These peaks were also found to be close to the projected m/z values calculated as shown in Table IV.

TABLE IV

<i>Range</i>	<i>monoMH-</i>	<i>Sequence</i>	<i>Identification</i>	<i># of glutamate units</i>	<i>Projected m/z</i>	<i>Observed m/z</i>
X-65 (Asp-N)	424.136	DEY	dNAP-1 (341-343)	10	1714.136	1714.865
X-64 (Asp-N)	1040.334	DENEED E Y	dNAP-1 (336-343)	10	2330.348	2329.895
X-66 (Trypsin)	567.315	H K ER	dNAP-1 (255-258)	5	1212.315	1212.92
X-67 (Trypsin)	302.162	ER	dNAP-1 (257-257)	5	947.162	947.675

Mass of a single glutamyl unit is 129 Da

MH- value of the sequence + (# of glutamyl units) X 129.

of native dNAP1 (Table IV). Since the central NAP-domain is highly conserved among the various members of the NAP-family of proteins, the polyglutamylation sites in dNAP1 were mapped upon the known structure of yeast NAP1. The first polyglutamylation site is represented as the unstructured CTAD (this domain was not modeled in the initial yNAP1 structure) and the second site is located at the loop connecting the β -hairpin comprising the NLS (Figure 25 A&B). The N-terminus could also be a potential target for this modification, but we have been unsuccessful in obtaining optimal fragmentation of the native dNAP1 N-terminus due to lack of a suitable enzyme for in gel digests and subsequent MS analysis.

In summary, the target residues identified so far for polyglutamylation are Glu-342, and associated with 10 glutamyl residues, and Glu-257, located at the NLS and containing five glutamyl acids. Experiments aimed at looking at the distribution of polyglutamylated dNAP1 between cytoplasmic and the nuclear extracts revealed the presence of a predominant K_H band in the nuclear fraction and both K_H and K_L bands in the cytoplasmic fraction (Figure 26). This may indicate a potential role of polyglutamylation in the regulation of the cellular localization of dNAP1. Aminoacid sequence alignment of human NAP1 & NAP2, dNAP1 and yNAP1 reveals that the residue dNAP1 Glu-342 and Glu-257 are conserved in the human NAP species but not in yNAP1 (Supplementary Figure A4.i and ii). This along with the fact that yNAP1 is not polyglutamylated (Supplementary Figure A5.i and ii A4.i and ii) might indicate the preference for this modification in higher eukaryotes.

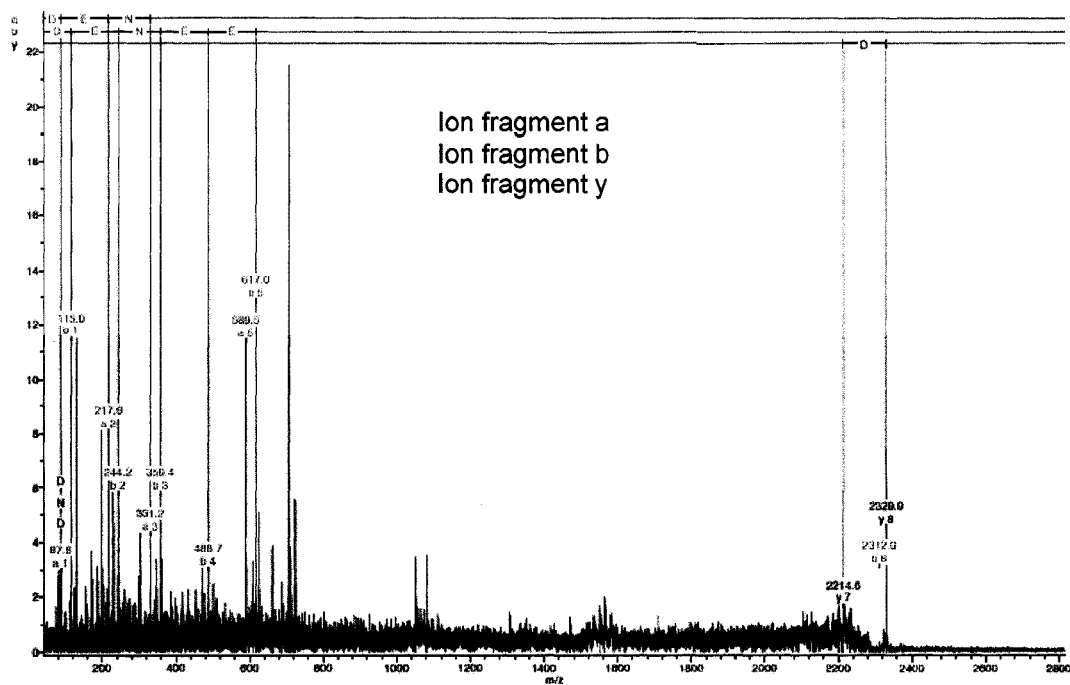


Figure 24: Glu 342 is the target residue for polyglutamylation of native dNAP1 at the C terminus. The raw MS/MS spectral analysis is represented above along with the corresponding masses of the various ion fragment peaks generated. The a, b and y ion fragments are represented in green, red and blue respectively. The correlation of the various masses with amino acid residues in the peptide fragment is represented in Table V. The m/z values range from 100-2500.

TABLE V

Calculated Masses of Ion Fragments
DENEED³⁴²Y - 10 Glutamic acid residues

N-term	Ion	a	b	y	C-term	Ion
1	D	88.0	116.0	182.1	8	Y
2	E	217.1	245.1	1598.5	7	E*
3	N	331.1	359.1	1713.6	6	D
4	E	460.2	488.2	1842.6	5	E
5	E	589.2	617.2	1971.6	4	E
6	D	704.2	732.2	2085.7	3	N
7	E*	2120.7	2148.7	2214.7	2	E
8	Y	2283.7	2311.7	2329.8	1	D

* Represents the Glu-342 residue containing 10 glutamyl units. The BioTools Version 3.0 software calculates the masses of the various possible ion fragments when the 10-glutamyl branched polyglutamylation modification is present on Glu-342. The peaks corresponding to these calculated values are then identified in the experimental data. Correlation between the calculated values and the experimental masses presents a valid model.

5.5 DISCUSSION

NAP1 is a multifunctional protein and is in the midst of a highly complex network of cellular processes (102,119). While the fundamental function of NAP1 is that of a H2A/H2B dimer chaperone (117,139), it is capable of numerous other fundamental cellular processes (108,119). This is largely due to the diverse protein binding partners, regulated cellular localization, and potentially also because of the ability of NAP1 to be posttranslationally modified (108,119).

NAP1 is a substrate for a number of posttranslational modifications. Recently it has been shown that regulation of γ NAP1 phosphorylation is essential for its nuclear import and normal cell-cycle progression (125). NAP1 is also a substrate for p300-mediated acetylation, presumably in a cell-cycle dependent manner (126). Human NAP1 and NAP2 are also known to be polyglutamylated.

In this study we provide strong evidence to support a difference in the chromatin-modulating function between native dNAP1 and recombinant dNAP1. We have shown the purified native dNAP1 is polyglutamylated in at least two positions. One of two polyglutamylation target sites identified in this study lies in the acidic C-terminus (128,129). Most importantly we have shown that the polyglutamylated species with 10 glutamyl units in the C-terminal domain could make native dNAP1 capable of nucleosome dissociation *in vitro*. In particular, this modification may compensate for the difference in acidic amino acid content at the CTAD of dNAP1 (when compared to γ NAP1 CTAD) making it compete enough to change nucleosome structure. This is further confirmed by the ability

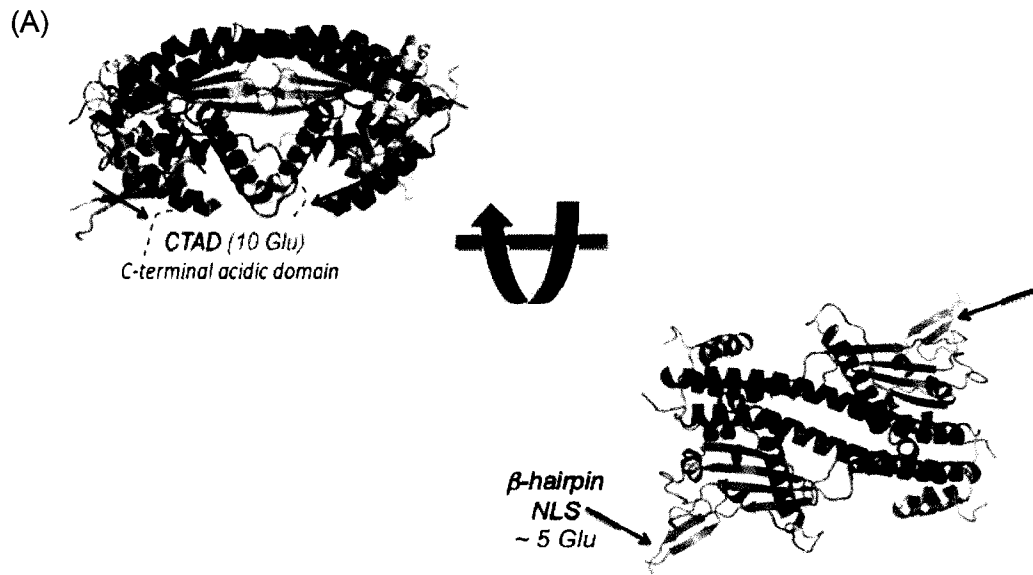
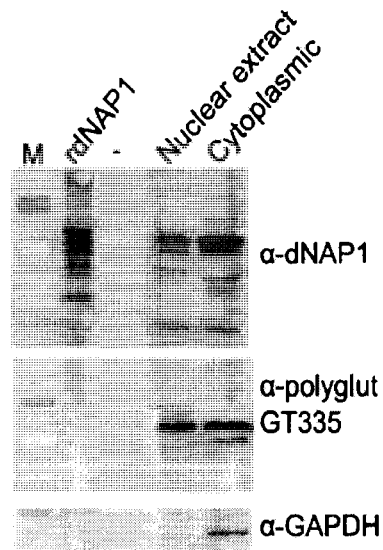


Figure 25: Target dNAP1 polyglutamylation sites in a structural context. The yNAP1 structure was used to locate the target modifications sites in dNAP1 since the central NAP domain is conserved among the different NAP-family members. (A) Putative dNAP1 polyglutamylation site at the C terminus acidic domain (CTAD) and (B) Second putative dNAP1 polyglutamylation site located at the NLS (β -hairpin). The black arrows represent the target sites superimposed on the yNAP1 structure and the number of glutamyl units associated with these sites is indicated in red.



15% SDS PAGE, Western Blot

Figure 26: Cellular localization of polyglutamylated dNAP1. Nuclear and cytoplasmic extracts purified from *Drosophila* embryos were probed with dNAP1 antibodies (α -dNAP1) and anti-polyglutamate antibodies (α -polyglut GT335). GAPDH antibodies (α -GAPDH) were used to probe for the presence of GAPDH- a cytoplasmic marker. Recombinant dNAP1 (rdNAP1) was used as a positive antibody control.

of the dNAP1 construct with the CTAD of yNAP1 to mediate nucleosome dissociation. The implications of NAP-mediated nucleosome dissociation *in vivo* remain unknown, but transcription by RNA polymerase II is known to be accompanied by increased chromatin dynamics including nucleosome eviction and deposition (73-76). In particular, H2A/H2B chaperone-FACT travels with the pol II complex, binds H2A/H2B dimer and mediates nucleosome disassembly and reassembly in a transcription-dependent manner (140). It is possible that NAP1 has a similar nucleosome dissociation function *in vivo* and the presence of a competent CTAD is essential to mediate this process.

The obvious explanation for the difference in activity of native dNAP1 versus recombinant dNAP1 (rdNAP1) with respect to nucleosome dissociation would be difference in affinity for binding to H2A/H2B dimers. Unpublished quantitative data in our lab suggests no difference in the affinity of histone-dimer binding to yNAP1/domain swap NAP1 (the two constructs with competent acidic C-terminal tail) and recombinant dNAP1. The other explanation for this difference in activity is based on the ability of the acidic C-terminus of NAP1 to potentially compete with nucleosomal DNA for binding H2A/H2B dimers in the nucleosomal context. The outcome of this competition results in nucleosome sliding/relocation and, in extreme cases, nucleosome disassembly (131). So far the exact mechanism of NAP-mediated disassembly and sliding has not been elucidated. However, this study reinstates the importance of a competent CTAD in NAP1-mediated regulation of nucleosome fluidity and the ability of higher eukaryotes to maintain C-terminus function through polyglutamylation.

Our studies have also indicated the possibility of a second site for polyglutamylation: Glu257 in the core domain of dNAP1 containing five glutamyl units. Amino acid sequence alignments with yNAP1 reveal that this residue resides in the flexible loop connecting the short anti-parallel β sheet containing β 5- β 6 (121). This highly basic region is known to contain the Nuclear Localization Sequences (NLS) (121,125). Glu257 is not conserved among other NAP1 species (Supplementary Figure A4.ii). It is possible that, apart from the nucleosome disassembly function imparted by the C terminal modification, polyglutamylation in the core dNAP1 domain also serves to regulate nuclear localization. Both the polyglutamylated dNAP1 species (Figure 26) are represented in the cytoplasmic fraction of the *Drosophila* embryos (though not in equal amounts). However, only the slower migratory species is well represented in the nuclear fraction, indicating a potential correlation between the patterns of dNAP1 polyglutamylation and its cellular localization. Nuclear localization of NAP1 is essential for its function in leaf development and cell proliferation in *Arabidopsis thaliana*. In particular, NAP1 promotes cell division as a function of its farnesylation status (127) – a posttranslational modification that promotes anchoring of proteins to lipid membranes.

The nature and cellular localization of the modifying enzyme/s involved in the maintenance of dNAP1 polyglutamylation remain unknown to date. α and β tubulin proteins show different levels of polyglutamylation both in terms of percentage of modified species and in the length of the polyglutamic acid branch during neuronal differentiation (134,135). It has also been shown that the binding

of some microtubule-associated proteins is a function of the length of the polyglutamic acid chain in tubulin (141,142). One can therefore speculate that the polyglutamylation of dNAP1 species can regulate association with various proteins (like transcription factors) and hence regulate NAP1 function.

Regnard and colleagues have shown that hNAP1 may also be polyglutamylated at the N-terminus with five glutamyl units (128). This remains a possibility in native dNAP1 as well.

This study as well as others have demonstrated that NAP1 is polyglutamylated in humans, *Xenopus* (128) and *Drosophila*, but not in yeast (*Saccharomyces cerevisiae*). The target polyglutamylation residue in the CTAD of dNAP1 (Glu-342) is conserved in human NAP1 and NAP2 and is replaced by an aspartate residue in yNAP1. Taken together with the fact that hNAP1, xNAP1 and dNAP1 have fewer acidic amino acids in the CTAD when compared to yNAP1, it is possible that this NAP-modification is more pronounced in higher eukaryotes.

In summary we have shown native dNAP is polyglutamylated and contains at least two target sites for this modification: the CTAD and the NLS. We have also demonstrated that the C-terminal polyglutamylation could regulate dNAP1-mediated nucleosome disassembly. This is based on the fact that the unmodified dNAP1 is incapable of nucleosome dissociation but, when its CTAD is substituted with the more acidic yNAP1 CTAD, it is made competent for this function. Polyglutamylation may be a mechanism by which NAP1 in higher

eukaryotes is supplemented with acidic amino acids at the CTAD to propagate chromatin-modulating function.

5.6 Acknowledgements

I would like to thank Dr. Carsten Janke for the monoclonal anti-polyglutamylation antibodies (mAb GT335), Dr. Takashi Ito for the dNAP1 antibodies and Sue Koplín-Krueger at the Macromolecular Resource Facility at Colorado State University for her help with the mass spectrometry data. A special thanks to Dr. Jim Kadonaga for the frozen dechorionated *Drosophila* embryos and Dr. Natalie Ahn. Dr. Paul J. Laybourn for his help with the S190 extracts and for reagents. This work would not be possible without the help of Pam Dyer for the reagents, Kitty Brown and Dr. YoungJun Park for their advice support and reagents.

5.7 SUPPLEMENTARY DATA

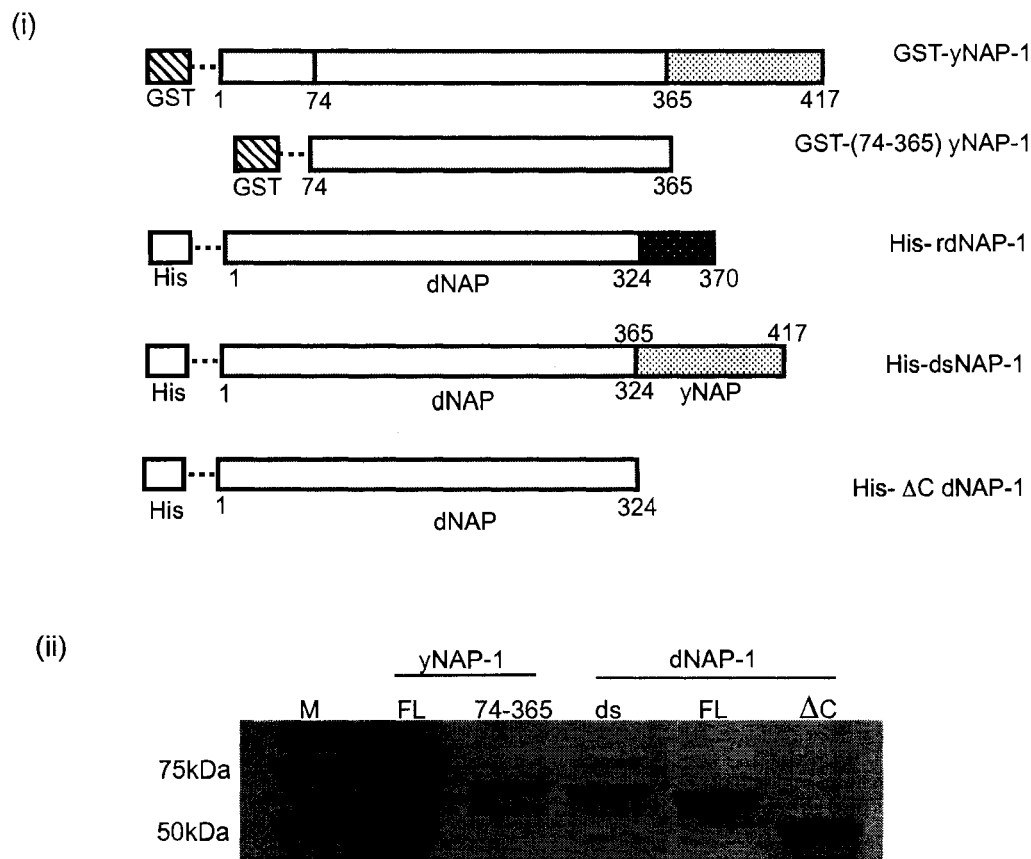


Figure A1: The recombinant NAP1 species used in this study. (i) Schematic of all the recombinant NAP1 constructs used in this study. Recombinant dNAP1 and Domain swap NAP1 are referred to as rdNAP1 and dsNAP1 in this study. (ii) 15% SDS-PAGE gel stained with coomassie showing all the purified recombinant proteins. All the proteins contain GST/His tags to help distinguish NAP1-dimer complexes from NAP1 alone in subsequent assays.

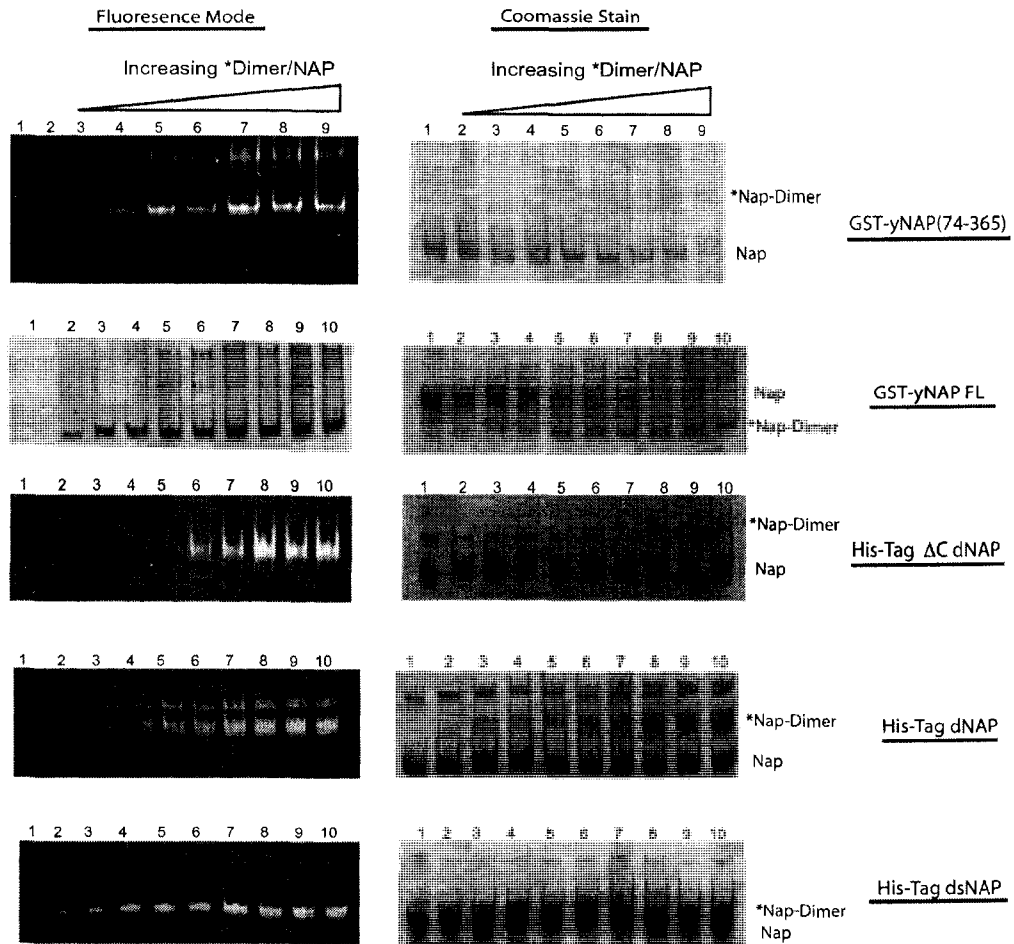


Figure A2: All the recombinant NAP constructs bind labeled histone dimers. The concentration of NAP in each reaction is 10 μ M. Lane 1 represents the NAP without histone dimer. Lanes 2-10 represent 0.2, 0.3, 0.4, 0.5, 0.6, 0.7, 0.8, 0.9, 1.0 molar excess of labeled dimer. The NAP1-dimer complexes were analyzed on a 5% Native gel and first viewed in the fluorescent mode and then stained with coomassie stain for visualization of the protein content.

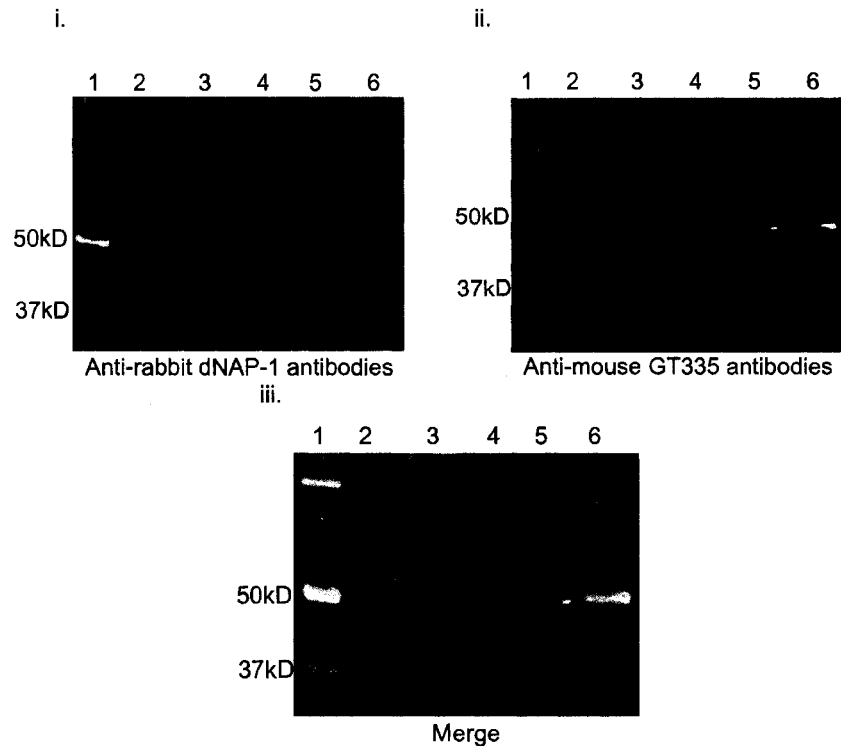


Figure A3: Colocalization of dNAP1 and polyglutamylation signal. The samples used in Figure 4 were used for probing with anti-rabbit dNAP1 antibodies and anti-mouse mAb-GT335, but with secondary antibodies that are differentially labeled for visualization of dNAP1 and polyglutamylation signal on the same gel using different channel laser sources in an Odyssey® Infrared Imaging system. The 800nm channel allows for visualization of the bands probed with anti-rabbit secondary antibodies (green), while the 700nm channel allows for the visualization of the bands probed with anti-mouse secondary antibodies (red). A yellow signal is observed when there is comigration of the red and green signal. (i) Represents a western blot analysis indicating the migration of the NAP1 bands in green (800nm channel) and (ii) represents the same blot indicating the polyglutamylation bands in red (700nm channel). (iii) Represents a merged image obtained from both the channels. Lane 1: protein molecular weight marker, Lane 2: recombinant yNAP1, Lane 3: recombinant dNAP1, Lane 4: waste, Lane 5: native dNAP1 fraction I and Lane 6: native dNAP1 fraction II.

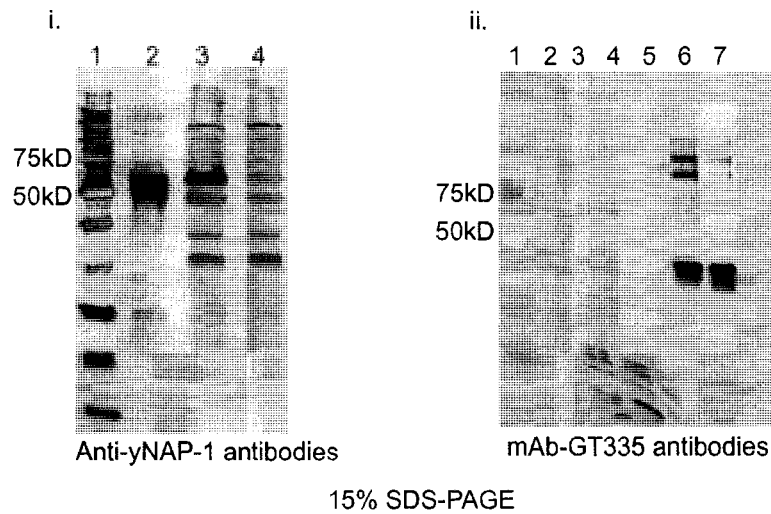


Figure A4: Native yNAP1 is not polyglutamylated. Extracts from wild-type yeast, Δ yNAP1 and Δ VPS75 (yNAP1 homologue) strains were prepared and probed with anti-yNAP1 antibodies (i) and mAb-GT335 antibodies (ii). In both panels, Lane1: protein molecular weight markers, Lane 2: recombinant yNAP1, Lane 3: extracts of wild-type yeast strain, Lane 4: extracts of Δ yNAP1 yeast strain. In Panel (ii) Lane 6: native dNAP1 fraction I and Lane 7: native dNAP1 fraction II. The native dNAP1 fractions were used as positive controls for blot analysis with mAb-GT335.

CHAPTER 6

Contribution to other publication

The temperature of flash-cooling has dramatic effects on the diffraction quality of nucleosome crystals.

Acta Crystallogr D Biol Crystallogr. 2005 Jul;61(Pt 7):891-8.

Edayathumangalam RS, Luger K.

In this paper, I helped in the harvesting, treatment and data collection process for nucleosome crystals subjected to cryo-cooling at liquid propane temperatures of 173K, 153K, 133K and 113K. The paper demonstrated that changing the optimal temperature (~153K) for propane cooling of nucleosome crystals results in increased crystal fragility, tendency for high mosaicity, and lattice changes.

CHAPTER 7

Perspective and Future Directions

The first part of my dissertation focused on examining the effect of sequence-specific DNA cross-linking drugs on nucleosomal DNA. Most studies involving DNA cross-linking agents focus their effects on unassembled, linear DNA. The results in Chapter 2 demonstrates the ability of the photoreactive anti-cancer drug NVOC to preferentially monoalkylate nucleosomal DNA when compared to unassembled DNA. This is consistent with the notion that the packaging of DNA into nucleosome protects genomic DNA from DNA damaging agents. Our studies also revealed that NVOC-mediated cross-links on linear DNA decrease *in vitro* transcription and chromatin assembly levels when used as a template. We propose that the ability of this class of compounds to act at the level of transcription and chromatin assembly may contribute significantly to their observed efficacy as anti-cancerous agents.

In order to understand the preferential ability of the photoreactive NVOC to mediate monoalkylation on nucleosomal DNA versus unassembled DNA, attempts were made to co-crystallize FR900482 and FK317 with nucleosomes (Chapter 3). A partially refined structure of the FK317-nucleosome complex was obtained at 3.4Å. The structure did not reveal conclusive evidence that could explain the preferential NVOC-mediated monoalkylation on nucleosomes. Crystals formed with these drugs resulted in reduced diffraction quality and high

mosaicity. Further efforts should be directed towards improving the overall resolution and the occupancy of the drug in the co-complex with nucleosomes. A vast number of crystallization screens and cryoprotectant screens should help in obtaining crystals with optimal resolution. A quantitative system must be developed to look at the affinity of binding of the different derivatives to nucleosomal DNA. This will enable us to screen for those derivatives that will show a higher occupancy in the co-crystal structure.

Studies involving chromatin dynamics have revolved around histone modifications, histone chaperones, remodelers, etc. The second part of the dissertation investigates another factor in the regulation of chromatin dynamics: NAP1 modification. Our study showed that the incompetence of recombinant dNAP1 CTAD in chromatin-related function *in vitro* is alleviated by the presence of a unique branched acidic polypeptide post-translational modification: polyglutamylation. Two polyglutamylation sites were identified in native dNAP1, one was found at the C-terminus containing ten glutamyl units, while the second site was found at the Nuclear Localization Sequence (NLS) containing five glutamyl units. This is the first study that has provided evidence for the effect of any post-translational modification on the chromatin-related function of dNAP1 *in vitro*.

The *in vivo* role of the individual polyglutamylation modifications in dNAP1 function can be determined by *Drosophila* genetics. Since our lab does not have the expertise to conduct live cell imaging we hope to collaborate with experts in the field to look at localization of dNAP1 in the presence and absence of one or

both polyglutamylation modifications and its resultant effect on chromatin-related function.

The polyglutamylase enzyme that mediates this unique post-translational modification has been identified as the TTLL4 (Tubulin-Tyrosine Ligase-Like 4 protein family) in HeLa cells (129). However, the same enzyme in *Drosophila* embryo extracts has yet to be identified. Efforts should be directed towards identification and characterization of the dNAP1 polyglutamylase in *Drosophila* embryos. *In vitro* polyglutamylase reactions with this purified enzyme fraction will allow us to identify the target peptide sequence requirements for this enzyme as well as other potential substrates. This system can also help us determine the turnover of this polypeptide modification in the presence of a yet-to-be-identified deglutamylase. Thus, with an optimized *in vitro* polyglutamylase system, one can look at sequence requirements and regulation for polyglutamylation in a systematic manner.

It has been shown conclusively that NAP1 polyglutamylation is found in *Drosophila*, *Xenopus* and *Humans*, while it remains absent in *Saccharomyces cerevisiae* (current work and (128). Recent findings have shown that fission yeast (more than *S.cerevisiae*) may be a more ideal system to understand chromatin structure and function since a number of proteins involved in metazoan cell division, chromosome structure, and maintenance in *Schizosaccharomyces pombe* (*S.pombe*) but not in *S.cerevisiae* (143). In light of these studies, we would like to investigate the possibility of polyglutamylated yNAP1 in *S.pombe* using a similar approach as mentioned in Chapter 5.

We would also like to investigate the possibility of regulation of polyglutamylated dNAP1 through various stages of *Drosophila* development. For this purpose we would require *Drosophila* samples at the different larval and pupal stages and finally the adult species. Western blot analyses of the extracts made from these samples with dNAP1 as well as anti-polyglutamylation antibodies (GT335) will enable us to look at the levels of polyglutamylated dNAP1 throughout the various developmental stages. α -tubulin antibodies will be used to probe for tubulin in these extracts not just as an internal load control but also to distinguish between the modified dNAP1 species versus modified tubulin species. Work to this effect is already underway with samples obtained from Dr. Noreen Reist at Colorado State University (Department of Biomedical Sciences).

As indicated earlier, NAP1 is subject to a number of other post-translational modifications (Figure 19). We hope to determine the target sites for this modification as well as their effect on NAP1 function. This will enable us to understand the mechanism by which NAP1 is capable of regulating chromatin dynamics and how this regulation is affected by NAP1 post-translational modifications. We believe that NAP1 modification may be another critical regulating nucleosome dynamics along with histone modifications.

REFERENCES

1. Zwelling, L. A., Anderson, T., and Kohn, K. W. (1979) *Cancer Res* **39**, 365-369
2. Millard, J. T. W., M.F.; Raucher, S.; Hopkins, P.B. (1990) *J. Am. Chem. Soc.* **112**, 3637-3641

3. Sastry, M., Fiala, R., Lipman, R., Tomasz, M and Patel, D.J. (1995) *J Mol Biol* **247**, 338-359
4. Rink, S. M., Lipman, R., Alley, S. C., Hopkins, P. B., and Tomasz, M. (1996) *Chem Res Toxicol* **9**, 382-389
5. Tomasz, M., Lipman, R., Chowdary, D., Pawlak, J., Verdine, G.L and Nakanishi, K. (1987) *Science* **235**, 1204-1208
6. Williams, R. M., Rajski, R.M. and Rollins, B.S. (1997) *Chemistry and Biology* **4**, 127-137
7. Iyer, V. N. a. S., W.A. (1963) *Proc. Nat. Acad. Scio, U.S.A* **50**, 355-362
8. Teng, S. P., Woodson, S. A., and Crothers, D. M. (1989) *Biochemistry* **28**, 3901-3907
9. Wolkenberg, S. E., and Boger, D. L. (2002) *Chem Rev* **102**, 2477-2495
10. Beckerbauer, L., Tepe, J.J., Eastman, A.R., Mixer, F.P., Williams, R.M. and Reeves, R. (2002) *Chemistry and Biology* **9**, 427-441
11. Judd, T. a. W., R.M. (2002) *Organic letters* **0**, A-D
12. Kornberg, R. D., and Klug, A. (1981) *Sci Am* **244**, 52-64
13. Workman, J. L., and Kingston, R. E. (1998) *Annu Rev Biochem* **67**, 545-579
14. Luger, K., Mader, A.W., Richmond, R.K., Sargent D.F. and Richmond, T.J. (1997) *Nature* **389**, 251-260
15. Davey, C. A., and Richmond, T. J. (2002) *Proc Natl Acad Sci U S A* **99**, 11169-11174
16. Richmond, T. J., and Davey, C. A. (2003) *Nature* **423**, 145-150
17. Millard, J. T., Spencer, R. J., and Hopkins, P. B. (1998) *Biochemistry* **37**, 5211-5219
18. Lawley, P. D., Lethbridge, J. H., Edwards, P. A., and Shooter, K. V. (1969) *J Mol Biol* **39**, 181-198
19. Sancar, A. (1996) *Annu Rev Biochem* **65**, 43-81
20. Sartorelli, A. C. (1986) *Biochem. Pharmacol.* **35**, 67-69
21. Tomasz, M. (1995) *Chem Biol* **2**, 575-579

22. Pratt, W. B., Ruddon, R.W., Ensminger, W.D., Maybaum, J. (ed) (1994) *The Anti-Cancer Drugs*, 2nd Ed., Oxford University Press, New York
23. Uchida, I., Takasae, S., Kayakiri, H., Kiyoto, S and Hashimoto, M. (1987) *J.Am.Chem.Soc* **109**, 4108-4109
24. Inami, M., Kawamura, I., Tsujimoto, S., Nishigaki, F., Matsumoto, S., Naoe, Y., Sasakawa, Y., Matsuo, M., Manda, T., and Goto, T. (2002) *Cancer Lett* **181**, 39-45
25. Naoe, Y., Inami, M., Kawamura, I., Nishigaki, F., Tsujimoto, S., Matsumoto, S., Manda, T., and Shimomura, K. (1998) *Jpn J Cancer Res* **89**, 666-672
26. Naoe, Y., Inami, M., Matsumoto, S., Nishigaki, F., Tsujimoto, S., Kawamura, I., Miyayasu, K., Manda, T., and Shimomura, K. (1998) *Cancer Chemother Pharmacol* **42**, 31-36
27. Naoe, Y., Inami, M., Matsumoto, S., Takagaki, S., Fujiwara, T., Yamazaki, S., Kawamura, I., Nishigaki, F., Tsujimoto, S., Manda, T., and Shimomura, K. (1998) *Jpn J Cancer Res* **89**, 1306-1317
28. Naoe, Y., Inami, M., Takagaki, S., Matsumoto, S., Kawamura, I., Nishigaki, F., Tsujimoto, S., Manda, T., and Shimomura, K. (1998) *Jpn J Cancer Res* **89**, 1047-1054
29. Naoe, Y., Kawamura, I., Inami, M., Matsumoto, S., Nishigaki, F., Tsujimoto, S., Manda, T., and Shimomura, K. (1998) *Jpn J Cancer Res* **89**, 1318-1325
30. Li, V. K., H. (1991) *J. Am. Chem. Soc.* **113**, 275-283
31. Kohn, H. L., V.; Shiltz, P.; Tang, M. (1992) *J. Am. Chem. Soc.* **114**, 9218-9220
32. Kumar, S., Lipman, R. and Tomasz, M. (1992) *Biochemistry* **31**, 1399-1407
33. Millard, J. T., Spencer, R.J. and Hopkins, P.B. (1998) *Biochemistry* **37**, 5211-5219
34. Dyer, P. N., Edatathumangalam, R.S., White, C.L., Bao, Y., Chakravarthy, S., Muthuraja, U.M. and Luger, K. (2004) *Methods Enzymol.* **375**, 23-44

35. Muthurajan, U. M., Park, Y. J., Edayathumangalam, R. S., Suto, R. K., Chakravarthy, S., Dyer, P. N., and Luger, K. (2003) *Biopolymers* **68**, 547-556
36. Sambrook, J., and Russell, D.W. (2001) *Molecular Cloning- A laboratory manual*, Third Ed., 2, Cold Spring Harbour Laboratory Press, New York
37. Fyodorov, D. V. K., J.T. (2003) *Methods Enzymol.* **371**, 499-515
38. Cech., T. R. (1981) *Biochemistry* **20**, 1431
39. Fletcher, T. M., Krishnan, U., Serwer, P. and Hansen, J. (1994) *Biochemistry* **33**, 2226-2233
40. Fletcher, T. M., Krishnan, U., Serwer, P. and Hansen, J. (1994) *Biochemistry* **33**, 10859-10863
41. Anderson, M. G. a. D., W.S. (1994) *Nucleic Acids Res* **22**, 3194-3201
42. Krude, T. (1999) *Eur. J. Biochem* **263**, 1-5
43. Tyler, J. K. (2002) *Eur J Biochem* **269**, 2268-2274
44. Kashanchi, F., Duvall, J. F., Kwok, R. P., Lundblad, J. R., Goodman, R. H., and Brady, J. N. (1998) *J Biol Chem* **273**, 34646-34652
45. Pan, S. S., Iracki, T., and Bachur, N. R. (1986) *Mol Pharmacol* **29**, 622-628
46. Rajski, S. R., Rollin, S.B. and Williams, R.M. (1998) *J.Am.Chem.Soc* **120**, 2192
47. Beckerbauer, L., Tepe, J.J., Cullision, J., Reeves, R. and Williams, R.M. (2000) *Chemistry and Biology* **7**, 805-812
48. Krude, T. (1995) *Curr. Biol* **5**, 1232-1234
49. Narlikar, G. J., Fan, H.Y. and Kingston, R.E. (2002) *Cell* **108**, 475-487
50. Kaufman, P. D., Kobayashi, R., Kessler, N., and Stillman, B. (1995) *Cell* **81**, 1105-1114
51. Nabatiyan, A. a. K., T. (2004) *Mol. Cell. Biol* **24**, 2853-2862
52. Oohara, I., and Wada, A. (1987) *J Mol Biol* **196**, 389-397
53. Oohara, I., and Wada, A. (1987) *J Mol Biol* **196**, 399-411

54. Allen, M. J., Dong, X. F., O'Neill, T. E., Yau, P., Kowalczykowski, S. C., Gatewood, J., Balhorn, R., and Bradbury, E. M. (1993) *Biochemistry* **32**, 8390-8396
55. Zhao, H., Zhang, Y., Zhang, S. B., Jiang, C., He, Q. Y., Li, M. Q., and Qian, R. L. (1999) *Cell Res* **9**, 255-260
56. Ito, T., Muramatsu, M., and Kadonaga, J. T. (1998) *Tanpakushitsu Kakusan Koso* **43**, 2087-2093
57. Simpson, R. T., and Stafford, D. W. (1983) *Proc Natl Acad Sci U S A* **80**, 51-55
58. Wang, H., Bash, R., Yodh, J. G., Hager, G. L., Lohr, D., and Lindsay, S. M. (2002) *Biophys J* **83**, 3619-3625
59. Norman, D., Live, D., Sastry, M., Lipman, R., Hingerty, B. E., Tomasz, M., Broyde, S., and Patel, D. J. (1990) *Biochemistry* **29**, 2861-2875
60. Gottesfeld, J. M., Melander, C., Suto, R. K., Raviol, H., Luger, K., and Dervan, P. B. (2001) *J Mol Biol* **309**, 615-629
61. Wemmer, D. E. (2000) *Annu Rev Biophys Biomol Struct* **29**, 439-461
62. Suto, R. K., Edayathumangalam, R. S., White, C. L., Melander, C., Gottesfeld, J. M., Dervan, P. B., and Luger, K. (2003) *J Mol Biol* **326**, 371-380
63. Edayathumangalam, R. S., Weyermann, P., Gottesfeld, J. M., Dervan, P. B., and Luger, K. (2004) *Proc Natl Acad Sci U S A* **101**, 6864-6869
64. Edayathumangalam, R. S., Weyermann, P., Dervan, P. B., Gottesfeld, J. M., and Luger, K. (2005) *J Mol Biol* **345**, 103-114
65. Fechter, E. J., and Dervan, P. B. (2003) *J Am Chem Soc* **125**, 8476-8485
66. Minor, Z. O. a. W. (1997) in *Methods in Enzymology* Vol. 276, pp. 307-326
67. Brunger, A. T., Adams, P. D., Clore, G. M., DeLano, W. L., Gros, P., Grosse-Kunstleve, R. W., Jiang, J. S., Kuszewski, J., Nilges, M., Pannu, N. S., Read, R. J., Rice, L. M., Simonson, T., and Warren, G. L. (1998) *Acta Crystallogr D Biol Crystallogr* **54**, 905-921
68. Jones, T. A., Zou, J. Y., Cowan, S. W., and Kjeldgaard, M. (1991) *Acta Crystallogr A* **47 (Pt 2)**, 110-119

69. Hansen, J. C. (2002) *Annu Rev Biophys Biomol Struct* **31**, 361-392
70. Polach, K. J., and Widom, J. (1995) *J Mol Biol* **254**, 130-149
71. Anderson, J. D., and Widom, J. (2000) *J Mol Biol* **296**, 979-987
72. Li, G., and Widom, J. (2004) *Nat Struct Mol Biol* **11**, 763-769
73. Bernstein, B. E., Humphrey, E. L., Liu, C. L., and Schreiber, S. L. (2004) *Methods Enzymol* **376**, 349-360
74. Kristjuhan, A., and Svejstrup, J. Q. (2004) *Embo J* **23**, 4243-4252
75. Lee, C. K., Shibata, Y., Rao, B., Strahl, B. D., and Lieb, J. D. (2004) *Nat Genet* **36**, 900-905
76. Schwabish, M. A., and Struhl, K. (2004) *Mol Cell Biol* **24**, 10111-10117
77. Kim, H. J., Seol, J. H., Han, J. W., Youn, H. D., and Cho, E. J. (2007) *Embo J* **26**, 4467-4474
78. Luger, K. (2006) *Chromosome Res* **14**, 5-16
79. Chakravarthy, S., Bao, Y., Roberts, V. A., Tremethick, D., and Luger, K. (2004) *Cold Spring Harb Symp Quant Biol* **69**, 227-234
80. Sullivan, S., Sink, D. W., Trout, K. L., Makalowska, I., Taylor, P. M., Baxevanis, A. D., and Landsman, D. (2002) *Nucleic Acids Res* **30**, 341-342
81. Chakravarthy, S., Park, Y. J., Chodaparambil, J., Edayathumangalam, R. S., and Luger, K. (2005) *FEBS Lett* **579**, 895-898
82. Suto, R. K., Clarkson, M. J., Tremethick, D. J., and Luger, K. (2000) *Nat Struct Biol* **7**, 1121-1124
83. Fan, J. Y., Gordon, F., Luger, K., Hansen, J. C., and Tremethick, D. J. (2002) *Nat Struct Biol* **9**, 172-176
84. Ausio, J., and Abbott, D. W. (2002) *Biochemistry* **41**, 5945-5949
85. Masumoto, H., Hawke, D., Kobayashi, R., and Verreault, A. (2005) *Nature* **436**, 294-298
86. Razin, S. V., Iarovaia, O. V., Sjakste, N., Sjakste, T., Bagdoniene, L., Rynditch, A. V., Eivazova, E. R., Lipinski, M., and Vassetzky, Y. S. (2007) *J Mol Biol* **369**, 597-607

87. Flanagan, J. F., Mi, L. Z., Chruszcz, M., Cymborowski, M., Clines, K. L., Kim, Y., Minor, W., Rastinejad, F., and Khorasanizadeh, S. (2005) *Nature* **438**, 1181-1185
88. Dorigo, B., Schalch, T., Bystricky, K., and Richmond, T. J. (2003) *J Mol Biol* **327**, 85-96
89. Gordon, F., Luger, K., and Hansen, J. C. (2005) *J Biol Chem* **280**, 33701-33706
90. Ruthenburg, A. J., Li, H., Patel, D. J., and Allis, C. D. (2007) *Nat Rev Mol Cell Biol* **8**, 983-994
91. Jenuwein, T., and Allis, C. D. (2001) *Science* **293**, 1074-1080
92. Becker, P. B. (2005) *Nat Struct Mol Biol* **12**, 732-733
93. Cairns, B. R. (2005) *Curr Opin Genet Dev* **15**, 185-190
94. McDaniel, I. E., Lee, J. M., Berger, M. S., Hanagami, C. K., and Armstrong, J. A. (2008) *Genetics* **178**, 583-587
95. Brown, E., Malakar, S., and Krebs, J. E. (2007) *Biochem Cell Biol* **85**, 444-462
96. Clapier, C. R., Langst, G., Corona, D. F., Becker, P. B., and Nightingale, K. P. (2001) *Mol Cell Biol* **21**, 875-883
97. Grune, T., Brzeski, J., Eberharter, A., Clapier, C. R., Corona, D. F., Becker, P. B., and Muller, C. W. (2003) *Mol Cell* **12**, 449-460
98. Langst, G., Bonte, E. J., Corona, D. F., and Becker, P. B. (1999) *Cell* **97**, 843-852
99. Auger, A., Galarneau, L., Altaf, M., Nourani, A., Doyon, Y., Utley, R. T., Cronier, D., Allard, S., and Cote, J. (2008) *Mol Cell Biol* **28**, 2257-2270
100. Lorch, Y., Zhang, M., and Kornberg, R. D. (1999) *Cell* **96**, 389-392
101. Schwanbeck, R., Xiao, H., and Wu, C. (2004) *J Biol Chem* **279**, 39933-39941
102. De Koning, L., Corpet, A., Haber, J. E., and Almouzni, G. (2007) *Nat Struct Mol Biol* **14**, 997-1007
103. Tagami, H., Ray-Gallet, D., Almouzni, G., and Nakatani, Y. (2004) *Cell* **116**, 51-61

104. Richardson, R. T., Batova, I. N., Widgren, E. E., Zheng, L. X., Whitfield, M., Marzluff, W. F., and O'Rand, M. G. (2000) *J Biol Chem* **275**, 30378-30386
105. Shintomi, K., Iwabuchi, M., Saeki, H., Ura, K., Kishimoto, T., and Ohsumi, K. (2005) *Proc Natl Acad Sci U S A* **102**, 8210-8215
106. Dutta, S., Akey, I. V., Dingwall, C., Hartman, K. L., Laue, T., Nolte, R. T., Head, J. F., and Akey, C. W. (2001) *Mol Cell* **8**, 841-853
107. Ray-Gallet, D., Quivy, J. P., Sillje, H. W., Nigg, E. A., and Almouzni, G. (2007) *Chromosoma* **116**, 487-496
108. Park, Y. J., and Luger, K. (2006) *Biochem Cell Biol* **84**, 549-558
109. Belotserkovskaya, R., Oh, S., Bondarenko, V. A., Orphanides, G., Studitsky, V. M., and Reinberg, D. (2003) *Science* **301**, 1090-1093
110. Angelov, D., Bondarenko, V. A., Almagro, S., Menoni, H., Mongelard, F., Hans, F., Mietton, F., Studitsky, V. M., Hamiche, A., Dimitrov, S., and Bouvet, P. (2006) *Embo J* **25**, 1669-1679
111. Ohkuni, K., Okuda, A., and Kikuchi, A. (2003) *Genetics* **165**, 517-529
112. Lankenau, S., Barnickel, T., Marhold, J., Lyko, F., Mechler, B. M., and Lankenau, D. H. (2003) *Genetics* **163**, 611-623
113. Rogner, U. C., Spyropoulos, D. D., Le Novere, N., Changeux, J. P., and Avner, P. (2000) *Nat Genet* **25**, 431-435
114. Daganzo, S. M., Erzberger, J. P., Lam, W. M., Skordalakes, E., Zhang, R., Franco, A. A., Brill, S. J., Adams, P. D., Berger, J. M., and Kaufman, P. D. (2003) *Curr Biol* **13**, 2148-2158
115. Namboodiri, V. M., Dutta, S., Akey, I. V., Head, J. F., and Akey, C. W. (2003) *Structure* **11**, 175-186
116. Muto, S., Senda, M., Akai, Y., Sato, L., Suzuki, T., Nagai, R., Senda, T., and Horikoshi, M. (2007) *Proc Natl Acad Sci U S A* **104**, 4285-4290
117. Ito, T., Bulger, M., Kobayashi, R., and Kadonaga, J. T. (1996) *Mol Cell Biol* **16**, 3112-3124
118. McBryant, S. J., Park, Y. J., Abernathy, S. M., Laybourn, P. J., Nyborg, J. K., and Luger, K. (2003) *J Biol Chem* **278**, 44574-44583

119. Zlatanova, J., Seebart, C., and Tomschik, M. (2007) *Faseb J* **21**, 1294-1310
120. Vardabasso, C., Manganaro, L., Lusic, M., Marcello, A., and Giacca, M. (2008) *Retrovirology* **5**, 8
121. Park, Y. J., and Luger, K. (2006) *Proc Natl Acad Sci U S A* **103**, 1248-1253
122. Altman, R., and Kellogg, D. (1997) *J Cell Biol* **138**, 119-130
123. Zimmerman, Z. A., and Kellogg, D. R. (2001) *Mol Biol Cell* **12**, 201-219
124. Li, M., Strand, D., Krehan, A., Pyerin, W., Heid, H., Neumann, B., and Mechler, B. M. (1999) *J Mol Biol* **293**, 1067-1084
125. Calvert, M. E., Keck, K. M., Ptak, C., Shabanowitz, J., Hunt, D. F., and Pemberton, L. F. (2008) *Mol Cell Biol* **28**, 1313-1325
126. Asahara, H., Tartare-Deckert, S., Nakagawa, T., Ikehara, T., Hirose, F., Hunter, T., Ito, T., and Montminy, M. (2002) *Mol Cell Biol* **22**, 2974-2983
127. Galichet, A., and Gruissem, W. (2006) *Plant Physiol* **142**, 1412-1426
128. Regnard, C., Desbruyeres, E., Huet, J. C., Beauvallet, C., Pernollet, J. C., and Edde, B. (2000) *J Biol Chem* **275**, 15969-15976
129. van Dijk, J., Miro, J., Strub, J. M., Lacroix, B., van Dorsselaer, A., Edde, B., and Janke, C. (2008) *J Biol Chem* **283**, 3915-3922
130. Ikegami, K., Horigome, D., Mukai, M., Livnat, I., MacGregor, G. R., and Setou, M. (2008) *FEBS Lett* **582**, 1129-1134
131. Park, Y. J., Chodaparambil, J. V., Bao, Y., McBryant, S. J., and Luger, K. (2005) *J Biol Chem* **280**, 1817-1825
132. Loyola, A., and Almouzni, G. (2004) *Biochim Biophys Acta* **1677**, 3-11
133. Rougeulle, C., and Avner, P. (1996) *Mamm Genome* **7**, 606-607
134. Schnieders, F., Dork, T., Arnemann, J., Vogel, T., Werner, M., and Schmidtke, J. (1996) *Hum Mol Genet* **5**, 1801-1807
135. Redeker, V., Le Caer, J. P., Rossier, J., and Prome, J. C. (1991) *J Biol Chem* **266**, 23461-23466
136. Warrens, A. N., Jones, M. D., and Lechler, R. I. (1997) *Gene* **186**, 29-35

137. Bulger, M., Ito, T., Kamakaka, R. T., and Kadonaga, J. T. (1995) *Proc Natl Acad Sci U S A* **92**, 11726-11730
138. Park, Y. J., Dyer, P. N., Tremethick, D. J., and Luger, K. (2004) *J Biol Chem* **279**, 24274-24282
139. Ishimi, Y., Hirosumi, J., Sato, W., Sugasawa, K., Yokota, S., Hanaoka, F., and Yamada, M. (1984) *Eur J Biochem* **142**, 431-439
140. Formosa, T., Ruone, S., Adams, M. D., Olsen, A. E., Eriksson, P., Yu, Y., Rhoades, A. R., Kaufman, P. D., and Stillman, D. J. (2002) *Genetics* **162**, 1557-1571
141. Boucher, D., Larcher, J. C., Gros, F., and Denoulet, P. (1994) *Biochemistry* **33**, 12471-12477
142. Larcher, J. C., Boucher, D., Lazereg, S., Gros, F., and Denoulet, P. (1996) *J Biol Chem* **271**, 22117-22124
143. Forsburg, S. L. (1999) *Trends Genet* **15**, 340-344